The Transport and Magnetic Resonance Properties of the Organic Superconductor $NMe_4[Ni(dmit)_2]_2$.

Geoffrey Stockham.

University of St. Andrews.

July 1996

For the degree of Doctor of Philosophy.

ABSTRACT

The organic superconductor $NMe_4[Ni(dmit)_2]_2$ has been studied by ^{13}C and ^{1}H Nuclear Magnetic Resonance, Electron Spin Resonance, Magnetic Susceptibility and Resistivity techniques.

Resistivity measurements show transitions at 100K and at 20K with hysteresis between the cooling and warming data. No sign of a superconducting transition was detected, as only ambient pressure measurements were taken.

Magnetic susceptibility experiments show a Curie tail dominating the results at low temperatures, from which estimates of the number of paramagnetic impurities are presented. The 20K transition in single-crystal samples can be seen, as well as a possible antiferromagnetic ordering at 4K.

Nuclear Magnetic Resonance experiments show a double peak for the ^{1}H spectra at room-temperature due to the methyl groups which freeze to produce a triplet at low temperatures. ^{13}C spectra show four peaks from the $Ni(dmit)_2$ molecule, and one from the NMe_4 cations. Knight shift and spin-lattice relaxation results are presented, and these contain of contributions from both *s*- and *p*-character orbitals.

Electron Spin Resonance results show sample dependent peaks at low temperatures due to paramagnetic impurities. At 45K unusual sharp peaks appear in the spectra, which broaden out and disappear by 60K. A possible mechanism of conduction "filaments" is used to explain this phenomenon.

I, Geoffrey John Stockham, hereby certify that this thesis, which is approximately 30,000 words in length, has been written by me, that it is the record of work carried out by me and that it has not been submitted in any previous application for a higher degree. I was admitted as a research student in October 1992; the higher study for which this is a record was carried out in the University of St. Andrews between 1992 and 1996.

23.07.96

I hereby certify that the candidate has fulfilled the conditions of the Resolution and Regulations appropriate to the degree of PhD. in the University of St. Andrews and that the candidate is qualified to submit this thesis in application for that degree.

23.07.96

In submitting this thesis to the University of St. Andrews I understand that I am giving permission for it to be made available for use in accordance with the regulations of the University Library for the time being in force, subject to any copyright vested in the work not being affected thereby. I also understand that the title and abstract will be published, and that a copy of the work may be made and supplied to any *bona fide* library or research worker.

23.07.96

Acknowledgements.

I would like to record my thanks to my supervisor, Dr. David Tunstall, for his help and guidance over the last four years, particularly throughout his absence from the department due to ill-health.

I am also indebted to a number of people for their assistance with various experiments: Solange Doidge-Harrison and John Irvine in the Department of Chemistry at the University of Aberdeen for preparing the samples; Dominic Hunter and John Ingledew from the Department of Biochemistry at the University of St. Andrews for the preliminary ESR spectra; Terry Hall and Peter Edwards in the Department of Chemistry at the University of Birmingham for the main ESR experiments; Gavin Whittaker and Andrew Harrison in the Department of Chemistry at the University of Edinburgh for the SQUID measurements.

My thanks are also extended to my colleagues in the Solid State Physics group - Wendy, Heather, Guangping, Bernd and Phil - for their many helpful discussions.

I would also like to thank my family, John and Valerie Stockham, and Jill and Bob Moore, for their support throughout my student years.

Last but by no means least, I would like to thank my wife, Leila, for her patience, understanding and proof-reading while I was writing this thesis. Danke schön!

For Leila

Take Carbon for example then
What shapely towers it constructs
To house the hopes of men!
A. M. Sullivan.

1. Introduction.

1.1. Superconductivity.

1.1.1. Introduction.

Only in the last few years has the prospect of achieving superconductivity at room temperature become a realistic proposition. Until 1986 it remained strictly a low temperature phenomenon, inspiring many theoretical studies, and creating a few practical applications. However, these applications, such as the production of large, homogeneous magnetic fields, required cooling to near-absolute zero temperatures with expensive liquid helium. The discovery of ceramic compounds which become superconducting above the boiling point of liquid nitrogen, which is much cheaper to produce, brings with it many new possibilities, such as faster electronic components and magnetically levitated trains.

All the publicity surrounding the new high-temperature superconductors has slightly overshadowed the parallel field of organic superconductors. These materials, based on carbon, are usually highly one-dimensional, and were originally predicted to have superconducting transitions as high as 2000K as long ago as the 1960s. In fact, the highest transition temperatures in organic superconductors have yet to break the liquid nitrogen barrier at 77K *(see Figure 1.1)*, but they remain a fascinating area of research, showing many new and unusual physical properties.

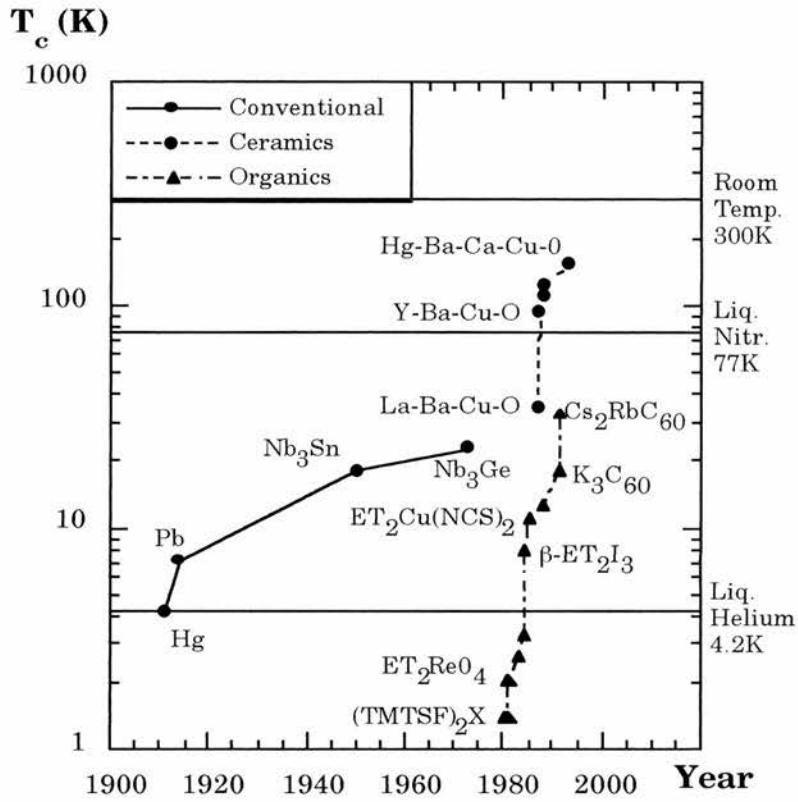

Figure 1.1. *The variation of T_c with time. It can be seen that the rate of increase of T_c in organic materials rivals that of the high-Tc materials.*

1.1.2. Conventional Superconductors.

In 1908, after almost 10 years of experimental work, the Dutch physicist Kamerlingh-Onnes first produced liquefied helium[1]. At that time, it was an enormous engineering feat to cool helium to its transition temperature of 4.2K. He realised that many new solid-state properties of matter could be probed so near to absolute zero, without the thermal motion of the atoms concealing them. At the time, there were contrasting theories about what would happen to the resistivity of metals as they approached absolute zero[2] *(see Figure 1.2)*. Kamerlingh-Onnes began a

---

1 H. K. Onnes: *Proc. Acad. Sci. Amst.*, **11**, 168 (1908).

2 See G. Vidali: *Superconductivity - the Next Revolution*, Cambridge Univ. Press (1993), for a flavour of the state of physics in the years surrounding the discovery of superconductivity.

systematic study of the resistivity of metals at liquid helium temperatures. His results appeared to be dependent on sample purity, so in 1911 he decided to investigate mercury, as it could be obtained in a very pure form. To his surprise, the resistance dropped abruptly to zero at 4.2K. He named this new phenomenon "superconductivity"[3] and a new branch of physics was born.

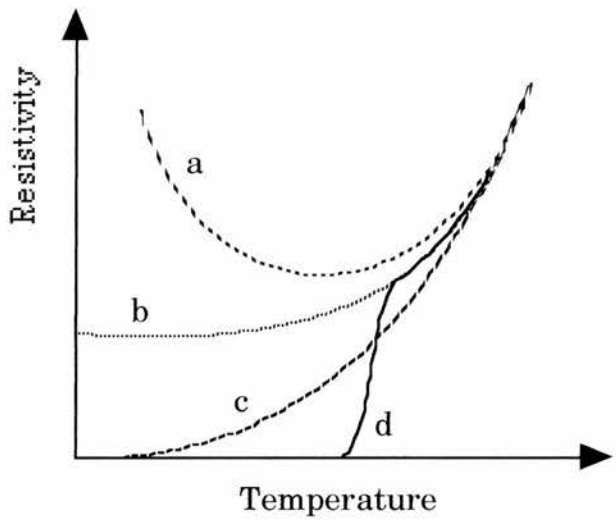

Figure 1.2. *At the turn of the century, there were differing views as to what would happen to a metal at low temperature. One possibility was that the 'cloud' of electrons would condense onto their atoms, and the resistivity would rise (a). Another idea was that as lattice vibrations stopped, the resistance would go to zero (c) although this may flatten off depending on impurities (b). In a superconductor, the resistance drops abruptly to zero (d).*

Many of the elements were subsequently discovered to be superconducting, of which niobium has the highest transition temperature of 9.26K. Unusually, the metals that are the best electrical conductors at higher temperatures turn out to be bad superconductors, a property which led to a theoretical understanding of the conventional superconductors, which will be explained below.

---

3 H. K. Onnes: *Leiden Comm.*, **124c** (1911).

The search for better superconductors led to alloys and compounds, such as Nb_3Sn, which has a T_c of 18K. The materials which have turned out to have the highest T_c have all belonged to the A-15 family of alloys, with stoichiometry A_3B. Characteristic of this group are the chains of linear, one-dimensional A atoms, a property that inspired studies on organic systems with similar metallic chains[4]. The record for the highest T_c was held by a thin film of Nb_3Ge with a T_c of 22.3K[5] until 1986 *(see Figure 1.1)*.

1.1.3. Properties of Superconductors.

The first indication of superconductivity was the observation of a state of zero resistance. Although it is impossible to actually measure zero resistance because of experimental error, the latest measurements show that the resistance is actually less than $10^{-27}\ \Omega.cm$[6].

One of the most visible properties of superconductors was discovered by Meissner and Ochsenfeld in 1933[7]. A superconductor cooled below T_c will expel an external magnetic field, provided the field is not larger than a critical value, H_c *(see Figure 1.3)*. This is due to electric currents, known as *screening currents*, flowing on the surface of the superconductor so as to oppose the external magnetic field. Therefore, the superconductor behaves as if the magnetic susceptibility, χ, is -1, characteristic of a *perfect diamagnet*. A spectacular demonstration of this effect, known as the *Meissner effect*, can be seen when a superconductor placed above a magnet is cooled below T_c. The superconductor can be seen to levitate above the magnet.

---

4 K. Krogmann and H. D. Hausen: *Z. Anorg. Allg. Chem.*, **358**, 67 (1968).

5 L. R. Testardi, J. H. Wernick and W. A. Royer: *Solid State Comm.*, **15**, 1 (1974).

6 See V. Kresin and S. A. Wolf: *Fundamentals of Superconductivity*, Plenum (1990).

7 W. Meissner and R. Ochsenfeld: *Naturwiss.*, **21**, 787 (1933).

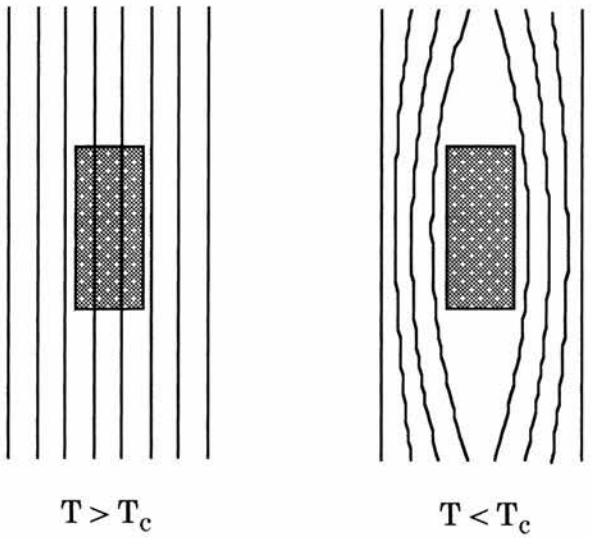

Figure 1.3. *Exclusion of magnetic flux from a superconductor. The magnetic field, H, must be less than the critical field* H_c.

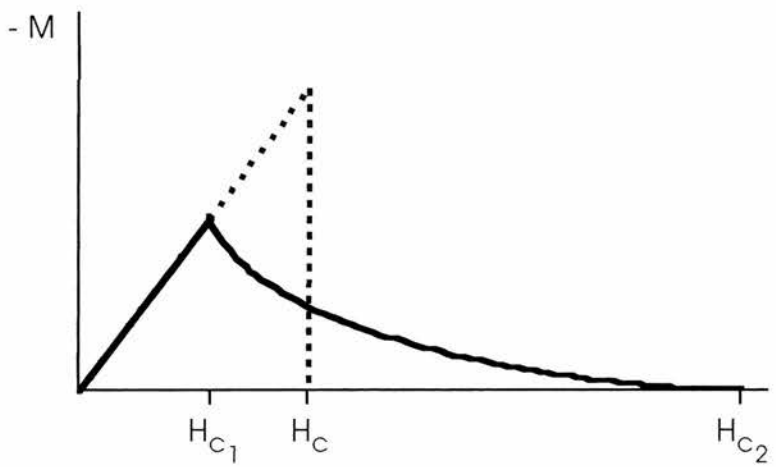

Figure 1.4. *Magnetism as a function of temperature for Type I and Type II superconductors. In reality, these show slight hysteresis due to impurities in the materials.*

The behaviour of superconductors in a magnetic field divides them into two distinct groups, known as *Type I* or *Type II* superconductors *(see Figure 1.4)*. All pure elements except for niobium are Type I, and their superconductivity is destroyed by a modest magnetic field, H_c. Type II

superconductors behave as Type I up to a lower critical field H_{c1}, above which there is partial flux penetration. At an upper critical field H_{c2}, superconductivity is completely destroyed. Between the two critical fields, the superconductor exists in a mixed state, with flux penetrating through some normal regions, whilst the rest remains superconducting.

The field associated with a current flowing through a superconductor means that there is also a critical current, I_c, that can flow. This is known as *Silsbee's hypothesis*[8]. Because of this, it is Type II superconductors that are used for all practical applications, as they can support much larger currents. Commercial superconducting magnets are presently able to produce highly homogeneous magnetic fields higher that 10T.

Although a complete theory of superconductivity could not be found, many phenomenological theories were founded to explain and predict many of the experimental results. Gorter and Casimir[9] proposed the "two-fluid" model in which the electrons in the system form a liquid of "normal" and "superconducting" components† . At T=0 there are only superconducting electrons, but as T increases the "normal" fraction grows until the "superconducting" fraction disappears at $T=T_c$.

In 1935, H. and F. London[10] showed that the magnetic field does not abruptly disappear at the surface of a superconductor, but exponentially decays with a characteristic length, λ, known as the *penetration depth (see Figure 1.5)*. The screening currents are set up in this surface layer. The penetration depth is given by

---

8 F. B. Silsbee: *J. Wash. Acad. Sci.*, **6**, 597 (1916).

9 C. J. Gorter and H. B. G. Casimir: *Physica*, **1**, 306 (1934).

† As superconductivity is a collective phenomenon, it is incorrect to say that each electron is either "normal" or " superconducting".

10 F. London and H. London: *Proc. Royal Soc. (London)*, **A149**, 71, (1935).

$$\lambda = \left(\frac{m}{\mu_0 n_s e^2} \right)^{\frac{1}{2}} \tag{1.1}$$

where n_s is the number of "superconducting" electrons as given by the two-fluid model.

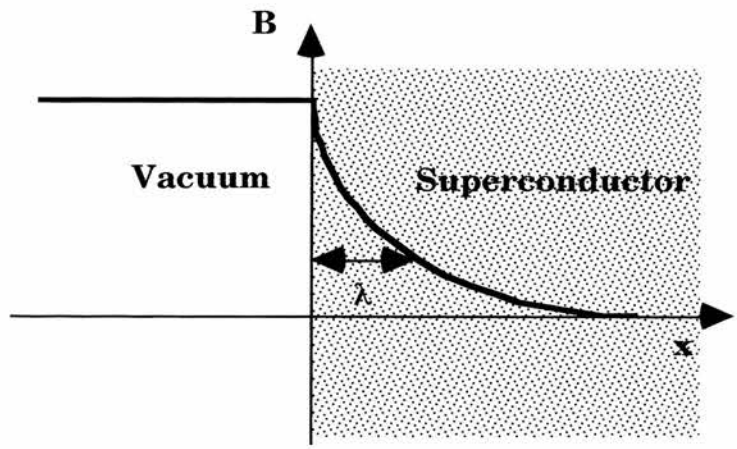

Figure 1.5. *Variation of magnetic field within a superconductor. The field decreases exponentially with a characteristic length λ.*

Pippard discovered that this penetration depth depended on impurity concentration. He found that λ increased when the mean free path, *l*, fell below a certain distance, now known as the *Pippard coherence length*, ξ_P. This phenomenological approach was later justified by the microscopic theory of superconductivity.

All the experimental evidence from superconducting systems points to the existence of a gap in the energy spectrum of the system. The gap, Δ, can be thought of as separating the superconducting electrons from the normal electrons. It vanishes at $T=T_c$, and has its maximum value at T=0. Experiments on the heat capacity of the system show that the energy gap is of the order of $k_B T_c$.

One of the most influential discoveries led to the microscopic theory of superconductivity. A study of the variation of T_c with respect to the isotope mass number[11] showed that

$$T_c M^{1/2} = \text{const} . \qquad (1.2)$$

Because the mass number is related to the frequency of lattice vibrations, or *phonons*, in the material, it was realised that superconductivity arose from interactions between electrons and phonons. This mechanism was the subject of an independent study by Fröhlich[12] while the experimental investigation was underway. Ironically, the mechanism that caused electrical resistance, electron-phonon interaction, was also responsible for superconductivity. This explains the absence of superconductivity in good metals, as the electron-phonon interaction in these metals is weak.

1.1.4. BCS Theory.

Eventually, in 1957, a microscopic theory of superconductivity was proposed by Bardeen, Cooper and Schrieffer, which became known as the BCS theory.

A year earlier, Cooper had studied the effect of the electron-phonon interaction[13]. He considered an electron moving through an ionic lattice. The electron deforms the lattice, creating a region of positive charge, which can exceed the charge on the electron. Another electron can then be attracted to this net positive charge. The interaction can be thought of as two electrons exchanging a virtual phonon *(see Figure 1.6)*. This

---

11 E. Maxwell: *Phys. Rev.*, **78**, 477 (1950); C. A. Reynolds, B. Serin, W. H. Wright and L. B. Nesbitt: *Phys. Rev.*, **78**, 487 (1950).

12 H. Fröhlich: *Phys. Rev.*, **79**, 845 (1950).

13 L. N. Cooper: *Phys. Rev.*, **104**, 1189 (1956).

pairing of electrons in a bound state became known as a *Cooper pair*. For two isolated electrons, this interaction would be very weak, but Cooper showed that near the surface of the Fermi sphere, electrons could form a bound state, no matter how weak the attractive interaction was.

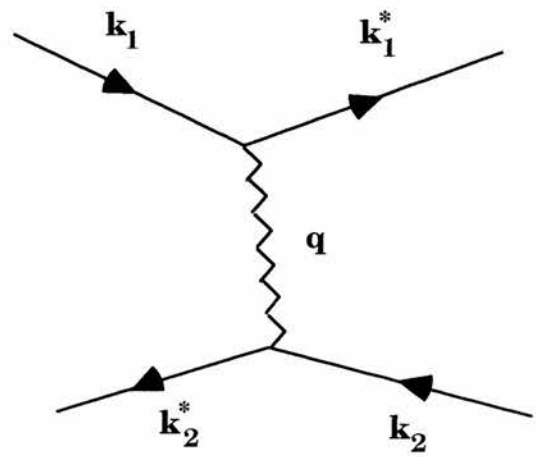

Figure 1.6. *Feynman diagram representing the interaction of two electrons via a virtual phonon.*

This approach was extended by Bardeen, Cooper and Schrieffer[14]. They showed that at T=0, all the electrons form bound pairs. As the temperature increases, the pairs are broken by thermal excitations. Because superconductivity is a co-operative phenomenon, the binding energy of the remaining pairs falls, and the energy gap becomes smaller. The theory provides a good fit to the experimental data of the temperature dependence of the energy gap. According to BCS theory the gap is given by

$$\Delta(0) = 1.76 k_B T_c \,. \tag{1.3}$$

---

14 J. Bardeen, L. N. Cooper, J. R. Schrieffer: *Phys. Rev.*, **106**, 162 (1957); *Phys. Rev.*, **108**, 1175 (1957).

The average distance between electrons in a Cooper pair is known as the *BCS coherence length*, and is given by

$$\xi_0 = \frac{\hbar v_F}{\pi \Delta(0)} \,. \tag{1.4}$$

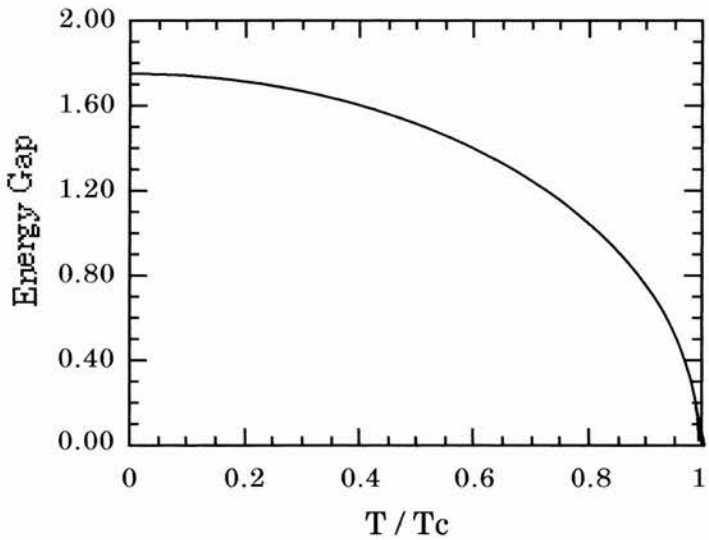

Figure 1.7. *The variation of energy gap with respect to temperature as predicted by BCS theory.*

For many years it was assumed that the BCS theory was the definitive superconductivity theory, as it was so successful. Because it predicted that all the Cooper pairs would be broken by thermal excitation, it seemed unlikely that superconductivity would be found above about 30K.

1.1.5. Unconventional Superconductors.

Until the discovery of the high-T_c oxide superconductors in 1986, most superconductors known were BCS-like. However, there were two other types of superconductors, both discovered at approximately the same time. One of them, the *organic superconductors*, will be described in more detail later. The other, *heavy fermion superconductors*, were first discovered in 1979 by Steglich *et al.*[15]. They do not have high transition temperatures (< 1K), but do have a number of interesting properties. Among them is the large value of effective mass, several hundred times that of the free electron, and anomalous temperature-dependence of heat capacity. Most evidence points to *p*-wave pairing of electrons, rather than BCS-like *s*-wave pairing[16]. This is similar to the pairing mechanism in superfluid ^{3}He[17].

The discovery in 1986 by Bednorz and Müller[18] of superconductivity at up to 40K in a La-Ba-Cu-O system earned them the Nobel Prize the following year. The swiftness of the award highlights the significance of their find. In early 1987, Chu and Wu[19] discovered the Y-Ba-Cu-O system had a T_c of 93K, the first time a superconductor had been found above the boiling point of liquid nitrogen. To date, the

---

15 F. Steglich, J. Aarts, C. Bredle, W. Lieke, D. Merschede, W. Franz and H. Schafel: *Phys. Rev. Lett.*, **43**, 1892 (1979).

16 For reviews of heavy fermion superconductors, see, for example: G. R. Stewart: *Rev. Mod. Phys.*, **56**, 755 (1984).

17 D. R. Tilley and J. Tilley: *Superfluidity and Superconductivity, 3rd Edition*, IOP Publishing (1990).

18 J. G. Bednorz and K. A. Müller: *Z. Phys. B*, **64**, 189 (1986).

19 M. K. Wu, J. R. Ashburn, C. J. Torng, P. H. Hor, R. L. Meng, L. Gao, Z. J. Thiang, Y. Q. Wang and C. W. Chu: *Phys. Rev. Lett.*, **58**, 908 (1987).

highest T_c found is in $HgBa_2Ca_2Cu_3O_{8+\partial}$ at 135K, which increases to 153K under 150kbar pressure[20].

A common feature among high-T_c oxides is the presence of many copper-oxygen planes. This gives them very anisotropic properties. The transition temperature approximately scales with the number of adjacent Cu-O planes. They are hole, rather than electron, conductors, and usually stem from an antiferromagnetic parent compound, which must be doped to add holes to the Cu-O planes. Although these materials exhibit many properties of BCS behaviour, such as electron pairing and the opening of an energy gap, there are many inconsistencies, such as the high transition temperature. The coherence length is very short, and the behaviour of the materials' elastic constants shows anomalous behaviour. As yet, there have been no conclusive theories to explain the superconductivity, but with the vast number of papers being published every year, there remains huge interest in the phenomenon.

1.2. Development of Organic Superconductors.

1.2.1. The First Organic Conductors.

Although predictions of high conductivity in organic compounds had been made as long ago as 1911[21], the first experimental evidence came from Akamuta *et al.* in 1954[22]. They reported a resistivity of as low as $\sim 10^2$ Ω.cm in a perylene-bromine complex, compared to a resistivity of

---

20 C. W. Chu, L. Gao, F. Chen, Z. J. Huang, R. L. Meng and Y. Y. Xue: *Nature.*, **365**, 323 (1993).

21 H. H. McCoy and W. C. Moore: *J. Am. Chem. Soc.*, **33**, 1273 (1911); H. J. Kraus: *J. Am. Chem. Soc.*, **34**, 1732 (1913)

22 H. Akamuta, H. Inokuchi and Y. Matsunaga: *Nature*, **173**, 168 (1954).

$\sim 10^{22}$ Ω.cm in perylene itself. However, many of the complexes that were synthesised were unstable, and didn't keep their unusual properties for long.

The first stable molecule synthesised was TCNQ (7,7,8,8-tetracyano-p-quinodimethane)[23], which was discovered to form many electrically conductive salts. This sparked an interest in the many new and exciting properties of one-dimensional conducting solids.

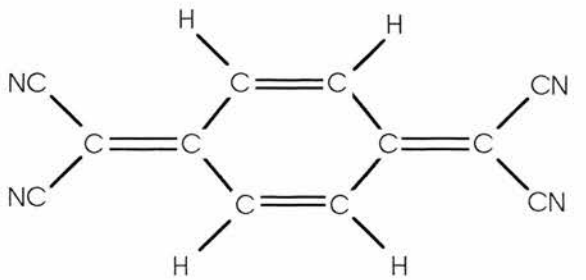

Figure 1.8. *Tetracyanoquinodimethane, or TCNQ.*

1.2.2. Little's Prediction.

A bold prediction of superconductivity with a transition temperature of up to 2000K was made by Little[24] in 1964. He had been interested in the possibility of a superconducting state in biological molecules such as DNA. A few years previously, the BCS theory of superconductivity had been published, and Little saw a way of adapting this to a certain type of molecule.

The BCS theory involves an electron causing a disturbance in the ionic lattice, which in turn attracts another electron to form a bound "Cooper" pair. Little's hypothetical molecule consisted of a "spine" of

---

23 L. R. Melby, R. J. Harder, W. R. Hertler, W. Mahler, R. E. Benson and W. E. Mochel: *J. Am. Chem. Soc.*, **84**, 273 (1962).

24 W. A. Little: *Phys. Rev. A*, **134**, 1416 (1964); *Sci. Am.*, **212**, 21 (1965).

carbon atoms, with periodic side chains which are highly polarisable. An electron moving along the spine would therefore polarise the side chains. This would induce a positive charge near the spine, to which a second electron would be attracted.

By adapting another aspect of BCS theory, the isotope effect, an possible transition temperature can be calculated. Unlike a conventional superconductor, in which the ions in the lattice move when polarised by the passing electron, in Little's molecule it is the electron in the side chains which move. The mass of the electron is approximately 10^{-5} that of the ion. According to the isotope effect, the transition temperature varies as the square root of the difference in mass *(see Equation 1.1)*, i.e. 316 times that of a conventional metallic superconductor, or about 2000K.

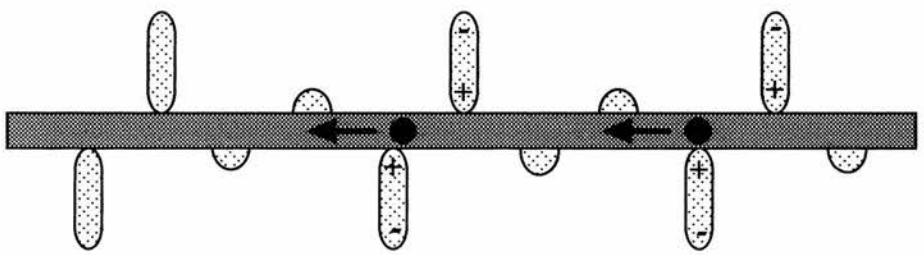

Figure 1.9. *A hypothetical polymer molecule as proposed by Little. An electron can move freely along the spine of the polymer, and as it does so, it polarises the electrons on periodic side chains, inducing a positive charge at the end near the spine. Another electron is then attracted to this net positive charge.*

Needless to say, such a molecule has yet to be successfully synthesised, but these ideas created an impetus which led to many discoveries along different avenues in the field. Only one polymer superconductor has been found[25], and the development of polymer conductors has more recently been directed towards the production of

---

25 Polysulphur nitride (T_c=0.3K).

polymer LEDs, whilst the progress of organic superconductors developed with 'mixed-stack' or 'charge-transfer' compounds, a completely different type of compound to Little's original proposal.

1.2.3. TTF-TCNQ.

The planar molecule TTF (tetrathiafulvalene)[26], first synthesised in 1970, was found to be a good electron donor. It produced many metallic salts with anions such as chlorine, bromine and iodine[27]. When combined with the electron-acceptor TCNQ, it forms one of the archetypal organic metals, TTF-TCNQ[28]. Two chains are formed, one of each molecule, with a transfer of electrons taking place from one chain to the other. This is characteristic of most quasi-one-dimensional systems, and leaves at least one chain with a partially filled electron energy band.

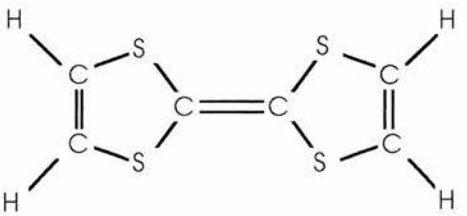

Figure 1.10. *Tetrathiafulvalene, or TTF.*

The salt exhibits metallic properties down to 54K, when there is a structural transition to an insulating state. The increase in conductivity before this transition, originally reported to be about 500 times the room-temperature value, was originally ascribed to superconducting

---

26 F. Wudl, G. M. Smith and E. J. Hufnagel: *J. Chem. Soc. Chem. Comm.*, **1970**, 1453 (1970).

27 For a review of TCNQ salts see B. A. Scott, S. J. LaPlaca, J. B. Torrance, B. B. Silverman and B. Welber: *Ann. N. Y. Acad. Sci.*, **313**, 369 (1978).

28 J. Ferraris, D. O. Cowan, V. V. Walatka and J. H. Perlstein: *J. Am. Chem. Soc.*, **95**, 948 (1973)

fluctuations[29], although this was later proved to be an experimental artefact[30], with the real increase nearer 50 times the room-temperature value.

Nevertheless, a whole family of quasi-one-dimensional salts was produced from the basis of TTF-TCNQ, which can really be considered as the first organic metal. It remained the prototype for studies until 1980.

1.2.4. The First Organic Superconductors.

In 1976, a new family of organic conductors were grown electrochemically by K. Bechgaard[31]. They consisted of a chain of TMTSF (tetramethyltetraselenafulvalene) cations separated by inorganic anions, such as PF_6, BF_4 etc.. These (TMTSF)2X salts, which became known as Bechgaard salts, remained metallic down to ~20K prompting Jérome *et al.*[32] to study their pressure dependence to try and drive this lower. They discovered that at 12kbar the PF_6 salt became superconducting with a T_c of 0.9K. Bechgaard then synthesised $(TMTSF)_2ClO_4$, which was predicted to have a smaller chain spacing[33], and discovered the first ambient pressure organic superconductor, with a T_c=1.3K.

---

29 L. B. Coleman, M. J. Cohen, D. J. Sandman, F. G. Yamagishi, A. F. Garito and A. J. Heeger: *Sol. State. Comm.*, **12**, 1125 (1973).

30 G. A. Thomas, (+ 29 other authors): *Phys. Rev. B*, **13**, 5105 (1976).

31 K. Bechgaard, D. O. Cowan and A. N. Bloch: *Mol. Cryst. Liq. Cryst.*, **32**, 227 (1976).

32 D. Jérome, A. Mazaud, M. Ribault and K. Bechgaard: *J. Phys. Lett.*, **41**, L95 (1980).

33 K. Bechgaard, K. Carneiro, M. Olsen, F. B. Rasmussen and C. S. Jacobson: *Phys. Rev. Lett.*, **46**, 852 (1981).

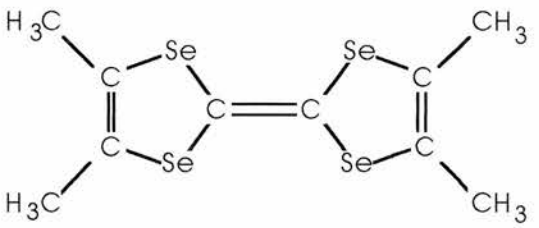

Figure 1.11. *Tetramethyltetraselenafulvalene, or TMTSF.*

The next organic superconductor discovered was based on a hybrid molecule, BEDT-TTF, which is normally abbreviated to ET. It is essentially an extended TTF molecule, and the salt $(ET)_4(ReO_4)_2$ was found to be superconducting at 4.5kbar with T_c=2K[34]. Unlike the Bechgaard salts, ET molecules forms many different crystal structures. Often, there are many different phases from one chemical composition, and these are labelled α–, β–, γ– etc.

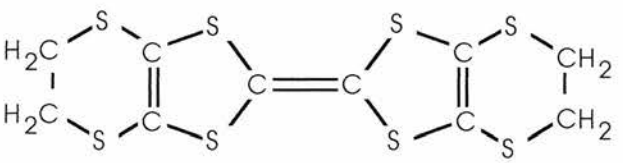

Figure 1.12. *BEDT-TTF.*

Excluding the fullerenes *(see Section 1.2.6)*, the highest ambient pressure T_c is held by κ-$(ET)_2Cu[N(CN)_2]Br$ at 11.6K[35]. An isostructural salt, κ-$(ET)_2Cu[N(CN)_2]Cl$ has a transition temperature of 12.8K, but only after a pressure of 0.3kbar is applied to suppress an insulating ground state.

---

34 S. S. P. Parkin, E. M. Engler, R. R. Schumaker, R. Lagier, V. Y. Lee, J. C. Scott and R. L. Greene: *Phys. Rev. Lett.*, **50**, 270 (1983).

35 A. M. Kini, U. Geiser, H. H. Wang, K. D. Carlson, J. M. Williams, W. K. Kwok, K. G. Vandervoort, J. E. Thompson, D. L. Stupka, D. Jung and M.-H. Whamgbo: *Physica.*, **C166**, 57 (1990).

1.2.5. $M(dmit)_2$ Salts.

All of the compounds discussed so far have been based on donor molecules. In 1986, the acceptor molecule $Ni(dmit)_2$ was found to form a highly conducting salt with TTF[36]. Under pressure, it was found to be superconducting, with a T_c of 1.62K at 7kbar[37]. This was the first observation of superconductivity in a material containing a transition-metal complex.

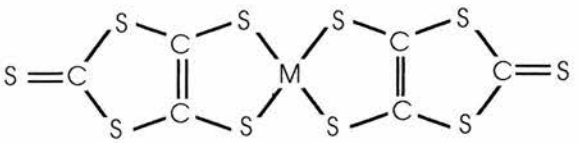

Figure 1.13. *bis(1,3-dithiol-2-thione-4,5-dithiolate)nickelate, or $Ni(dmit)_2$.*

In 1987, the complex $NMe_4[Ni(dmit)_2]_2$ was shown to be a superconductor[38] with a T_c of 5K at 7kbar. This was an interesting development, as the NMe_4 cations take no part in the conduction, and therefore the superconductivity must arise solely because of the $Ni(dmit)_2$ stacks.

These properties will be discussed in more detail in the next chapter.

---

36 M. Bousseau, L. Valade, J.-P. Legros, P. Cassoux, M. Garbauskas and L. V. Interrante: *J. Am. Chem. Soc.*, **108**, 1908 (1986).

37 L. Brossard, M. Ribault, M. Bousseau, L. Valade, P. Cassoux: *Physica*, **143B,** 378 (1986).

38 H. Kim, A. Kobayashi, Y. Sasaki, R. Kato and H. Kobayashi: *Chem. Lett.*, **1987**, 1799 (1987); A. Kobayashi, H. Kim, Y. Sasaki, R. Kato, H. Kobayashi, S. Moriyama, Y. Nishio, K. Kajita and W. Sasaki: *Chem. Lett.*, **1987**, 1819 (1987).

1.2.6. Organic Superconductors Today.

The startling discovery of a new, third form of carbon in 1985[39] has led to another branch of organic superconductors. The C_{60} molecule, or "buckyball"† can be doped with atoms such as potassium or rubidium to give T_cs up to 33K. With these discoveries, the rapid rise of T_c in the last few years in organic superconductors has rivalled the High-T_c ceramics as can be seen in Figure 1.1. As yet, they have not reached such high transition temperatures, but have produced equally challenging properties to explore and explain.

---

39 H. W. Kroto, J. R. Heath, S. C. O'Brien, R. F. Cure and R. E. Smalley: *Nature,* **318**, 162 (1985).

† The molecule was named 'Buckminsterfullerene', as the structure resembled the geodesic dome, as made famous by the architect R. Buckminster-Fuller.

2. Organic Superconductors.

2.1. Properties of Quasi One-Dimensional Conductors.

A *quasi-one-dimensional conductor* can be defined as one in which the overlap of electron wavefunctions is much larger in one crystallographic direction than in the others. The material will therefore exhibit a high anisotropy in many properties, such as electrical conductivity. Most "charge-transfer" molecular conductors (as opposed to polymer conductors) consist of planar molecules stacked on top of each other, with many separate (although not necessarily independent) columns of these stacks. Usually, the larger wavefunction overlaps occur in between adjacent molecules within a stack, so that the highest conductivity is along the stacking direction.

2.1.1. Molecular Orbitals.

A criterion for an organic conductor is the presence of a delocalised electron orbital, as it is these electrons which form the conduction band of the conductor. In an organic molecule, the 2s- and 2p-orbitals of the carbon atom hybridise to form in-plane, or σ-orbitals[1]. In addition, π-molecular orbitals, are formed from the p_z-orbitals of the individual carbon atoms, which are perpendicular to the molecular plane. These π-orbitals have a much lower bonding energy than the σ-orbitals, and

---

1 See, for example, P. W. Atkins: *Molecular Quantum Mechanics (2nd Edition)*, Oxford University Press (1983).

therefore can move from atom to atom. In many calculations, it is only necessary to consider these π-orbitals, with the σ-orbitals, nuclei and inner electrons forming potential fields for the π-electrons. This is known as the *π-electron approximation*.

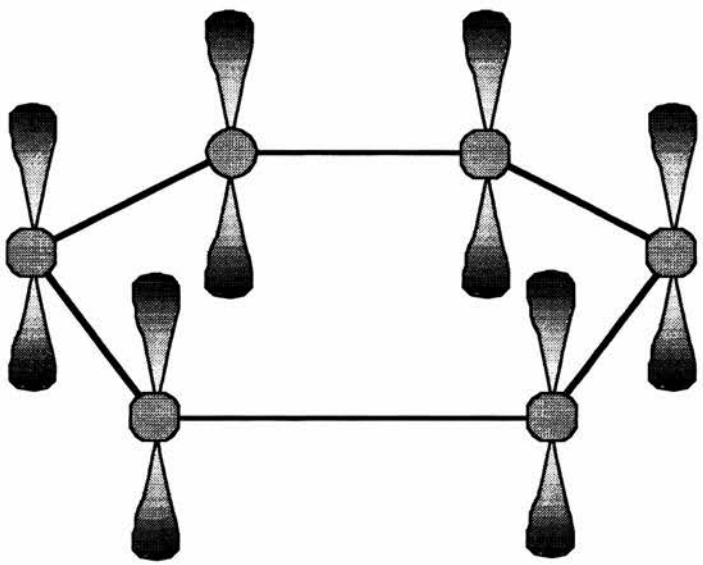

Figure 2.1. *Benzene π-orbitals.*

It is possible to approximate the electronic states of a molecule using a method known as the Hückel Molecular Orbital method (HMO). This uses the π-electron approximation, and assumes that the valence electrons are spread over the whole molecule. The molecular orbitals are approximated by a linear combination of the individual atomic orbitals.

An instructive example would be to take the case of benzene, which has 6 carbon atoms arranged in a ring *(see Figure 2.1)*. Each of these has a p_z-orbital which contributes an electron, which is delocalised over the molecule. Its wavefunction can be described as a linear combination of the atomic orbitals, or

$$\psi = \sum_{p=1}^{6} c_p \chi_p \ . \qquad (2.1)$$

These coefficients can be determined using the variational principle[2] to give

$$\sum_p \left(\mathscr{H}_{qp} - ES_{qp}\right)c_p = 0 \ . \tag{2.2}$$

The energies can therefore be found by solving

$$\det\left|\mathscr{H}_{qp} - ES_{qp}\right| = 0 \ . \tag{2.3}$$

According to Hückel theory, the following simplifications are then made:

1) The overlap integral S_{qp} is set to 1 if i = j, and otherwise is set to 0.

2) All diagonal Hamiltonians, H_{ii} are set to α, known as the *Coulomb integral*, on the assumption that all atoms are electronically equivalent.

3) All off-diagonal elements are set to 0, unless the atoms are neighbours, in which case they are set to β, known as the resonance integral.

We are therefore left with a 6 x 6 determinant

$$\begin{vmatrix} \alpha - E & \beta & 0 & 0 & 0 & 0 \\ \beta & \alpha - E & \beta & 0 & 0 & 0 \\ 0 & \beta & \alpha - E & \beta & 0 & 0 \\ 0 & 0 & \beta & \alpha - E & \beta & 0 \\ 0 & 0 & 0 & \beta & \alpha - E & \beta \\ 0 & 0 & 0 & 0 & \beta & \alpha - E \end{vmatrix} = 0 \ . \tag{2.4}$$

From this, the energy levels can be shown to be

---

2 See, for example, A. I. M. Rae: Quantum Mechanics (3rd Edition), IOP Publishing (1992).

$$\begin{array}{lll} \alpha - 2\beta & \alpha - \beta & \alpha + \beta \\ \alpha - \beta & \alpha + \beta & \alpha + 2\beta \end{array}$$

It can be seen that some of these orbitals are degenerate because of the high symmetry of the benzene molecule.

Generally in organic systems, an extended Hückel method is employed[3]. The resonance and Coulomb integrals can be semi-empirically estimated, and the potential fields from the σ-orbitals are included. Many computer programs are now available[4] which can calculate molecular orbitals, given atomic coordinates of the atoms in a unit cell.

2.1.2. Band Structure.

Because the materials discussed here are highly anisotropic, the electronic band structure can be approximated by the *tight-binding* band approximation[5]. Therefore, the energy band can be written as

$$E(k_a) = 2t_a \cos(k_a a), \tag{2.5}$$

where a is the direction of highest conductivity, and t_a is the electron transfer energy in the a-direction. For molecular stacks, the transfer energy is given by

$$t = \frac{1}{2} K\left(E_i + E_j\right) S_{ij} \tag{2.6}$$

---

3 R. Hoffmann: *J. Chem Phys.*, **39**, 1397 (1963).

4 For example: Computer Aided Calculation of Atomic Orbitals (CACAO) - public domain software for IBM PC.

5 See, for example, J. R. Hook and H. E. Hall: *Solid State Physics (2nd Edition)*, Wiley (1991).

where E_i is the energy level of the i^{th} atomic orbital, and S_{ij} is the overlap integral between molecular orbitals i and j. K is a constant between 1 and 2, usually given the value 1.75.

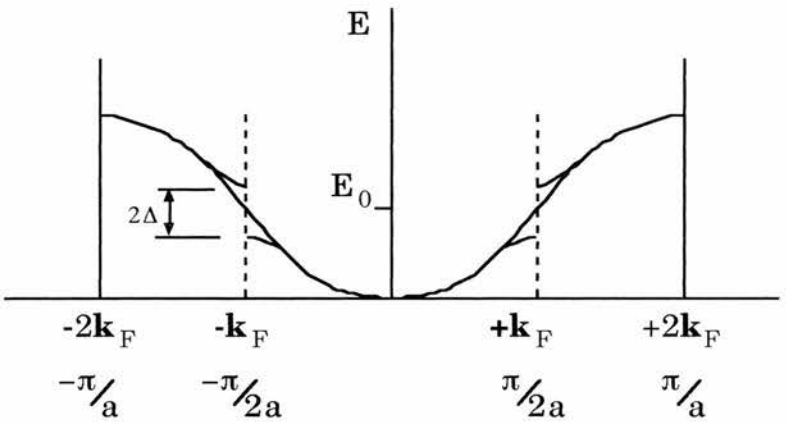

Figure 2.2. *Band structure of a one-dimensional system with a half-filled band. A transition to an insulating state opens up a gap at the Fermi surface E_F.*

2.1.3. Fermi Surface.

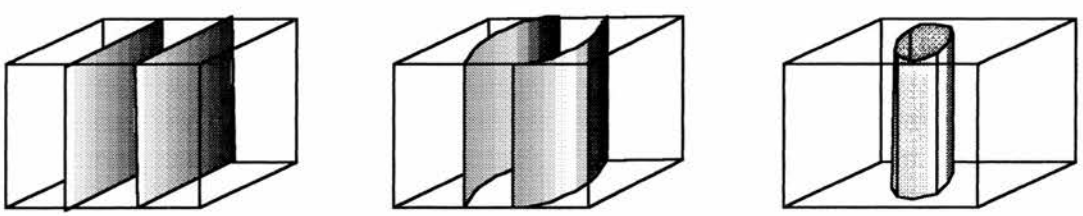

Figure 2.3. *(a) The Fermi surface of a truly one dimensional conductor. (b) A quasi-one-dimensional conductor, in which there is appreciable transverse interaction to 'warp' the sheets of the FS. (c) A two-dimensional conductor has a cylindrical FS. This would be warped slightly if there was appreciable interaction in the third direction.*

Because of the one-dimensional nature of the conductivity of organic conductors, the Fermi surface consists of planar parallel sheets

(see Figure 2.3). As the electron transfer energy in the b-direction, t_b, becomes more significant, the Fermi surface "warps" until it finally closes to form a cylindrical shape. If there is any interaction in the third direction, then this cylinder then becomes warped.

2.1.4. Peierls Transition.

It was Peierls, in 1955, who was the first to notice that a 1D chain of atoms is unstable against distortions of the underlying lattice[6]. In a one-dimensional system with a half-filled band, the molecules will tend to dimerise, which will effectively double the size of the unit cell. This will open a gap at the wave vector $\mathbf{k}_F$ resulting in a transition to an insulating state.

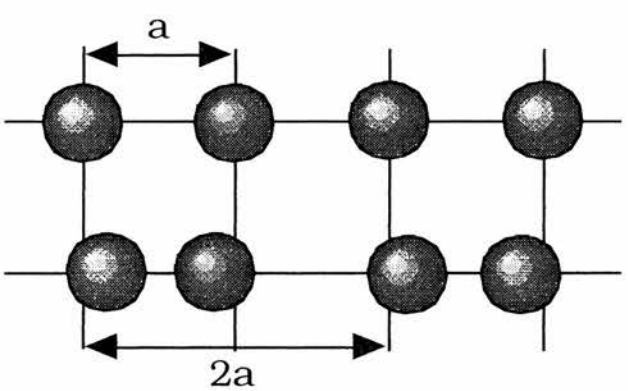

Figure 2.4. *Dimerisation of atoms in a one-dimensional system.*

This transition, at a characteristic temperature T_P, is a result of strong interactions between conduction electrons and acoustic phonons of wave vector $2\mathbf{k}_F$. This produces a dip in the frequency of the $2\mathbf{k}_F$ phonons, known as the Kohn anomaly[7]. Because in reality, the electrons are coupled to the underlying lattice, the perturbations due to the $2\mathbf{k}_F$

---

6 R. E. Peierls: *Quantum Theory of Solids*, Oxford Univ. Press (1955).

7 W. Kohn: *Phys. Rev. Lett.*, **2**, 393 (1959).

phonons also deforms the lattice. As the energy of these phonons becomes zero at the transition temperature T_P, the lattice distortion becomes time-invariant, and is "frozen in".

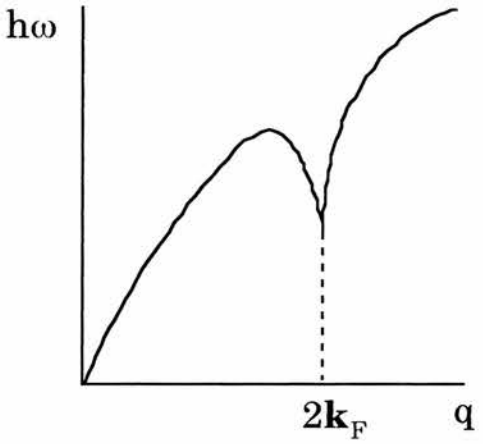

Figure 2.5. *The Kohn anomaly. The frequency of the $2k_F$ phonon mode falls to zero at the transition temperature.*

2.1.5. Charge and Spin Density Waves.

The distortion of the electron and lattice systems can be thought of as a modulation of the electron density. This structure is known as a *Charge Density Wave* (CDW). If the wavelength of the CDW corresponds to an integer multiple of the lattice spacing, it becomes "pinned" to the underlying lattice, and is said to be *commensurate*. Otherwise, it is said to be *incommensurate*. It is also possible to pin a CDW with crystalline imperfections.

In TTF-TCNQ, it was discovered that the high conductivity could not be explained by using a simple single-electron theory of conduction. The increased conductivity was ascribed to sliding CDW motion, which was borne out by pressure studies. The charge transfer of TTF-TCNQ increases linearly with pressure, and near 20kbar, there is a sharp drop

in conductivity, where the CDW becomes commensurate and is pinned to the lattice.

Another density wave phenomenon is found in the Bechgaard salts. The charge density of the two electron spin states is modulated so that overall, there is no change in the charge density, but the net spin polarisation changes. It is an antiferromagnetic-like state, but is due to delocalised rather than localised electrons. It is known as a *Spin Density Wave* (SDW) and, unlike the CDW, there is no underlying lattice distortion, so it can be difficult to identify. Just as a $2\mathbf{k}_F$ modulation of the charge density leads to an insulating state, a $2\mathbf{k}_F$ modulation of the spin density will open a gap at the Fermi surface to produce an insulating state.

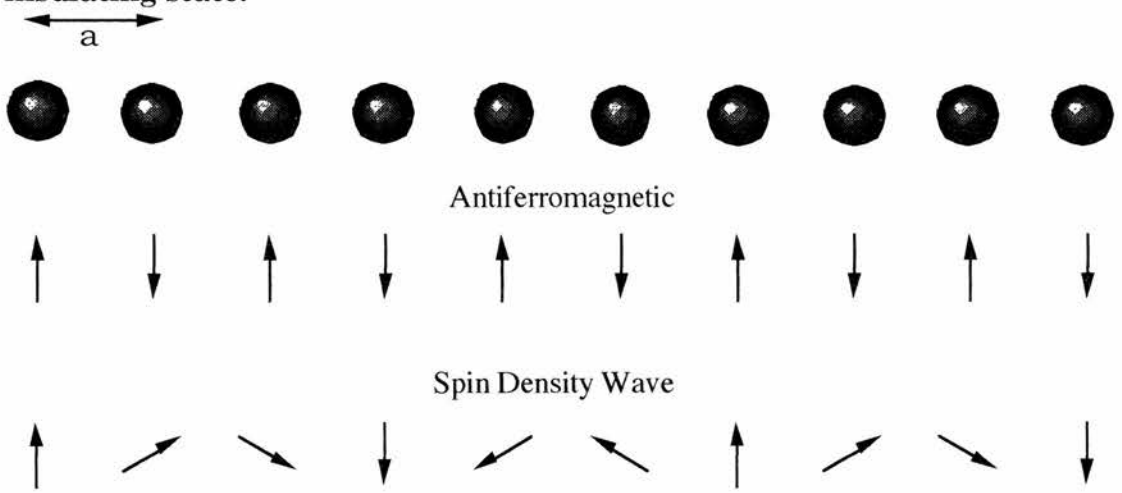

Figure 2.6. *In an antiferromagnetic chain, the spins alternate between up and down states. In a SDW chain, the spins are modulated.*

2.2.4. Spin-Peierls State.

A combination of the CDW and spin states is the *spin-Peierls* arrangement. In a ρ = 0.5 charge-transfer material such as the Bechgaard salts the normal $2\mathbf{k}_F$ transition would dimerise the stacks with one electron per dimer. A spin-Peierls state has an additional $4\mathbf{k}_F$

instability which pairs the spins in a singlet state. This is illustrated in Figure 2.7.

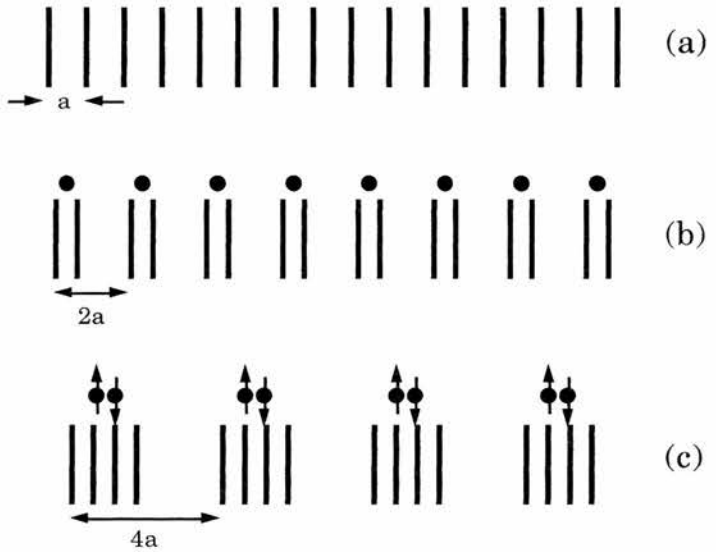

Figure 2.7. *With 1/2 electron per molecule (a), the stacks can be dimerised as in a normal Peierls transition (b) with one molecule per dimer, then paired in a spin-Peierls state (c) with the spins paired in a singlet state.*

2.2. The Bechgaard Salts.

Since their discovery in 1979, the Bechgaard salts have become something of a model system for the study of organic superconductors. They show a wide variety of ground states, such as Spin Peierls, Spin Density Wave, and Superconducting *(see Figure 2.8)*.

2.2.1. Structure.

All the $(TMTSF)_2X$ compounds form the same triclinic crystal structure (space group $P\bar{1}$), despite their differing low-temperature properties. The TMTSF molecules form staggered stacks, with the molecules slightly dimerised. These stacks are separated by the inorganic anions, such as PF_6^- or ClO_4^-.

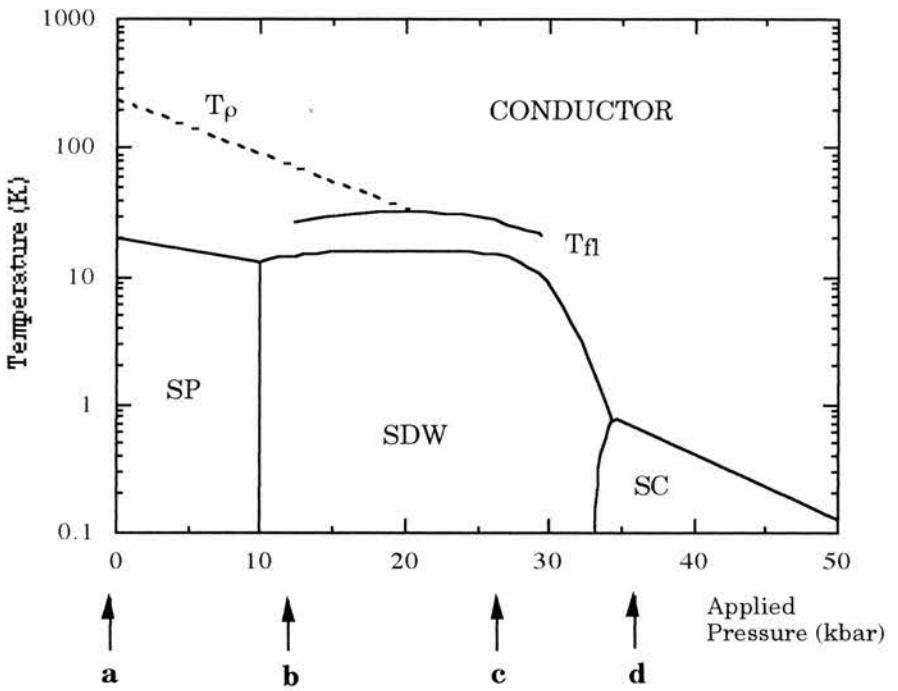

Figure 2.8. *Generic phase diagram for the Bechgaard salts. The possible ground states are Spin Peierls (SP), Spin Density Wave (SDW) or Superconducting (SC). T_ρ marks the onset of a 1D lattice instability, and T_{fl} shows a region of antiferromagnetic fluctuations. Positions of selected salts at ambient pressure are shown:* ***a*** *- $(TMTTF)_2PF_6$,* ***b*** *- $(TMTTF)_2Br$,* ***c*** *- $(TMTSF)_2PF_6$,* ***d*** *- $(TMTSF)_2ClO_4$. From ref.* [8].

The charge transfer ratio ρ is 0.5 for TMTSF, which gives overall charge of $(TMTSF)_2^+ \bullet X^-$. The shortest Se-Se distance is 3.87Å in $(TMTSF)_2PF_6$ which is shorter than the sum of the van der Waals radii (3.96Å). Although there is significant orbital overlap between molecules on adjacent stacks, the main overlap of π-orbitals occurs between molecules within a stack. This means that the main conduction path is along the a-axis, with a small but significant conduction along the b-axis. The anions separating the stacks mean that there is little conduction along the c-axis.

---

8 P. Wzeitek, F. Creuzet, C. Bourbonnais, D. Jérome, K. Bechgaard, P. Batail: *J. Phys. I France*, **3**, 171 (1993).

2.2.2. Spin Density Wave State.

Resistivity measurements on $(TMTSF)_2PF_6$ showed a transition to a semiconducting state at about 10K. This could not be ascribed to a CDW transition as X-ray measurements showed no sign of a lattice deformation. Evidence of a SDW state came from many magnetic measurements. Although in many ways indistinguishable from an antiferromagnetic semiconductor, an SDW has some characteristic details:

(i) anisotropic magnetic susceptibility.

(ii) characteristic *spin-flop* field*.

(iii) disappearance of NMR line.

The susceptibility of $(TMTSF)_2AsF_6$ can be seen in Figure 2.9. Along the "easy" axis along which the spins are aligned it drops to zero, whilst there is a slight increase in the other directions. At 0.45T there is an increase in the χ_b susceptibility to make it comparable with the other two directions. This demonstrates the spin-flop transition.

NMR measurements in $(TMTSF)_2PF_6$ demonstrate the broadening effect of the spins. Both the ^1H and ^{77}Se lines are broadened and disappear because of the appearance of local inhomogeneous fields due to the ordered spins[9].

---

* This is the field at which the direction of polarisation of the spins is flipped to reduce the energy.

9 W. M. Walsh Jr., F. Wudl, G. A. Thomas, D. Nalewajek, J. J. Hauser, P. A. Lee, T. Poehler: *Phys. Rev. Lett.*, **45**, 829 (1980);
A. Andrieux, D. Jerome, K. Bechgaard: *J. Physique Lett.*, **42**, L97 (1982);
J. C. Scott, H. J. Pedersen, K. Bechgaard: *Phys. Rev.*, **B24**, 475 (1981).

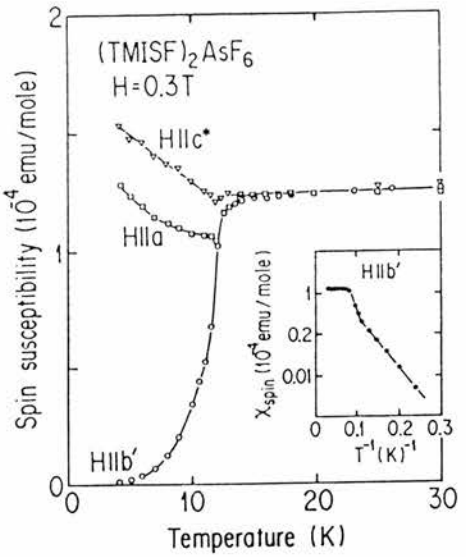

Figure 2.9. *Spin susceptibility of $(TMTSF)_2AsF_6$ with a field of H = 0.3 T. After Mortensen et al.* [10].

2.2.3. Anion Ordering.

Another transition is apparent in the Bechgaard salts, which is dependent on the method used to cool them while measuring. As the temperature is slowly lowered the anions order to form a superstructure. This has the same effect as the Peierls transition and results in a transition to an insulating state. A rapidly-cooled sample does not allow the anions to order, and they are left in random orientations.

There are many different effects produced by anion ordering. One of the most notable is $(TMTSF)_2ClO_4$ [11]. The slowly-cooled sample (0.1K/min) orders at 24K, but the superstructure is not formed along the stacking axis. The ordering actually enhances the conductivity by reducing phonon-scattering by the randomly-orientated anions. There is

---

10 K. Mortensen, Y. Tomkiewicz, K. Bechgaard: *Phys. Rev.*, **25**, 3319 (1982).

11 J. P. Pouget, G. Shirane, K. Bechgaard, J. M. Fabre: *Phys. Rev.*, **B27**, 5203 (1983).

then a transition to a superconducting state at 1.2K. The rapidly cooled samples freezes the random potential results in a SDW ground state with no superconducting state.

2.3. Dmit Salts.

2.3.1. Chemistry of the dmit Ligand.

In the search for better organic conducting materials, the dmit *(1,3-dithiole-2-thione-4,5-dithiolate)* molecule was considered an ideal candidate, as the large number of sulphur atoms on the ligands should encourage a multi-dimensional structure. Sulphur atoms have large atomic orbitals, which should increase the intermolecular overlap between columns.

The dmit ligand was first synthesised by Steimecke in 1975,[12] followed by the $Et_4N[Ni(dmit)_2]_2$ salt in 1979.[13] The $[M(dmit)_2]$ can form salts with three types of cation: *open*- and *closed*-shell, and inorganic. The closed-shell cations, such as NMe_4, or Et_4N do not contribute to the conductivity of the system, as they are effectively only providing structural and charge stability in the system, much as the anions in the Bechgaard salts do. The charge on each $[M(dmit)_2]$ should then depend on the stoichiometry of the system, i.e. 1/2 for the $NMe_4[Ni(dmit)_2]_2$ system.

Open-shell systems are more complicated. With an open-shell cation such as TTF the charge transfer between molecules is dependent on a number of factors. Therefore, a stoichiometry of 1:1 can have a

---

12 G. Steimecke, R. Kirmse, E. Hoyer: *Z. Chem.*, **15**, 28 (1975).

13 G. Steimecke, H. J. Sieler, R. Kirmse, E. Hoyer: *Phosphorus and Sulphur*, **7**, 49 (1979).

charge-transfer of ρ = 0.59, as in TTF-TCNQ. Conductivity in these systems is through a large number of inter- and intra-molecular sulphur-sulphur bonds which are smaller than the Van der Waals radius.

Systems with inorganic cations such as Cs and Na have been synthesised. The most successful, and most studied conductor is $Cs[Pd(dmit)_2]_2$ [14]. It has a very similar structure to many of the closed-shell systems, with the stacks of $Pd(dmit)_2$ molecules separated by the Cs cations.

Another possibility which has not been mentioned is the neutral $[Ni(dmit)_2]$ compound, which was formed as a by-product of $TTF[Ni(dmit)_2]_2$ [15], although this has a low conductivity (3.5×10^{-3} S.cm^{-1}).

2.3.2. Electronic Properties.

The most notable electronic property of the dmit systems is that when they form salts, the $M(dmit)_2$ acts as an acceptor rather than a donor, making these the first anion organic conductors.

By far the most studied dmit systems are those based on the $Ni(dmit)_2$ molecule, as these have produced the most conducting and superconducting systems. Many other systems, based on metals such as Pt, Pd and Au have also been studied, and these have also produced highly conducting and even superconducting examples.

The first highly conducting system was $TTF[Ni(dmit)_2]_2$. The conductivity was measured to be 300 S.cm^{-1} at room temperature which increased to ~10^5 S.cm^{-1} at 4K. Pressure-dependent studies showed a superconducting transition at 1.62 K at 7 kbar[16] *(see Figure 2.10.)*.

---

14 R. A. Clarke, A. E. Underhill: *Synth. Met.*, **27**, B515 (1988).

15 L. Valade, M. Bousseau, A. Gleizes, P. Cassoux, M. Garbauskas, L. V. Interrante: *J. Chem. Soc. Dalton Trans.*, **1985**, 783 (1985).

16 L. Brossard, M. Ribault, L. Valade, P. Cassoux: *Physica*, **143B**, 378 (1986).

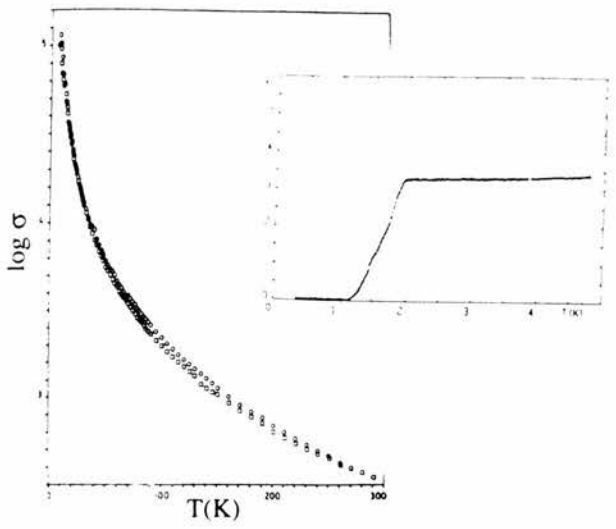

Figure 2.10. *Conductivity of TTF[Ni(dmit)$_2$]$_2$ at ambient pressure, and (inset) the superconducting transition T_c=1.62 K at 7kbar. From references 36, 37, Chapter 1.*

The onset of CDW instabilities has been observed in X-ray studies[17] which is unusual, as these are normally accompanied by a Peierls transition. There is no obvious transition in the conductivity data. This anomaly is explained[18] in terms of the unusual band structure of the system. The M(dmit)$_2$ molecule has a very weak splitting between the HOMO and LUMO (~0.4 eV) according to Hückel calculations[19]. In TTF[Ni(dmit)$_2$]$_2$ this leads to some electronic states of the HOMO having a higher energy than those built from the LUMO. The band structure is shown in Figure 2.11. NMR measurements (see next section) show that the CDW instabilities only affect some of the bands, so the material remains metallic to low temperatures.

---

17 S. Ravy, J. P. Pouget, L. Valade, J. P. Legros: *Europhys. Lett.*, **9**, 931 (1989).

18 L. Brossard, M. Ribault, L. Valade, P. Cassoux: *Phys. Rev. B*, **42**, 3935 (1990).

19 S. Ravy, E. Canadell, J. P. Pouget, P. Cassoux, A. E. Underhill: *Synth. Met.*, **41-43**, 2191 (1991).

Not all the $M(dmit)_2$ systems show this inversion of energy levels. In $NMe_4[Ni(dmit)_2]_2$ the band structure is more conventional, with the HOMO bands remaining at a lower energy than the LUMO bands.

Until 1993, all $M(dmit)_2$ superconductors had only been superconducting under pressure. The first ambient pressure superconductor was α-EDT-TTF[Ni(dmit)$_2$] with a T_c = 1.3 K [20].

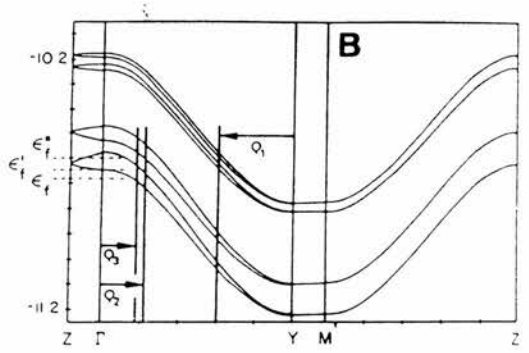

Figure 2.11. *Band structure of TTF[Ni(dmit)$_2$]$_2$ showing multiple band s built from the HOMO and LUMO.*

2.3.3. Magnetic Properties.

The coexistence of the CDW instabilities with the high conductivity of $TTF[Ni(dmit)_2]_2$ was confirmed by NMR measurements[21,22]. Spin-lattice relaxation rate (T_1) measurements[23] showed that the TTF stacks retained their metallic character to low temperatures, implying that the CDW instabilities affected only the $Ni(dmit)_2$ stacks. Locally resolved resonances from the carbon sites on

---

20 H. Tajima, M Inokuchi, A Kobayashi, T. Ohta, R. Kato, H. Kobayashi, H. Kuroda: *Chem. Lett.*, **1993**, 1235 (1993).

21 A. Vainrub, D. Jérome, M.-F. Bruniquel, P. Cassoux: *Europhys. Lett.*, **12**, 267 (1990).

22 A. Vainrub, E. Canadell, D. Jérome, P. Bernier, T. Nunes, M.-F. Bruniquel, P. Cassoux: *J. Phys. France*, **51**, 2465 (1990).

23 C. Bourbonnais, P. Wzietek, D. Jérome, F. Creuzet, L. Valade, P. Cassoux: *Europhys. Lett.*, **6**, 177 (1988).

the $Ni(dmit)_2$ molecule could be seen, with the Knight shifts of the outer carbons decreasing as the temperature was lowered *(see Figure 2.12.)*. This is due to the CDW instabilities affecting the outer carbons, which are associated with the conduction bands built from the LUMO, confirming the unusual band structure.

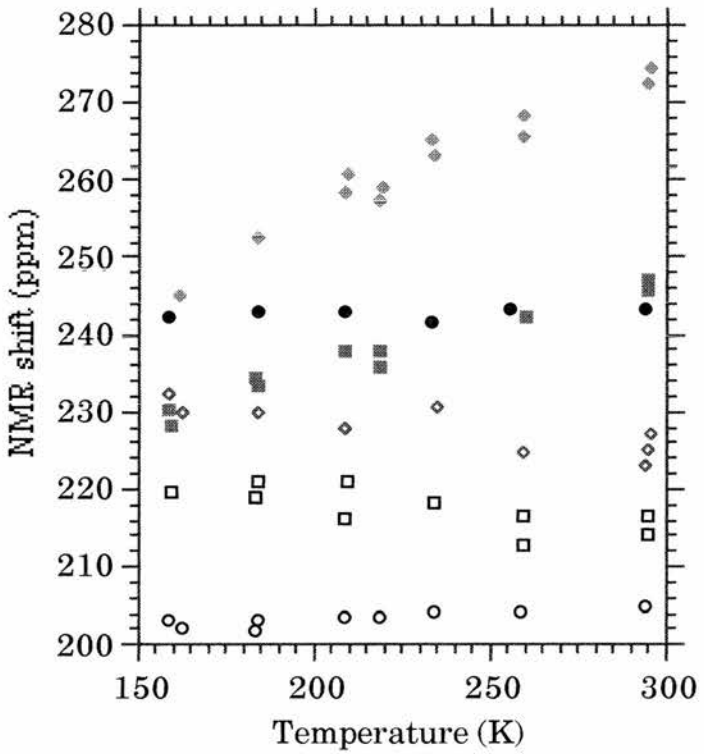

Figure 2.12. *NMR measurements on $TTF[Ni(dmit)_2]_2$ showing the decrease in Knight shift of two of the lines, while the others remain almost constant.*

Magnetic susceptibility measurements on $TTF[Ni(dmit)_2]_2$ [24] show a steady decrease in χ_S as the CDW instabilities affect the LUMO bands of the $Ni(dmit)_2$ stacks. More significant decreases occur at 42K and 8K *(see Figure 2.13.)* which are associated with the HOMO bands. The 8K transition can also be associated with a weak resistivity bump at 9K.

---

24 L. Brossard, E. Canadell, L. Valade, P. Cassoux: *Phys. Rev. B*, **47**, 1647 (1993).

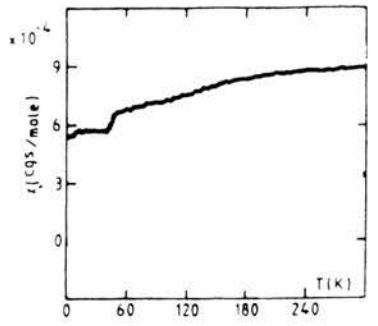

Figure 2.13. *Magnetic susceptibility measurements on TTF[Ni(dmit)$_2$]$_2$.*

2.3.4. Other dmit-Based Systems.

There are many other variations on the M(dmit)$_2$ molecule which have been investigated. One of the most promising is the substitution of the peripheral sulphur atoms with selenium[25]. The larger atomic orbital of selenium should increase the overlaps along the stacks, and increase the conductivity. So far a number of complexes have been synthesised, based mainly on the Pd(dmit)$_2$ molecule[26], but with conductivities still inferior to the sulphur analogs, and with no reported superconducting compounds.

There are many other systems which make slight adjustments to the structures of the existing compounds such as Ni(dmbit)$_2$ and Ni(dmbbip)$_2$ [27] and also systems with three dmit ligands such as

---

25 B. Olk, R.-M. Olk, J. Sieler, E. Hoyer: *Synth. Met.*, **41-43**, 2585 (1991).

26 R. Kato, Y.-L. Liu, H. Sawa, S. Aonuma, A. Ichikawa, H. Takahashi, N. Mori: *Sol. State Comm.*, **94**, 973, (1995);
C. Faulmann, J.-P. Legros, P. Cassoux, J. Cornelissen, L. Brossard, M. Inokuchi, H. Tajima, M. Tokumoto: *J. Chem. Soc. Dalton Trans.*, **1994**, 249 (1994).

27 D.-Y. Noh, J.-H. Choy: *Synth. Met.*, **70**, 1059 (1995).

$W(dmit)_3$ and $Mo(dmit)_3$ [28] although these still do not produce such effective conductors as the original $Ni(dmit)_2$ and $Pd(dmit)_2$ systems.

2.4. Summary of the $NMe_4[Ni(dmit)_2]_2$ System.

The $NMe_4[Ni(dmit)_2]_2$ system consists of stacks of $Ni(dmit)_2$ molecules which are slightly dimerised, separated by $N(CH_3)_4$ cations, as in Figure 2.14. The salt is monoclinic, with space group C2/c, and with unit cell parameters a = 13.856 Å, b = 6.498 Å and c = 36.053 Å. Adjacent stacks have slightly different orientations, which leads to two superimposed Fermi surfaces *(see Figure 2.15 (a).)*. The calculated band structure[29] shows more conventional behaviour than $TTF[Ni(dmit)_2]_2$ with the HOMO and LUMO bands not overlapping *(see Figure 2.15 (b).)*.

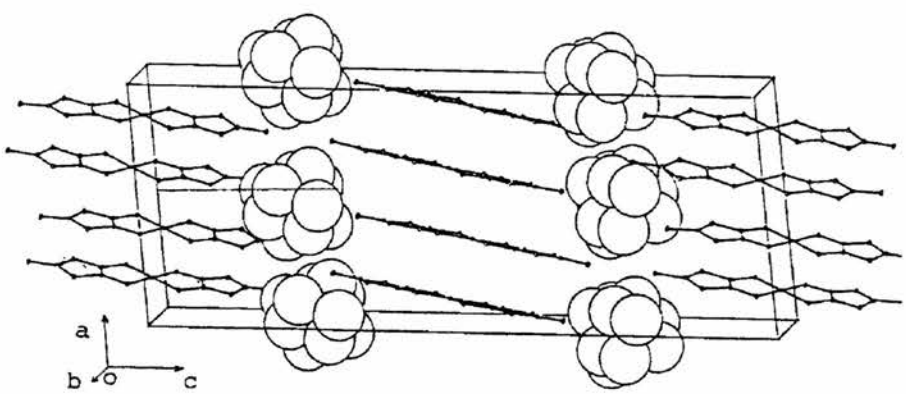

Figure 2.14. *Crystal structure of $NMe_4[Ni(dmit)_2]_2$.*

---

28 G. Matsubayashi, K. Douki, H. Tamura, M. Nakomo, W. Mori: *Inorg. Chem.*, **32**, 5990 (1993).

29 E. Canadell, S. Ravy, J.-P. Pouget, L. Brossard: *Sol. State Comm.*, **75**, 633 (1990).

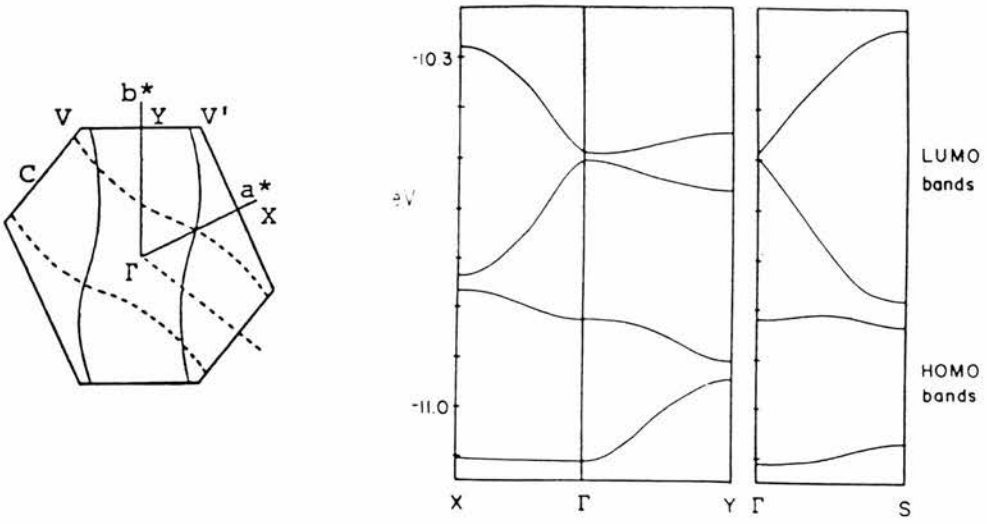

Figure 2.15. *Fermi surface of $NMe_4[Ni(dmit)_2]_2$ (a) and calculated band structure (b).*

Resistivity data shows unusual temperature dependence of the in-plane resistivity *(see Figure 2.16.)*. Most samples follow curve (b) with a jump in the resistivity at about 100K, followed by a transition at 20K, with hysteresis shown as the sample is warmed. However, after repeated thermal cycling samples follow curve (c), with the 100K transition suppressed although the 20K transition remains. Curve (a) shows the resistivity for the plane normal to the ab-plane.

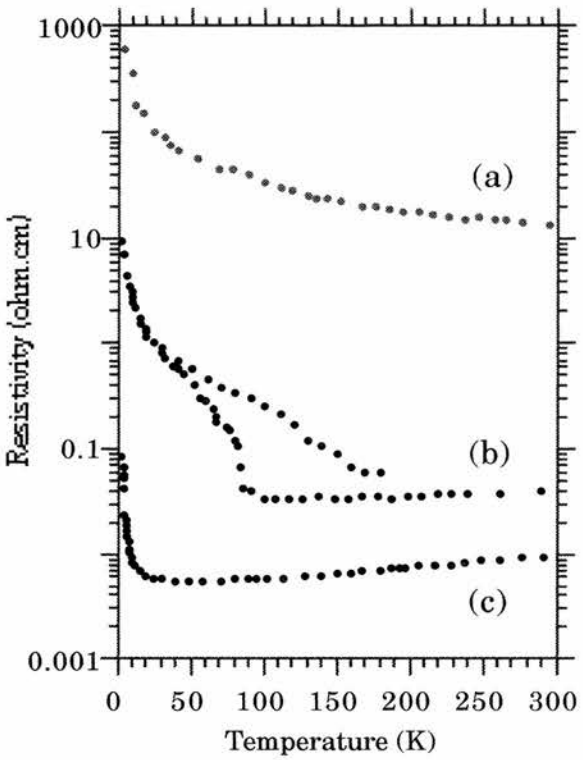

Figure 2.16. *Resistivity of $NMe_4[Ni(dmit)_2]_2$ showing resistivity normal to plane (a) and in-plane (b and c).*

With a pressure of 3.2 kbar, a superconducting transition is observed with T_c = 3.0K. This increases to T_c = 5.0K with a pressure of 7kbar, although this was only observed in one crystal. Studies on the related compound $NH_xMe_{4-x}[Ni(dmit)_2]_2$ attempted to repeat the measurements of a superconducting transition for x = 0 but without success[30]. They also failed to see the 100K transition, but the 20K transition was always present.

---

30 B. Pomarede, B. Garreau, I. Malfant, L. Valade, P, Cassoux, J.-P. Legros, A. Audouard, L. Brossard, J. P. Ulmet, M. L. Doublet, E. Canadell: *Inorg. Chem.*, **33**, 3401, (1994).

3. Sample Characterisation.

3.1. Sample Synthesis.

All samples were synthesised in the Chemistry Department, University of Aberdeen by Solange Doidge-Harrison, Christopher Milne and John Irvine.

3.1.1. Elemental Analysis.

Standard elemental analysis of a crystal of $NMe_4[Ni(dmit)_2]_2$ for carbon, hydrogen and nitrogen gives the ratios shown in Table 3.1.

	Carbon %	Hydrogen %	Nitrogen %
Measured	20.54	1.53	1.97
Theoretical			
C,H. x=0.64	20.6	1.53	1.80
C,N. x=0.73	21.18	2.02	1.73

Table 3.1. *Elemental analysis for $[Ni(dmit)_2] : x\,[N(CH_3)_4]$ with theoretical calculations matching C / H, and C / N ratios.*

Solving $[Ni(dmit)_2] : x\,[N(CH_3)_4]$ for the C and H ratios gives $x = 0.64$, whereas solving for C and N ratios gives $x = 0.73$. It can be seen from Table 3.1 that the first of these gives very close results. Absolute errors are estimated as being up to 0.3% weight, which leads to $x = 0.64 \pm 0.03$.

3.1.2. X-Ray Analysis.

X-Ray analysis of the powder sample confirmed the published unit cell parameters of a = 13.856Å, b = 6.498Å and c = 36.053Å. Analysis was performed in the Dept. of Chemistry, University of St. Andrews by Dr. P. Lightfoot.

3.2. Resistivity Measurements.

One of the most useful measurements on any new material is that of its electrical resistance. In many organic conductors, this should be also done at high pressures, as they often become superconducting. A standard four-point method of measuring resistance was used, but in a pressure cell (Unipress) within a continuous-flow cryostat.

3.2.1. Unipress Pressure Cell.

The Unipress pressure cell (serial number 476/94) is made of copper-beryllium, and has an outer diameter of 36mm. The inner chamber has a diameter of 10mm. Twelve wires are fed through to the inner chamber, one of which is made of constantan, the rest made of copper. The constantan wire and one copper wire are connected to make one junction of a thermocouple. Four wires are connected to measure the resistance of a single crystal of indium antimonide (InSb) in a standard four-point arrangement. The dependence of the resistivity with pressure and temperature is well known and therefore provides a good measure of the pressure in the cell.

Of the remaining six wires, only four are needed to measure the resistance of the sample. The connections are shown in figure 3.1. Crystals of $NMe_4[Ni(dmit)_2]_2$ are very fragile, and the weight of

connecting wires can break them. For these experiments, connections were made to the sample with 20 μm diameter gold wire (Goodfellows) attached with silver-loaded paint. The other end of the wires were soldered to the connecting pins. The sample was held in place with a small drop of GE varnish on a small strip of PTFE tape. This method is similar to that used successfully by Brossard *et al.* in their original measurements on TTF[Ni(dmit)$_2$]$_2$[1]. They noticed that crystals would break if the temperature was changed faster then about 1 K/minute.

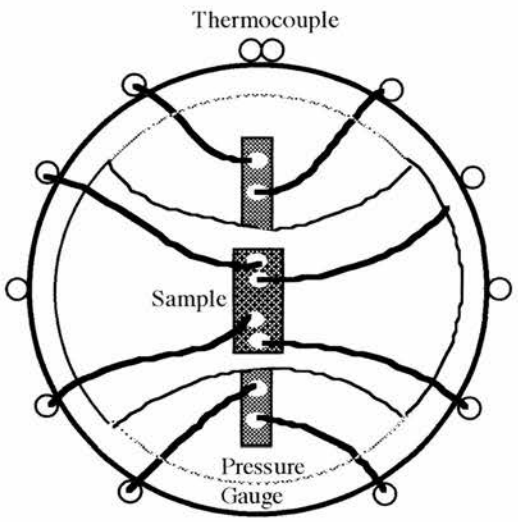

Figure 3.1. *Wiring diagram for the pressure cell. The sample sits on a "table" which fits over the pressure gauge.*

3.2.2. High Pressure Apparatus.

The experimental set-up was adapted from a home-built Van der Pauw resistivity system[2] *(see Figure 3.2.)*. There was no need to switch

---

1 L. Brossard, M. Ribault, M. Bousseau, L. Valade, P. Cassoux: *Physica*, **143B,** 378 (1986).

2 H. F. Booth: *PhD. Thesis*, St. Andrews (1995).

between different contacts as a standard four-point resistivity technique was used.

The ten wires from the pressure cell were separated in a "splitter" box to make connecting apparatus easier. The constantan wire was connected to a copper wire to make the reference junction for the thermocouple. This was then kept in a flask filled with liquid nitrogen. The thermocouple connections were then connected to an Oxford Instruments ITC-4 temperature controller. This can be calibrated for many different types of thermometer, and was set up for a copper-constantan thermocouple with 77.2K reference. The ITC-4 was connected to a Compaq Deskpro 286 PC by an RS-232 serial connection.

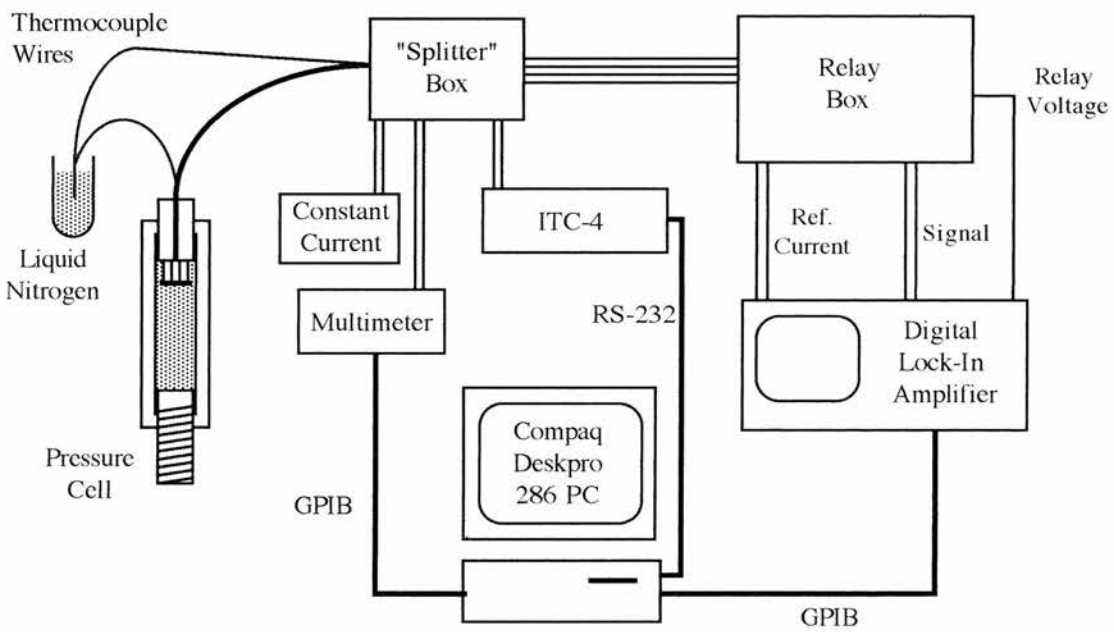

Figure 3.2. *Schematic diagram of the experimental set-up for high-pressure resistivity measurements.*

The pressure gauge was supplied with a current of 10 mA from a constant-current supply, and was constantly monitored. The voltage was measured with a Schlumberger Solartron multimeter, which was

connected to the PC. This allowed instant calculation of the pressure, as the temperature could be read from the ITC-4.

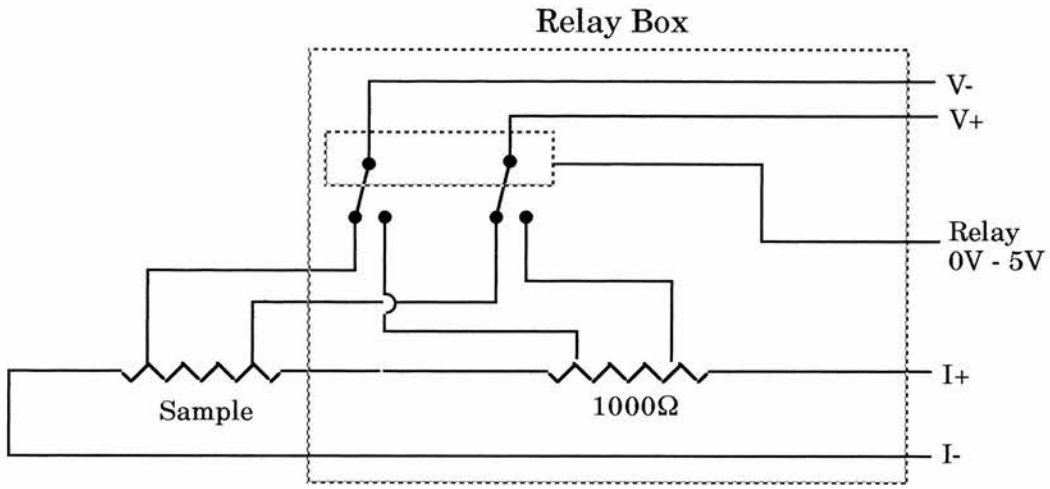

Figure 3.3. *Schematic diagram of the relay box. The switch is set by a controlling voltage from the lock-in amplifier.*

The four sample wires were fed into a relay box. By passing a current through and measuring the voltage, then switching to measure the voltage across a standard resistor the accurate resistance of the sample could be measured. This is shown diagramatically in Figure 3.3. The lock-in amplifier (Stanford Research Systems) provided an alternating current at 27 Hz to the sample. The voltage could then be read. Any out-of-phase components (usually due to bad contacts on the sample) show up clearly. The measurement could then be switched to a standard resistor (1000Ω) to provide an accurate measurement of the sample resistance. The relay switch was operated from the lock-in amplifier auxiliary output, which could be switched between 0V and +5V.

Temperature control of the system was provided by an Oxford Instruments continuous-flow cryostat (CF1200). A cryostat insert was made to hold the pressure cell.

A computer program was written to control as many aspects of data acquisition as possible. A program for the lock-in amplifier had

previously been written[3], into which were incorporated routines for measuring the temperature and voltage of the pressure gauge, and to calculate the pressure given these parameters. All the data could then be saved to disk for post-processing.

3.2.3. Results.

Preliminary results at ambient pressure without the Unipress cell are shown in Figure 3.4.

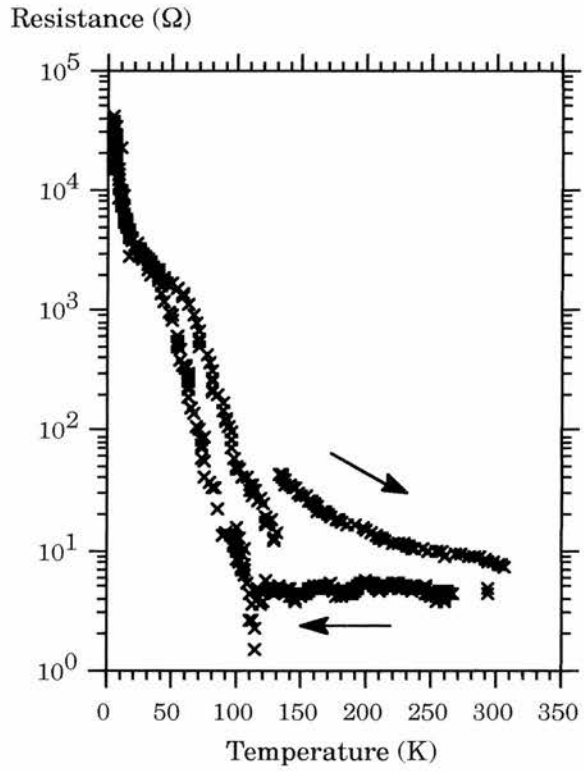

Figure 3.4. *Resistance at ambient pressure.*

The resistivity curves have the hysteresis effect that was observed by Kobayashi *et al.*, and the 20K transition is also present. The break in

---

3 P. J. Mason: A program to control the lock-in amplifier for Van-der Pauw measurements (LIAVDP.EXE).

the warming curve corresponds to the point at which the pump was switched off. Also, the crystal was found to be cracked when taken out of the cryostat. Presumably there was a fluctution in the temperature caused by the pump which caused the crystal to break. The sample could not then be used for further temperature runs, so the effects of repeated thermal cycling could not be investigated.

Attempts to measure a superconducting transition under pressure failed. Only three crystals were of a suitable size for resistivity measurements, and these all broke while wires were being attached or before measurements could be taken.

4. Nuclear Magnetic Resonance.

4.1. Background Theory.

The phenomenon of Nuclear Magnetic Resonance was discovered in the 1940s. At that time, it was a new and exciting area of study for physicists, but the discovery a few years later that the frequency of the resonance depended on the chemical environment opened up the technique to many different disciplines as a powerful tool. Since the first commercial spectrometer appeared in 1953, NMR has become a valuable resource for physicists, chemists, biologists and a host of others.

There are many detailed accounts of Nuclear Magnetic Resonance, both introductory[1,2,3,4] and advanced[5,6,7].

4.1.1. Zeeman Interaction.

All nuclei with odd mass numbers possess spin, $\mathbf{I}$, and therefore a spin angular momentum $\hbar\mathbf{I}$. The magnetic moment can then be given by

$$\boldsymbol{\mu} = \gamma\hbar\mathbf{I}$$

---

1 K. A. McLauchlan: *Magnetic Resonance*, Oxford (1972).

2 R. S. Macomber: *NMR spectroscopy*, Harcourt Brace Jovanovich (1988).

3 R. K. Harris: *Nuclear Magnetic Resonance Spectroscopy*, Longman (1986).

4 J. W. Hennel and J. Klinowski: *Fundamentals of Nuclear Magnetic Resonance*, Longman (1993).

5 C. P. Slichter: *Principles of Magnetic Resonance - 3rd Edition,* Springer-Verlag (1989).

6 A. Abragam: *Principles of Nuclear Magnetism*, Oxford (1961).

7 B. C. Gerstein and C. R. Dybowski: *Transient Techniques in NMR of Solids,* Academic Press (1985).

where γ is known as the gyromagnetic ratio, and is unique to each type of nucleus.

If a nucleus with magnetic moment μ is placed in an external magnetic field $\mathbf{B}_0$, then the Hamiltonian corresponding to the interaction between the two is given by

$$\mathcal{H} = -\mu \cdot \mathbf{B}_0 = -B_o \gamma \hbar I_z,$$

for $\mathbf{B_0}$ defining the z-axis of the system. Therefore, the energy levels of the system are given by

$$E(m) = -B_o \gamma \hbar m_I,$$

where m_I can take the values I, (I-1), ..., (-I+1), -I. This splitting in a magnetic field is known as the *Zeeman Effect*, and it can be seen that there are 2I + 1 Zeeman energy levels.

It can be seen in Figure 4.1 that the energy levels are separated by an energy of $\gamma \hbar B_0$. If energy is supplied to the system with a frequency of $\hbar\omega_0$ such that

$$\hbar\omega_0 = \gamma \hbar B_0,$$

or

$$\omega_0 = \gamma B_0,$$

then a transition occurs between adjacent levels. Here, ω_0 is called the *Larmor Frequency*, and because γ is unique for each nuclear species, the transition occurs at a unique frequency allowing identification of the nuclei present.

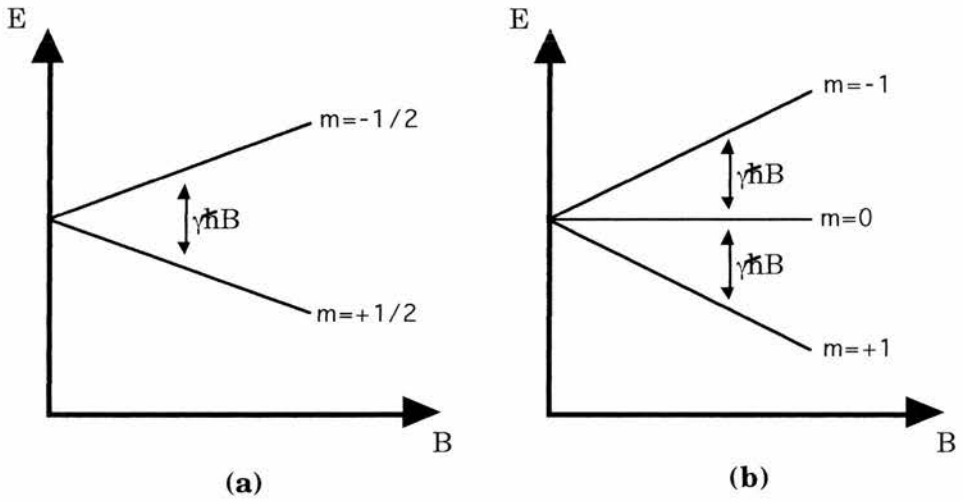

Figure 4.1. *Development of energy levels for a spin-1/2 (a) and spin-1 (b) nucleus in a magnetic field B.*

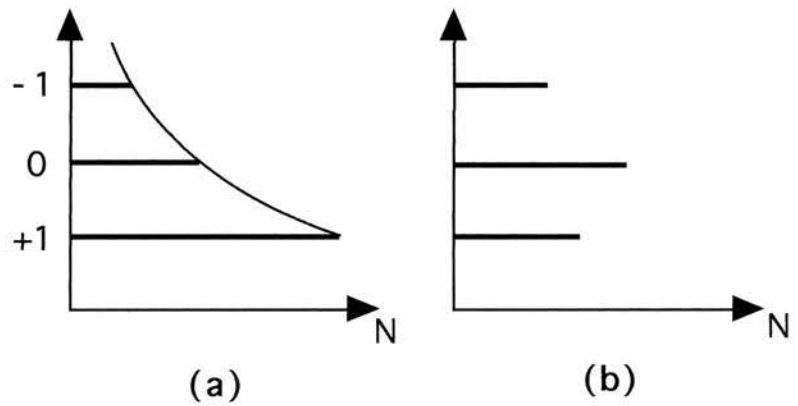

Figure 4.2. *Population of levels for a spin-1 system when in thermal equilibrium (a - exponential decrease) and away from equilibrium (b).*

4.1.2. Total Magnetisation.

In a real system, the total magnetisation **M** is composed of individual magnetic moments. The population of these in the energy levels for a two level system can be determined by Boltzmann statistics[8] such that

8 See for example, J. R. Hook and H. E. Hall: *Solid State Physics - 2nd Edition*, Wiley (1991).

$$\frac{N_{+1/2}}{N_{-1/2}} = e^{\gamma\hbar B_0/kT}.$$

The population difference between the levels can be shown to be

$$n = \frac{\gamma\hbar B_0}{2kT} N,$$

where N is the total number of nuclei in the sample. This ratio is $\sim 10^{-6}$ for ^{1}H nuclei (in 1 Tesla at room temperature), which means that NMR is a very insensitive technique. Because transitions between levels occur with equal probability, only the net magnetisation from the population imbalance contributes towards the NMR signal. The total magnetisation is given by

$$M_0 = n\mu_z = \frac{1}{2}\gamma\hbar n.$$

It is possible to treat the total magnetisation **M** as one treats a single magnetic moment in further calculations.

4.1.3. Relaxation Mechanisms.

The radiation-induced transitions disturb the equilibrium population distributions between the states. A system which has absorbed energy can be thought of as having increased its *spin temperature (see Figure 4.3)*, and will then try to reach thermal equilibrium with its surroundings. This takes place through a mechanism known as *spin-lattice relaxation*.

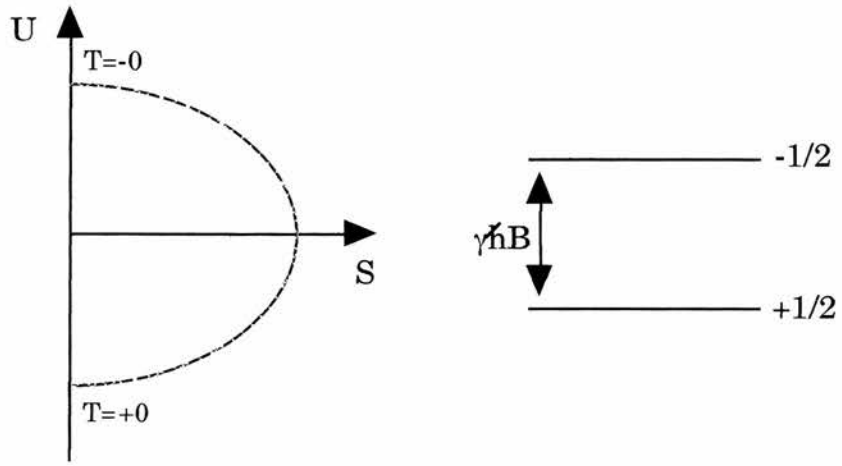

Figure 4.3. *The temperature of a spin system is given by dU/dS, where U is the energy, and S is the entropy. When the lower state is fully occupied, the entropy is low, and $T=0$. As the upper state becomes populated the temperature increases, through $T=\infty$ up to $T=-0$ when the upper state is fully occupied. For a more detailed look at spin temperature see Goldman*[9].

If the probabilities of upward and downward transitions in a two-level system are given by $w_\uparrow$ and $w_\downarrow$ then

$$\frac{dN_{-1/2}}{dt} = N_{+1/2}w_\uparrow - N_{-1/2}w_\downarrow \quad \text{and} \quad \frac{dN_{+1/2}}{dt} = N_{-1/2}w_\downarrow - N_{+1/2}w_\uparrow \ .$$

So,

$$\frac{dn}{dt} = 2N_{-1/2}w_\downarrow - 2N_{+1/2}w_\uparrow = N(w_\downarrow - w_\uparrow) - n(w_\downarrow + w_\uparrow) \ ,$$

or

$$\frac{dn}{dt} = \frac{n_0 - n}{T_1} \ ,$$

where

$$n_0 = N\frac{(w_\downarrow - w_\uparrow)}{(w_\downarrow + w_\uparrow)} \quad \text{and} \quad T_1 = \frac{1}{(w_\downarrow + w_\uparrow)} \ .$$

From this, it can be seen that the solution is

---

9 M. Goldman: *Spin Temperature and Nuclear Magnetic Resonance in Solids.*, Oxford (1970).

$$n = n_0\left(1 - e^{-t/T_1}\right) ,$$

so that the magnetisation approaches its equilibrium value exponentially with a time constant T_1, called the *spin-lattice relaxation time.*

Another mechanism determines the width of the resonance line. Nuclei interact with each other by the *dipolar interaction*, given by

$$\mathcal{H}_{dip} = \gamma_1\gamma_1\left\{\frac{\mathbf{I}_1\cdot\mathbf{I}_1}{r^3} - \frac{3(\mathbf{I}_1\cdot\mathbf{r})(\mathbf{I}_2\cdot\mathbf{r})}{r^5}\right\} ,$$

where r is the vector connecting the two spins. The local field around each moment is then slightly different from its neighbours, and there is a spread of Larmor frequencies, meaning there is a broadening of the line. This is known as *spin-spin relaxation*, and is denoted by T_2. In solution NMR, this does not have much effect, as the molecules are moving rapidly, and any broadening is averaged out, but it does significantly broaden lines in solid-state NMR. It should be noted that inhomogeneities in the magnetic field also produce a broadening of the line. The total broadening is represented by T^*, as opposed to T_2 for the dipolar broadening only.

4.1.4. Achieving Resonance.

So far, we have discussed transitions between levels, but have not mentioned how these transitions are achieved. A good method of visualising this is to use the classical perspective of a vector model of magnetic resonance.

Because a nuclear spin possesses angular momentum, a magnetic moment in a field has a torque, $\Gamma = \mu \times \mathbf{B}$, with the net effect that there is a precession around the axis of the magnetic field. For a two level system, the two states correspond to opposite orientations of the

magnetic moment vector *(see Figure 4.4)*, and a transition requires one vector to change orientation. For this to occur, a torque must be applied by a magnetic field $\mathbf{B}_1$ in a direction perpendicular to **B**. For this to be effective, $\mathbf{B}_1$ must be precessing at the same rate as the magnetic moment, or $\omega_0 = \gamma\mathbf{B}$, the Larmor frequency. This is the same conclusion arrived at previously.

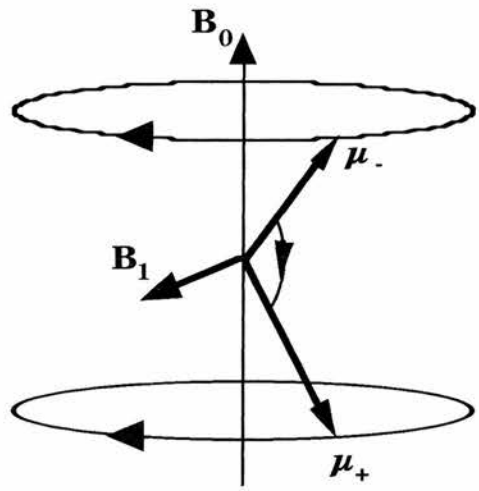

Figure 4.4. *The vector model of magnetic resonance. The magnetic moments precess around* $\mathbf{B_0}$ *at the Larmor frequency. To 'flip' from one state to the other, a field* $\mathbf{B_1}$ *is applied perpendicular to the axis of precession and at the Larmor frequency.*

Because the total magnetisation **M** can be thought of as an ensemble of magnetic moments, the same principles apply, and the torque is given by

$$\Gamma = \frac{d\mathbf{M}}{dt} = \gamma\mathbf{M} \times \mathbf{B}.$$

The components of this are given by

$$\frac{dM_x}{dt} = \omega M_y - \frac{M_x}{T_2}, \qquad \frac{dM_y}{dt} = -\omega M_x - \frac{M_y}{T_2}, \qquad \frac{dM_z}{dt} = -\frac{(M_z - M_0)}{T_1}$$

where we have introduced terms to account for the exponential relaxation. This approach was first formulated by Bloch[10], and the equations are known as the *Bloch equations*.

The sample can be placed in a coil in a magnetic field, and a pulse of $2B_1\cos\omega_1 t$ is applied. This can be expressed as $\left(B_1 e^{j\omega_1 t} + B_1 e^{-j\omega_1 t}\right)$ or two counter-rotating components. Only one is rotating in the same sense as the magnetisation and has any effect, and the other can be ignored. The remaining component can be described as

$$\mathbf{B}_1 = B_1\left(\mathbf{i}\cos\omega_1 t - \mathbf{j}\sin\omega_1 t\right).$$

The motion of the total magnetisation can then be described including the additional field as

$$\frac{d\mathbf{M}}{dt} = \gamma\left(\mathbf{M}\times\mathbf{B}_0\right) + \gamma\left(\mathbf{M}\times\mathbf{B}_1\right) - \frac{\left(\mathbf{i}M_x + \mathbf{j}M_y\right)}{T_2} - \frac{\mathbf{k}\left(M_z - M_0\right)}{T_1}.$$

It is easiest to view this in a frame of reference that is rotating at the same frequency as the rf field, ω_1, so that all the rotating components appear stationary. This frame will be represented by the coordinate system (x', y', z)† , and called the *rotating frame*.

In the rotating frame, the motion of the magnetisation is given by

$$\frac{d\mathbf{M}'}{dt} = \gamma\left(\mathbf{M}'\times\left(\mathbf{B}'_0 + \frac{\omega_1}{\gamma}\right)\right) + \gamma\left(\mathbf{M}'\times\mathbf{B}'_1\right) - \frac{\left(\mathbf{i}'M_{x'} + \mathbf{j}'M_{y'}\right)}{T_2} - \frac{\mathbf{k}'\left(M_z - M_0\right)}{T_1}$$

---

10 F. Bloch, *Phys. Rev.*, **70**, 460 (1946).

† Note that the z and z' axes coincide.

which, for $\omega_1 = \gamma B$ and large $\mathbf{B}_1$ reduces to the simple picture of the magnetisation precessing around the x'-axis with a frequency of $\gamma\mathbf{B}_1$. When the pulse ends, the magnetisation will relax back to its equilibrium position, inducing a signal in the coil, which is the resonance signal. The signal is dependant on the size of the magnetisation along $\mathbf{B}_1$, so the maximum signal is obtained when the magnetisation rotates 90°, or when $t=\pi/2\gamma\mathbf{B}_1$. The T_2 term has the effect of de-phasing the magnetisation in the x'-y' plane *(see Figure 4.6).*

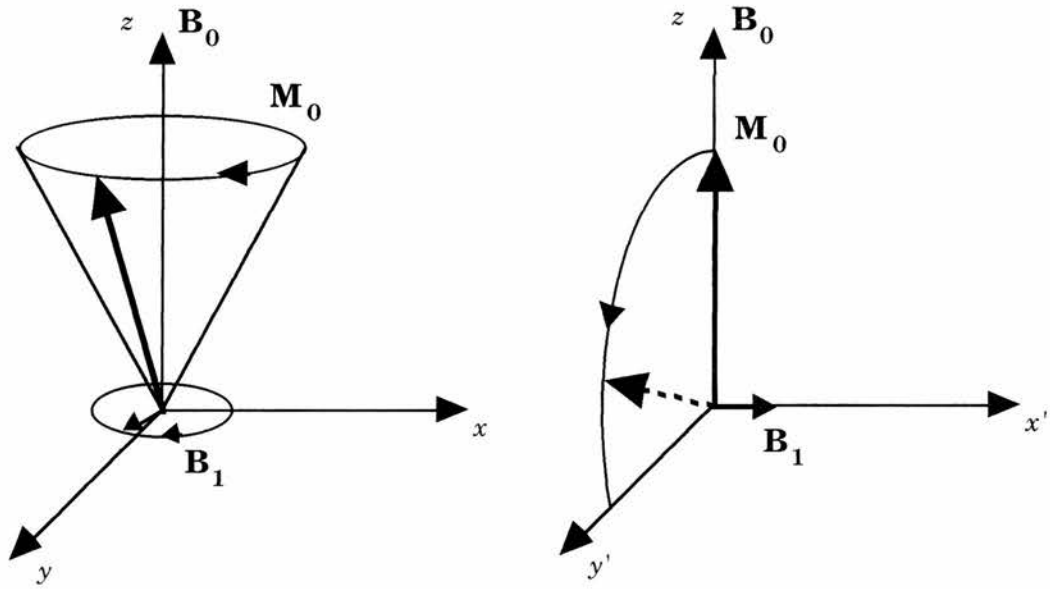

Figure 4.5. *In the laboratory frame (x, y, z), the magnetisation precesses at the Larmor frequency, and the rf field must rotate with it to induce a transition. In the rotating frame (x', y', z), the magnetisation is stationary, and the rf field can be applied along the x'-direction.*

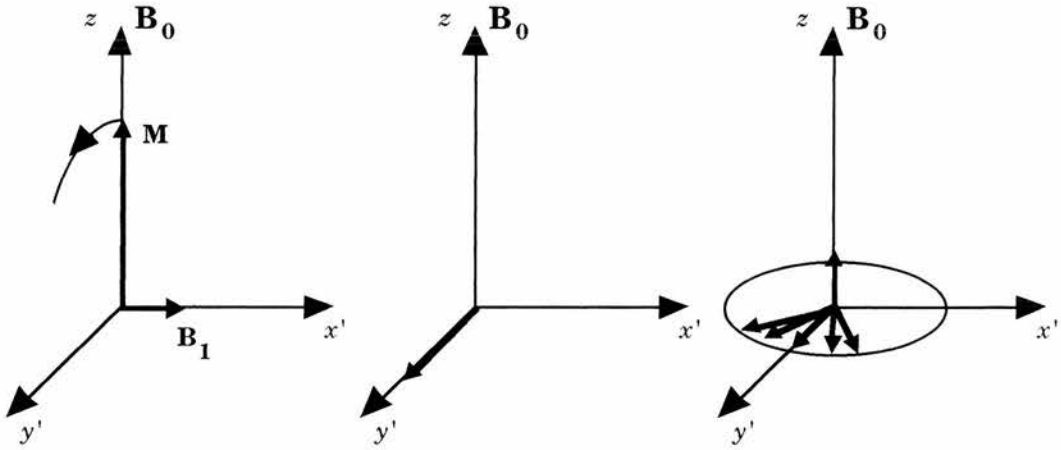

Figure 4.6. *The application of a pulse along x' rotates the magnetisation around the x'-axis. For a 90° pulse, this will leave M along the y'-axis. It will then grow exponentially along the z-axis to reach equilibrium. Simultaneously, the magnetisation in the x'-y' plane will 'de-phase', as the individual 'isochromats' precess at slightly different rates.*

4.1.5. Chemical Shift.

Although each type of nucleus precesses with a different Larmor frequency, this is of very limited use for analytical purposes. In 1949, the discovery that the resonance frequency was slightly different for nuclei in different chemical environments[11] meant that NMR could be a useful tool for structure elucidation. The slight shifts from the expected position are known as *chemical shifts*, and are due to the screening of nuclei from the applied field by electrons.

The resonance condition can be modified to include a term for the shielding effect,

$$\omega_0 = \gamma B_0(1-\sigma),$$

where σ is known as the shielding constant. Because the resonant frequency is dependant on $\mathbf{B}_0$, the chemical shift (or difference between

---

11 W. C. Dickinson, *Phys. Rev.*, **77**, 736 (1950); W. G. Proctor and F. C. Yu, *Phys. Rev.*, **77**, 717 (1950).

the actual and Larmor positions of the line) will vary with $\mathbf{B}_0$ if measured in Hertz. If the shift is measured in ppm (parts per million), which is the measurement in Hz divided by the frequency of spectrometer operation ν_0, then the shifts are independent of spectrometer characteristics - a much more useful comparison between spectra.

In reality, the shielding constant is actually a tensor, and is represented by σ_{ij}. The chemical shift Hamiltonian can then be written as

$$\mathcal{H}_{cs} = \gamma\hbar\mathbf{I}\cdot\sigma\cdot\mathbf{B}_0.$$

The frequency of resonance associated with the orientation of the tensor i given by

$$\omega_0 = -\gamma B_0\left(\sigma_{xx}\cos^2\alpha\sin^2\beta + \sigma_{yy}\sin^2\alpha\sin^2\beta + \sigma_{zz}\cos^2\beta\right),$$

where σ_{xx}, σ_{yy} and σ_{zz} are the principal-axis values of the chemical shift.

This can be integrated over all angles to give the absorption spectrum of a powder sample. For an axially symmetric chemical shift tensor $\left(\sigma_{xx} = \sigma_{yy} = \sigma_{\perp};\quad \sigma_{zz} = \sigma_{//}\right)$ the lineshape will look like Figure 4.7a, whereas for a non-axially symmetric tensor it will look like Figure 4.7b. It can be seen that the principal values of the tensor can easily be found from the lineshape.

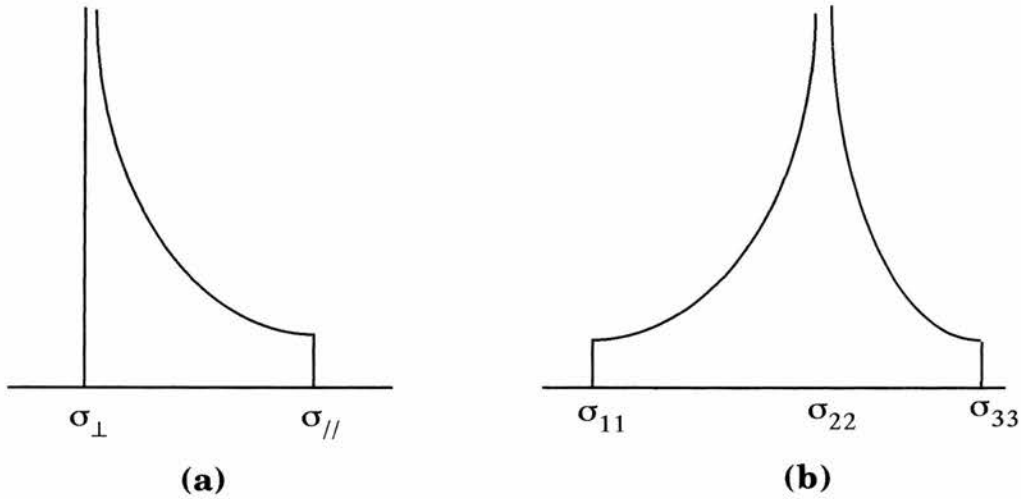

Figure 4.7. *Powder spectra for an axially symmetric (a) and non-axial symmetric (b) chemical shift tensor.*

4.1.6. The Knight Shift.

In a metal, the conduction electrons are free to move. Each nucleus will effectively 'see' the magnetic field of all the conduction electrons simultaneously. This mechanism is known as the *s-state hyperfine coupling*[12].

The interaction betwen the nucleus and electron is given by the *Fermi contact interaction*[13]

$$\mathcal{H}_{en} = \frac{8\pi}{3}\gamma_e\gamma_n\hbar^2\mathbf{I}\cdot\mathbf{S}\delta(\mathbf{r})$$

or

$$\mathcal{H}_{en} = \frac{8\pi}{3}g\beta\gamma_n\hbar\mathbf{I}\cdot\mathbf{S}\delta(\mathbf{r})$$

using our term for the gyromagnetic ratio for the electron. For a metallic system this is summed over all conduction electrons, l, to give

---

12 The s-state of the electron is the only one which is non-zero at the nucleus, and therefore the only one which can interact with it.

13 See ref. 5, Chapter 4.

$$\mathcal{H}_{en} = \frac{8\pi}{3} g\beta\gamma\hbar \sum_{j,l} \mathbf{I}_j \cdot \mathbf{S}_l \delta(\mathbf{r}_l - \mathbf{R}_j),$$

which can be shown to be analagous to an additional magnetic field ΔB such that

$$K = \frac{\Delta B}{B_0} = \frac{8\pi}{3} \left\langle |u_k(0)|^2 \right\rangle_{E_F} \chi_s ,$$

Here, $\left\langle |u_k(0)|^2 \right\rangle_{E_F}$ is the square of the s-wave function at the nucleus averaged over the electrons at the Fermi surface, and χ_s is the spin-susceptibility of the electrons. This shift in the resonance line due to the extra field is called the *Knight Shift*, after its discoverer, Walter Knight[14].

In 1950, Korringa showed that for a metallic system the fluctuations in the hyperfine field led to spin-lattice relaxation through the conduction electrons[15]. He found that K and T_1 were related by the *Korringa law*,

$$K^2 T_1 T = \frac{\hbar}{4\pi k} \left(\frac{g\beta}{\hbar\gamma} \right)^2 = \text{constant}.$$

Other mechanisms can contribute to the relaxation, so that often there are deviations from the Korringa behaviour.

---

14 W. D. Knight, *Phys. Rev.*, **76**, 1259 (1949).

15 J. Korringa, *Physica*, **16**, 601 (1950).

4.2. Experimental Techniques.

The spectrometers used in this study were a Bruker MSL500, and a home-built ^{1}H spectrometer, which will be described more fully in sections 4.2.8. to 4.2.10. Before this, the techniques used will be described along with the basic hardware of a NMR spectrometer.

4.2.1. Basic NMR Spectrometer.

The basic components of a pulsed NMR spectrometer are shown in a schematic diagram in Figure 4.8.

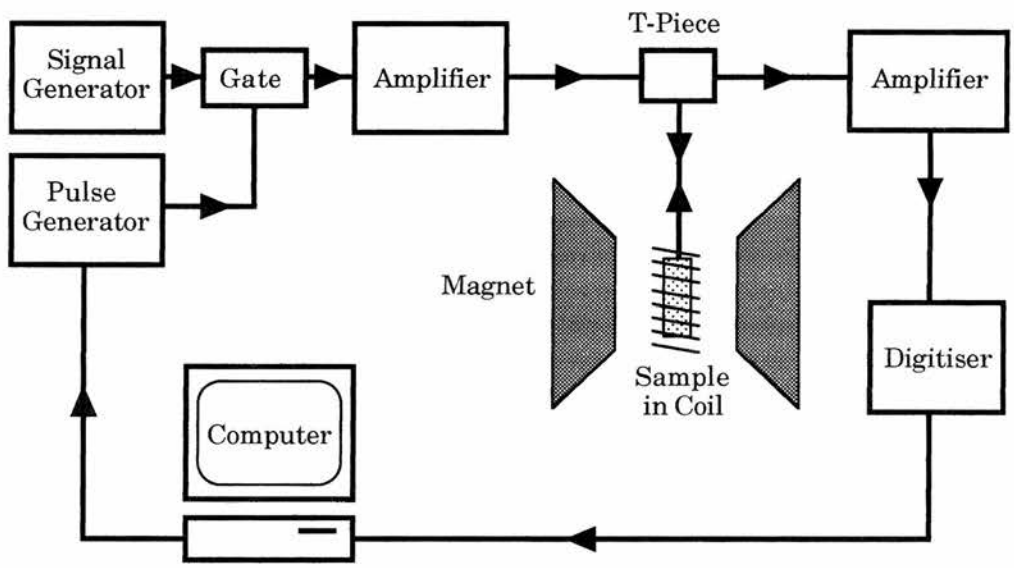

Figure 4.8. *Schematic diagram of a modern NMR spectrometer.*

A signal generator is used to provide a stable continuous frequency close to the appropriate Larmor frequency. Because pulses of this frequency are needed, a pulse generator is used to control a gate, only allowing the rf through during a pulse. This has the advantage of the rf always being a coherent source. Because the power required is typically over 100 Watts the signal must be amplified to a suitable level, so the amplifier must be sophisticated enough to cope with short pulses.

The rf pulse must then be directed to a sample. Because the same coil is used as a transmitter and receiver it is necessary to isolate the receiver section from the huge rf power. This is done through a "T-piece" which directs the incoming rf pulse to the sample, and the received signal to the receiver section of the spectrometer.

Typically, received signals from NMR are in the microvolt range. Therefore, the main function of the receiver section is to amplify this signal without introducing any noise. The signal must be dissociated from the "carrier" frequency at the Larmor frequency, which is done by subtraction from the signal generator frequency. The signal can then be digitised to allow easy manipulation by a computer.

The computer is an integral part of most modern spectrometers as it can be used to control most functions. Also, it is invaluable for performing Fourier Transformations of the signal for spectral analysis *(see Section 4.2.2)*.

Because it is easily possible to change the frequency of the signal generator, it is not really necessary to adjust the magnetic field, unless this feature is expressly desired. A persistent superconducting magnet can be powered to produce the correct magnetic field, and then disconnected. The current will then circulate indefinitely with no significant decay. Highly stable and homogeneous magnetic fields can be produced, with additional adjustable shim coils for increasing the field homogeneity.

4.2.2. Fourier Transforms.

The signal obtained from an NMR spectrometer is in the form of an electrical signal induced in the coil from the magnetisation in the y' direction, and will slowly decay because of transverse relaxation. If all the nuclei being observed are chemically equivalent there will only be one

signal present and the signal is easy to interpret, as resonance can be found easily *(see figure 4.9.)*.

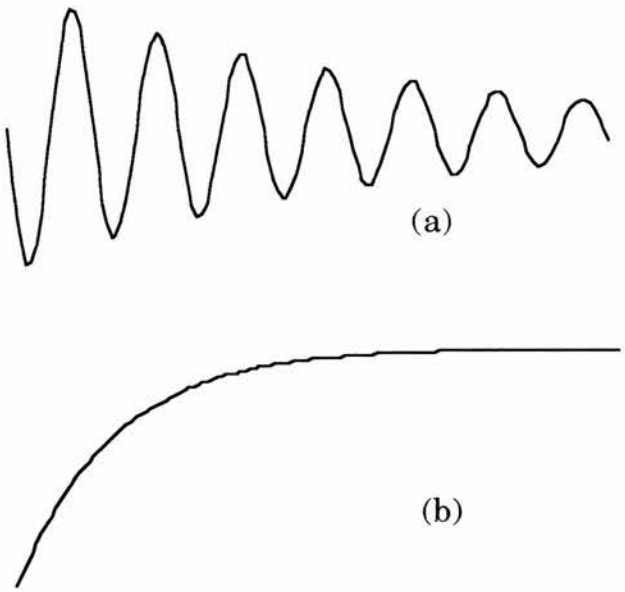

Figure 4.9. *Simulated FID for a single nucleus (a) slightly off resonance an (b) exactly on resonance.*

If there is more than one resonance present, then the FID will be a complex superposition of the decaying signals *(see Figure 4.10.)*.

Figure 4.10. *Simulated FID of three inequivalent nuclei, all off resonance.*

This transient decay can be interpreted by converting it from the time domain to the frequency domain. This is done through a mathematical

algorithm known as a Fourier Transform[16]. The approach is simple, but long-winded, and is an ideal operation to be performed by a computer.

The two domains are related by the formulae

$$F(\upsilon) = \int_{-\infty}^{\infty} f(t) \exp\{-i 2\pi \upsilon t\} \, \mathrm{d}\, t$$

$$f(t) = \int_{-\infty}^{\infty} F(\upsilon) \exp\{+i 2\pi \upsilon t\} \, \mathrm{d}\, \upsilon$$

Normally, two signals are detected - the real signal and the quadrature (which is 90° out of phase) although algorithms exist that will take a single real signal[17]. The resulting transformation will then have a real and imaginary part which is a mix of the absorption and dispersion signals. The phase of these can be adjusted to give pure absorptive and dispersive signals, or with less accuracy, a magnitude calculation can be performed.

4.2.3. High-Power Decoupling.

For studying a spin system such as an organic compound, it is useful to observe the carbon nuclear resonance. Because the most abundant isotope is ^{12}C, which has spin-0, only the ~1% of carbon nuclei which are ^{13}C (spin 1/2) can be seen. Although they are so dilute that homonuclear interactions can effectively be ignored there is a strong coupling to the abundant spin-1/2 ^{1}H nuclei. A ^{1}H bonded to a ^{13}C can have two possible spin states, and this produces two different Larmor frequencies, and lines will be split.

---

16 For the use of Fourier transforms in NMR see for example, I. J. Lowe, R. E. Norberg: *Phys Rev.*, **107**, 46 (1957); R. R. Ernst, W. A. Anderson: *Rev. Sci. Instrum.*, **37**, 93 (1966).

17 J. W. Cooper: *Introduction to Pascal for Scientists.*, Wiley (1981).

This effect can be removed by a technique known as broadband decoupling. If a second rf signal at the Larmor frequency of the ^1H nuclei is applied, with some spread so that all possible ^1H resonances are covered, then transitions can be induced between the ^1H states. This has the effect of time-averaging out the interactions, and the doublets collapse to a single line. Because a large decoupling field is required in solids, a high power is needed, giving rise to the term *High-Power Decoupling*.

4.2.4. Cross Polarisation.

An ingenious experimental technique by Hartmann and Hahn[18], known as cross-polarisation, allows enhanced sensitivity of a dilute spin such as ^{13}C through contact with an abundant spin such as ^1H.

The proton spins are prepared in state with a low spin temperature T_p. The carbon spins, at the lattice spin temperature T_l are put into contact with the large proton reservoir, and cool to a temperature near that of the protons (because the protons have a much larger heat capacity). This results in a large initial carbon polarisation, which is what is required for a large signal. Additionally, the protons must then be decoupled to provide higher resolution.

To cool the protons, a technique known as spin-locking is used. A 90° pulse is applied at the proton Larmor frequency to flip the magnetisation along the y'-axis. The rf power is then immediately applied along the y'-axis. In the rotating frame the magnetisation only sees the $\mathbf{B_1}$ field if the rf power is applied exactly on resonance. This effectively "locks" the magnetisation along the y'-axis, although it will decay back to its original state with a characteristic time $T_{1\rho}$. Because the temperature is determined by the Boltzmann statistics *(see section*

---

18 S. R. Hartmann, E. L. Hahn: *Phys. Rev.*, **128**, 2042 (1962).

4.1.2) the spin temperature is less than that of the lattice. The temperature is related to the populations of the two levels by the relation

$$\frac{N_{-\frac{1}{2}}}{N_{+\frac{1}{2}}} = \exp\left(-\frac{\hbar\gamma B_0}{kT_l}\right) = \exp\left(-\frac{\hbar\gamma B_1}{kT_s}\right),$$

from which it can be seen that the spin and lattice temperatures are related by

$$\frac{T_s}{T_l} = \frac{B_1}{B_0} \quad .$$

Because $B_1 << B_0$ then $T_s << T_l$.

To make thermal contact between the carbon and proton spins, they must be rotating with the same Larmor frequency, or

$$\gamma_c B_{1c} = \gamma_p B_{1p},$$

which is known as the *Hartmann-Hahn condition.* Because two different resonant frequencies are required, the probe must be capable of this. Either two separate coils will be required, or a specially tuned double-resonance coil.

Another feature of this technique is that a longer contact pulse can actually begin to destroy the signal instead of enhancing it[19]. The proton polarisation decays as the carbon polarisation grows. This is shown graphically in Figure 4.11.

---

19 E. O. Stejskal, J. D. Memory: *High Resolution NMR in the Solid State*, Oxford (1994).

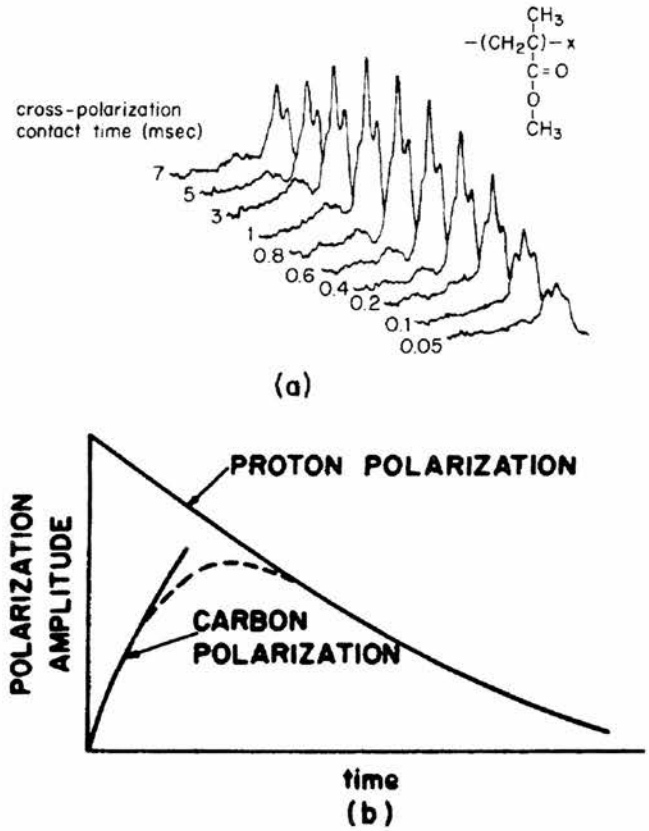

Figure 4.11. *The signal intensity depends on the contact pulse length. The signal can be seen to have an optimum value (a), which is because of the* $T_{1\rho}$ *processes causing the proton intensity to decay (b). From Shaefer et al.*[20].

4.2.5. Magic Angle Spinning.

It was shown in Section 4.1.3 that the direct dipolar coupling between spins contained a term $\left(3\cos^2\theta - 1\right)$ where θ is the angle between the magnetic field and the axis between the spins. In liquids this term is time-averaged out, and lines are narrow, but in solids the term becomes significant and broadens the lines considerably. If the angle θ is 54.74° then this term reduces to zero, and the interaction disappears. This is known as the *magic angle*.

In order to achieve this experimentally, a technique known as Magic Angle Spinning (MAS) is used[21]. The sample is placed in a rotor

---

20 J. Shaefer, E. O. Stejskal, R. Buchdahl: *Macromolecules*, **10**, 384 (1977).

21 E. R. Andrew: *Prog. NMR Spectroscopy*, **8**, 1 (1971).

which is suspended in a stator block at the magic angle. Bearing air is then passed through the stator to suspend the rotor, and simultaneously drive air is pumped in to spin it. Typically spin rates are in excess of 10kHz. A schematic diagram of this is shown in Figure 4.12.

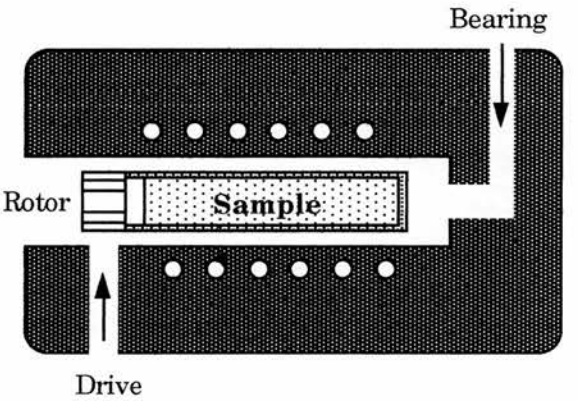

Figure 4.12. *Schematic Diagram of a MAS stator block.*

The purpose of this spinning is to average any spin-spin interactions along the magic angle. If two nuclei are spun around an axis sufficiently fast, then the vector connecting them can be considered to lie along this axis. The rate of rotation must be much greater than the linewidth in Hz to successfully eliminate the dipolar interaction[22].

By spinning the sample, extra lines are introduced in the spectrum. These spinning sidebands are spaced at the spinning frequency, and therefore are easily eliminated by adjusting the spinning speed to discover which lines move. The envelope of the sidebands actually corresponds to the chemical shift anisotropy of the sample, and this knowledge can be used to elicit the anisotropy of each individual line[23].

---

22 I. J. Lowe: *Phys. Rev. Lett.*, **2**, 285 (1959).

23 M. M. Maricq, J. S. Waugh: *J. Chem. Phys.*, **70**, 3300 (1979); J. Herzfeld, A. E. Berger: *J. Chem. Phys.*, **73**, 6021 (1980).

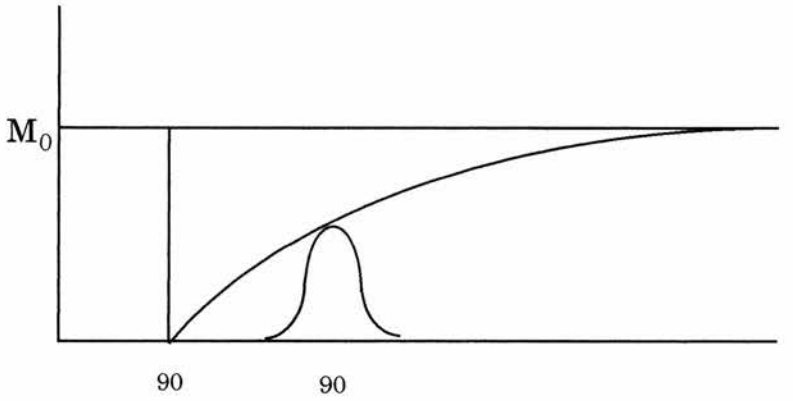

Figure 4.13. *Evolution of the magnetisation along the z-axis after a 90° pulse. If another pulse is applied before the magnetisation has recovered, the signal will be smaller.*

4.2.6. Non-Quaternary Suppression.

Although CP/MAS allows clearer spectra by removing spin-spin coupling, it can also be a hindrance, as it makes assigning specific carbon resonances more difficult. A slight adaptation of the pulse sequence solves this problem. If the decoupling is switched off briefly, then protonated carbons rapidly decay, whereas quaternary carbons do not decay as quickly. Signals from the non-quaternary carbons will disappear, which is why the technique is known as Non-Quaternary Suppression[24]. There are exceptions to this though. Methyl carbons will still produce signals, as the rapid internal rotation causes a slower decay of the signal, and therefore peaks will remain in the spectra.

4.2.7. T_1 Pulse Sequences.

If a spin system is subjected to a 90° pulse, then the magnetisation is flipped into the x-y plane. It will then gradually decay back to its original position along the z-axis with a characteristic time T_1. If another 90° pulse is applied before the magnetisation reaches its

---

24 R. K. Harris: *Nuclear Magnetic Resonance Spectroscopy*, Longman (1986).

maximum, then the height of the resultant peak will be proportional to the magnetisation along the z-axis at that time.

By varying the delay between the two 90° pulses, the evolution of the magnetisation with time can be found, as the peak height follows the relationship

$$\frac{M(t)}{M_o} = 1 - \exp\left(-\frac{t}{T_1}\right) .$$

This is known as a *saturation recovery* experiment for determining T_1.

A similar pulse sequence is known as the *inversion recovery* experiment. The first pulse is instead a 180° pulse, which inverts the magnetisation. The recovery follows the relation

$$\frac{M(t)}{M_o} = 1 - 2\exp\left(-\frac{t}{T_1}\right) .$$

Both of these techniques have their advantages and disadvantages. The inversion recovery experiment is ideal for narrow lines, as it is easy to determine the length of the 180° pulse, as the FID will reduce to zero. However, it is necessary to wait until the magnetisation has fully recovered to its original state before repeating (usually about $3T_1$).

The saturation recovery experiment is more convenient for broader lines. Because it is difficult to accurately set a 90° pulse for broad lines a saturating comb can be used. A series of pulses, of approximately 90° will destroy the magnetisation in the z-direction. Also, the comb can begin immediately after the observation pulse, making the technique much more efficient.

For a more detailed account of these pulse sequences see for example Fukushima and Roeder[25].

4.2.8. Bruker MSL500 Spectrometer.

The Bruker MSL500 is a commercial NMR spectrometer. It is based around an Oxford Instruments superconducting cryomagnet (11.74T) with an 89mm bore. Interchangeable probes can be inserted, although all experiments for this study used a Bruker MAS probe. An Aspect 3000 computer contols three independent channels allowing simultaneous data manipulation and acquisition, using Bruker's proprietary DISMSL software. Frequencies from 17MHz to 215MHz are attainable, and also 500MHz for proton frequencies from a separate transmitter.

A number of shim coils can be used for high-resolution work to adjust the field homogeneity. The setting for these are stored in a parameter file (SHIMMAS.ANDR) and could be recalled before each session, so that shimming was not necessary.

Two samples were used for this study. The first was a rotor full of powdered $NMe_4[Ni(dmit)_2]_2$. This was used for preliminary tests, and for a series of cross-polarisation spectra. During one run, this rotor broke in half, destroying the sample, so another batch had to be made. This did not contain enough $NMe_4[Ni(dmit)_2]_2$ to fill the rotor completely, so the ends of the rotor were packed with a small amount of powdered KBr. Because the ends of the rotor are not within the coil, this was expected to have little difference on the signal. Also, KBr is a useful comparison for ^{13}C spectra, as the resonance of ^{79}Br is near to that of ^{13}C, so it can be

---

25 E. Fukushima, S. B. W. Roeder: *Experimental Pulse NMR. A Nuts and Bolts Approach.*, Addison-Wesley (1981).

used to check the magic-angle, and other spectrometer operations without the need to re-tune the spectrometer.

A number of acquisition parameters can be adjusted; the resonance frequency for ^{13}C is 125.758MHz (SF) which can be offset in Hertz using O1. The number of points acquired is set by TD, with the number of points in the Fourier transorm set by SI. This must always be greater or equal to TD, with the difference being filled with zeroes to increase resolution[26]. The separation of points is set by DW (in μs) which corresponds to a spectral width of SW (= 1/(2xDW)). The number of averages can be set by NS, or for indefinite averaging NS can be set to -1.

Before each session using the spectrometer a reference sample must be run. Adamantane was used as its distinctive double peak is easily seen with a single acquisition. The peaks occur at 38.56 and 29.51 ppm relative to TMS, the generally accepted standard. This allows the spectral reference (SR) to be set so that the system is calibrated.

For a simple High-Power Decoupling pulse sequence the program HPDEC.PC was used *(see Appendix B1)*. The parameters for this are summarised in table 4.1.

Parameter	Description	Typical Value
D0	Repetition rate	2.0 s
D1	1st pulse width	4 μs
D3	Dead time	30 μs
D7	Acq./Decoupling time	30 ms

Table 4.1. *Parameters for HPDEC.PC High-Power Decoupling sequence.*

26 Zero filling interpolates points between those calculated for a normal FFT. It does not enhance resolution, but can *smooth* noisy spectra.

For the slightly more complicated Cross-Polarisation sequence the program CPCYCL.PC was used *(see Appendix B2)*. The parameters for this are summarised in Table 4.2.

Parameter	Description	Typical Value
D0	Repetition rate	2.0 s
D1	1st pulse width	4 μs
D3	Dead time	30 μs
D5	Contact pulse	10 ms
D7	Acq./Decoupling time	30 ms

Table 4.2. *Parameters for CPCYCL.PC High-Power Decoupling sequence.*

The Non-Quaternary Suppression program NQS.PC is actually an adaptation of the CPCYCL.PC program, with the decoupling window simply being an extension of the dead-time *(see Appendix B3)*. Parameter D3 is increased in the range 50 - 80 ms with the rest of the parameters staying the same.

For T_1 measurements no suitable programs were available so an existing sequence had to be adapted. Because cross-polarisation does not work as well in the $NMe_4[Ni(dmit)_2]_2$ system[27] the T_1 program was based on the HPDEC.PC program. As the lines are narrow, an inversion-recovery sequence was used. This involved adding a variable delay and a second pulse *(see Appendix B4)*. The parameters are summarised in table 4.3.

---

27 Because the carbon sites of interest on the $Ni(dmit)_2$ molecule are far away from protons, only the NMe_4^+ carbons would be enhanced.

Parameter	Description	Typical Value
D0	Repetition rate	2.0 s
D1	1st pulse width	8 μs
VD	Variable delay	< 2 s
D2	2nd pulse width	4 μs
D3	Dead time	30 μs
D7	Acq./Decoupling time	30 ms

Table 4.3. *Parameters for GJSHPDT1.PC inversion recovery sequence based on the High-Power Decoupling program HPDEC.PC.*

For proton measurements, the second transmitter was used (500.180 MHz) using the simple pulse sequence ONEF2.PC *(see Appendix B5)*. This is just a single 90° pulse followed by a dead-time delay, then acquisition. As proton signals are much stronger, 16 averages were sufficient to obtain a good signal. The reference used was acetone, which has a sharp peak at 2.2ppm relative to TMS.

Low temperature operation down to approximately 200K is possible with the Bruker MAS probe. The air supply is replaced with an oxygen-free Nitrogen gas supply which is then passed through a dewar of liquid nitrogen to cool the gas. This is shown schematically in Figure 4.14.

The nitrogen cylinders used last for about 3 hours each. Two are connected with one in reserve. When the level gets too low the reserve can be used while the others are changed allowing continuous operation. The nitrogen dewar can be continuously topped up as the liquid doesn't pass through to the probe as with other cooling systems. For ambient temperature measurements the air-flow can be switched to bypass the liquid nitrogen.

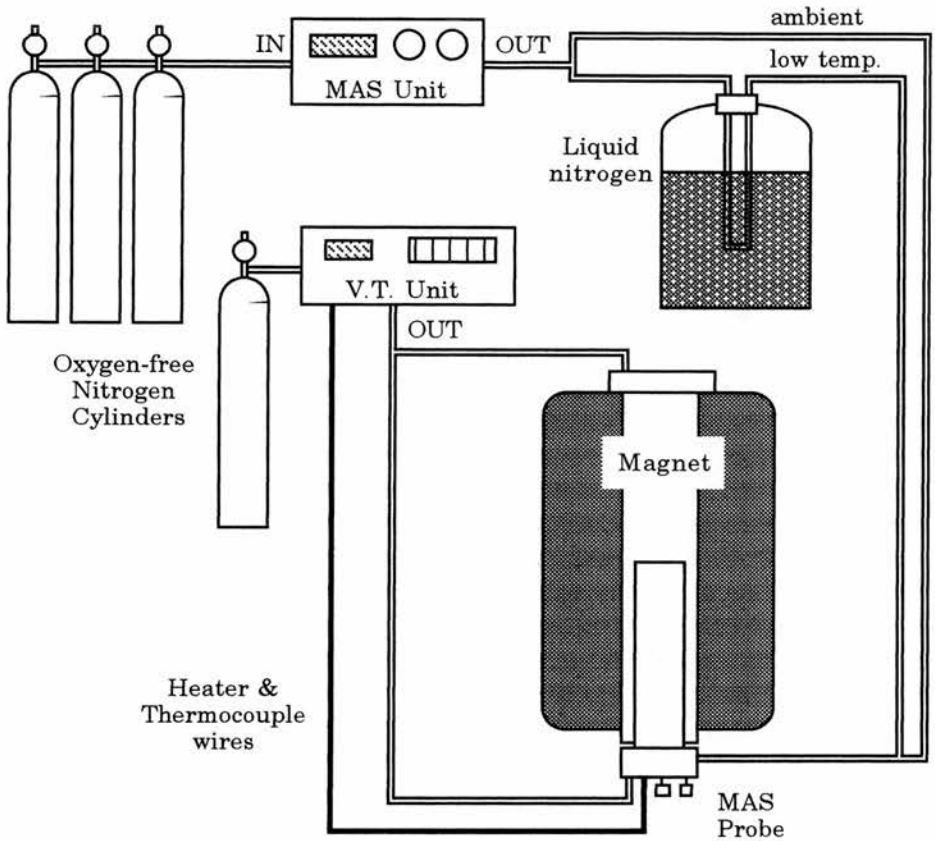

Figure 4.14. *Schematic diagram of the air-flow for low temperature MAS operation.*

Another oxygen-free nitrogen cylinder is connected to provide flushing gas to the electronics of the MAS probe and the magnet bore. This stops icing at lower temperatures and provides stability in the tuning and other settings. Temperature control is provided by a thermocouple and heater controlled from the Variable Temperature unit of the MSL500.

4.2.9. Custom ^{1}H Spectrometer.

The electronics for the custom ^{1}H NMR spectrometer were based on previous experiments[28]. The receiver system was optimised for about 100MHz which correspond to a magnetic field of about 2.5T. The magnet

---

28 B. Ctortecka, *MSc. Thesis, University of St. Andrews* (1994).

used was a custom 12T fast-sweep superconducting magnet (Oxford Instruments). The magnetic field was monitored with a non-inductively wound magprobe fed with a current of 51.04mA.

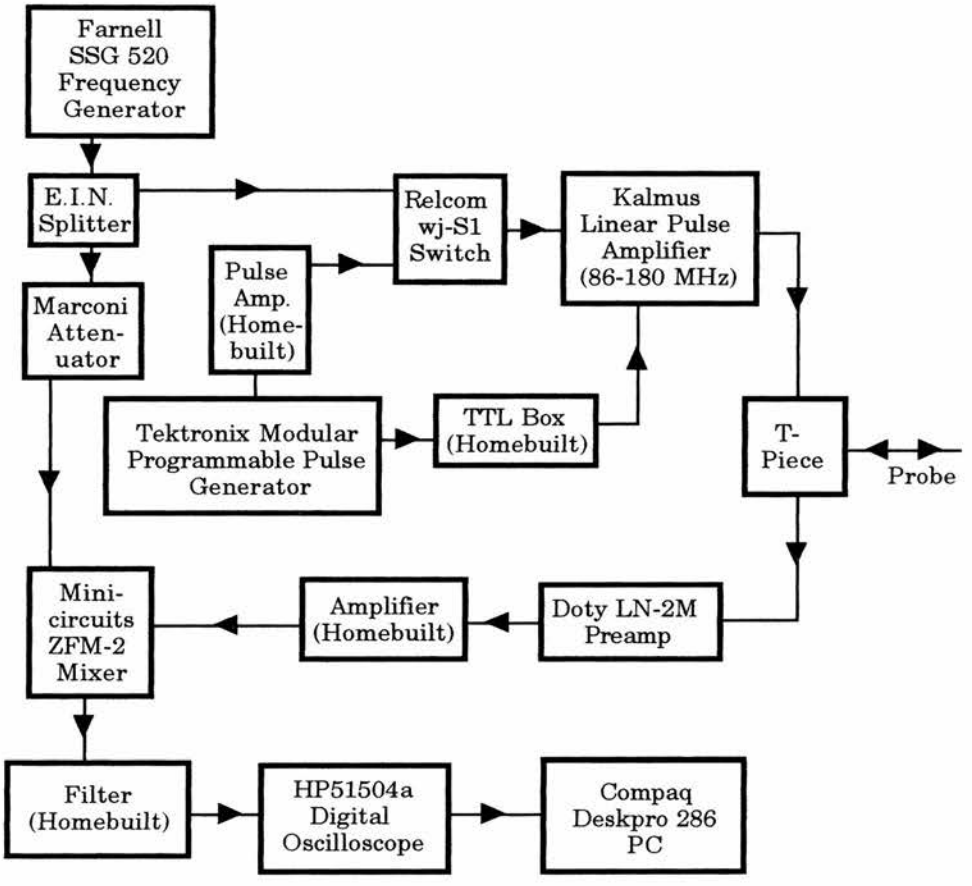

Figure 4.15. *Electronics of the custom ^1H NMR spectrometer.*

The experimental arrangement of the electronics of the system is shown in figure 4.15. Essentially this is identical to the schematic spectrometer in section 4.2.1. with some additional equipment. The Splitter divides the signal from the Frequency Generator to feed it as a reference signal to the receiver section where it is subtracted from the received signal by the mixer. The amplifiers and the attenuator are purely to bring signals to within limits determined by the equipment used. The TTL Box uses Transitor-Transistor Logic to convert the output from the pulse generator into a form which will control the gate of the

Linear Pulse Amplifier. The Pulse Generator consists of five modules which can be interconnected to produce a number of different pulse sequences.

The signal is then digitised by the oscilloscope. This is connected to the PC by a GPIB interface. A program was written to download spectra from the oscilloscope and store them in ASCII format (SCOPE.EXE - see Appendix A2). A separate program was written to analyse the spectra, allowing pulse dead-time to be removed and Fourier transforms to be performed (FT3.EXE - see Appendix A3).

4.2.10. Custom Spectrometer Probe Design.

The probe was designed for operation at 4.2K. A simplified diagram of the end of the probe can be seen in Figure 4.16. Helium could be filled through the central tube. The coil was wound to fit the sample (the second sample as used in the MSL500). A match capacitor (24pF) was connected in parallel with the coil, and a variable tuning capacitor (10pF) was connected in series. This could be adjusted by a rod fed through to the top of the probe.

To measure the temperature, two thermocouples were fed to the end of the probe, a Gold-Chromel (1K-300K), and a Copper-Constantan (77K-300K). These were shielded from the rf within a metal tube. Although the system is not a complete variable-temperature system, heater wires were installed to allow the helium to be boiled off, and provide limited temperature control to ~50K. These are not shown on the diagram, but were fed through the main can (shielded with aluminised tape) and then wound around the outside of the lower half of the can. Also not shown is the helium dipstick which was mounted at the end of the probe near the variable capacitor. This was a length of superconducting wire attached to a strip of veroboard. As the helium level increased more of the wire became superconducting, and the

resistance of the circuit changed. This could be monitored with a homebuilt meter. As the bottom of the dipstick was well above the sample, as long as the meter was reading that there was helium present then the sample was immersed.

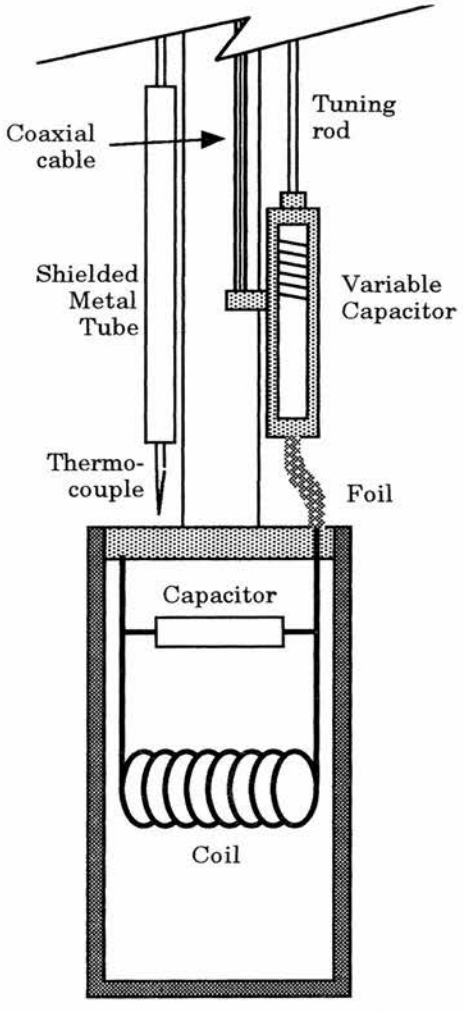

Figure 4.16. *Probe head of the spectrometer. The helium dipstick and heater wires are not shown for clarity.*

4.3. Results.

4.3.1. 1-H NMR.

Room temperature proton measurements were carried out using the Bruker MSL500 as described in Section 4.2.8 The reference was acetone which has a single peak at 2.2ppm relative to TMS (Tetramethylsilane). Two peaks can be seen for $NMe_4[Ni(dmit)_2]_2$ at 3.6ppm and 1.4ppm of almost equal intensity, with sidebands from the ~5800Hz spinning speed. Lowering the temperature produced slight shifts in the peak positions, and a more marked effect in the peak heights, with a decrease beginning at about 260K. Spectra from room temperature to 220K can be seen in Figure 4.17. and plots of the peak positions and heights can be seen in Figures 4.18. and 4.19. respectively.

Low temperature measurements using the home-built spectrometer as described in section 4.2.9. show much broader lines. When Fourier-transformed, some spectra show peaks near 1MHz, but these correspond to those when the heater was switched on. Because the main peaks appear below this frequency then the spectra have been cropped below this frequency. A series of spectra are shown in Figure 4.20.

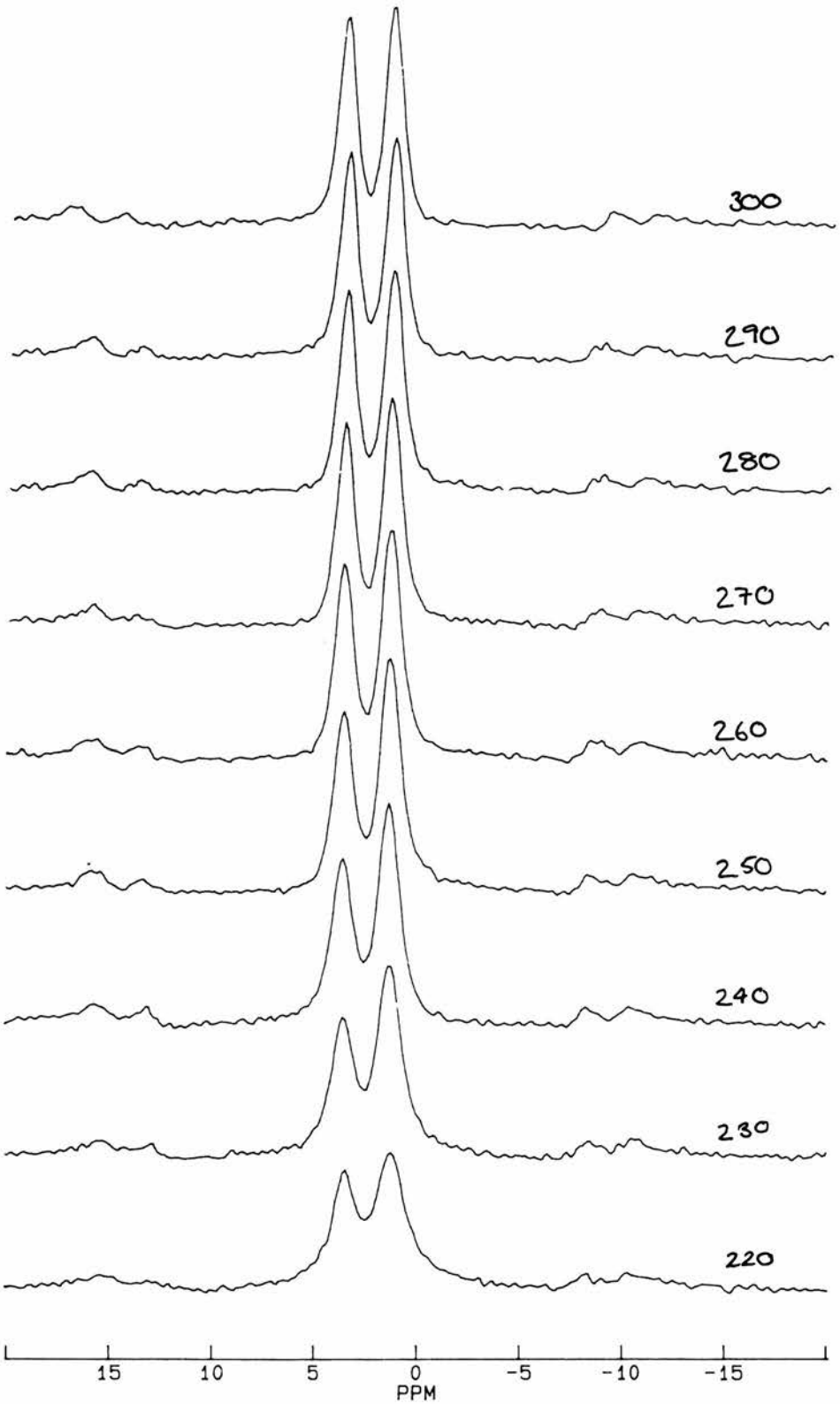

Figure 4.17. *Proton spectra from 220K to room temperature using the Bruker MSL500.*

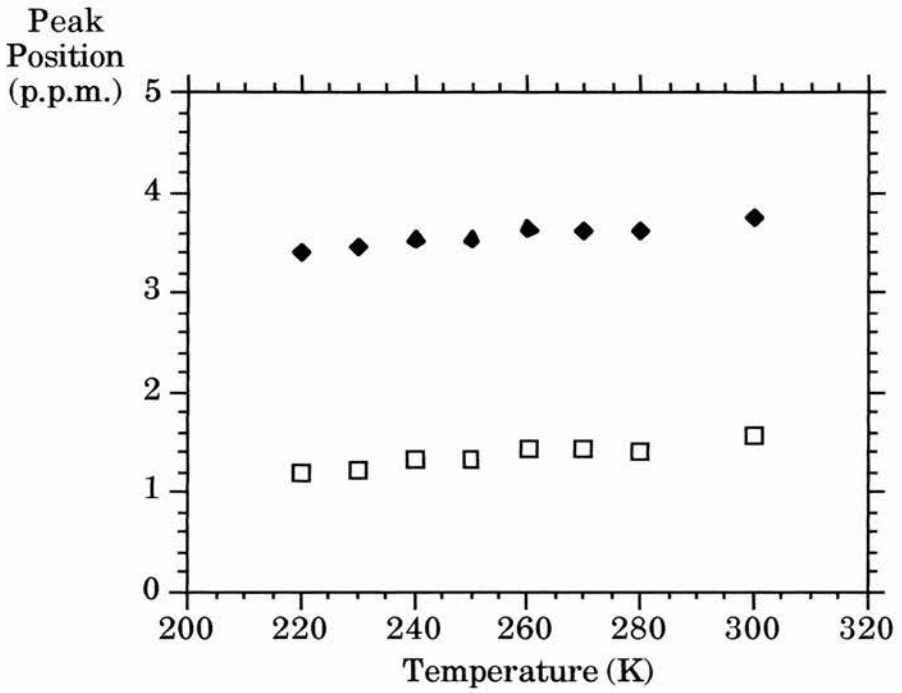

Figure 4.18. *Variation of proton NMR peak position with temperature (relative to TMS).*

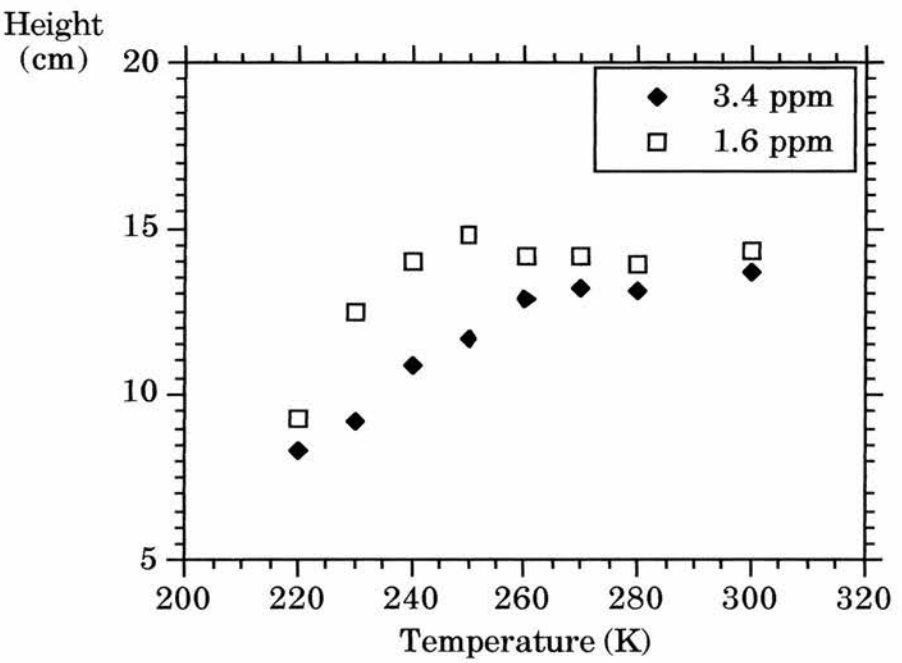

Figure 4.19. *Variation of proton NMR peak height with temperature.*

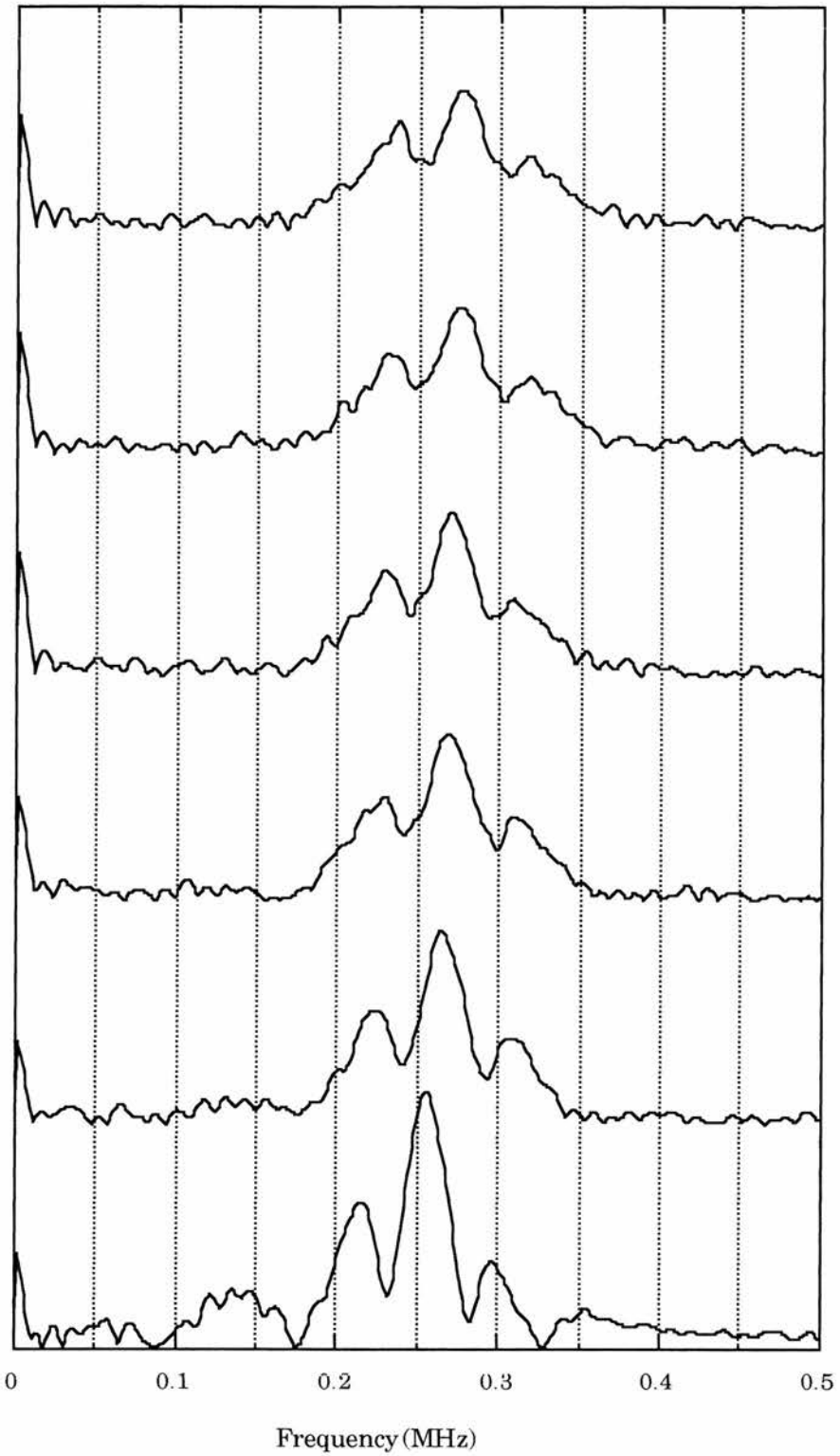

Figure 4.20. *Low temperature proton NMR spectra. It can be seen that there is a slight shift in the position of the central peak.*

It can be seen that the spectra broaden as the temperature is increased. There is a slight shift in the position of the central peak, which can be seen more clearly in Figure 4.21.

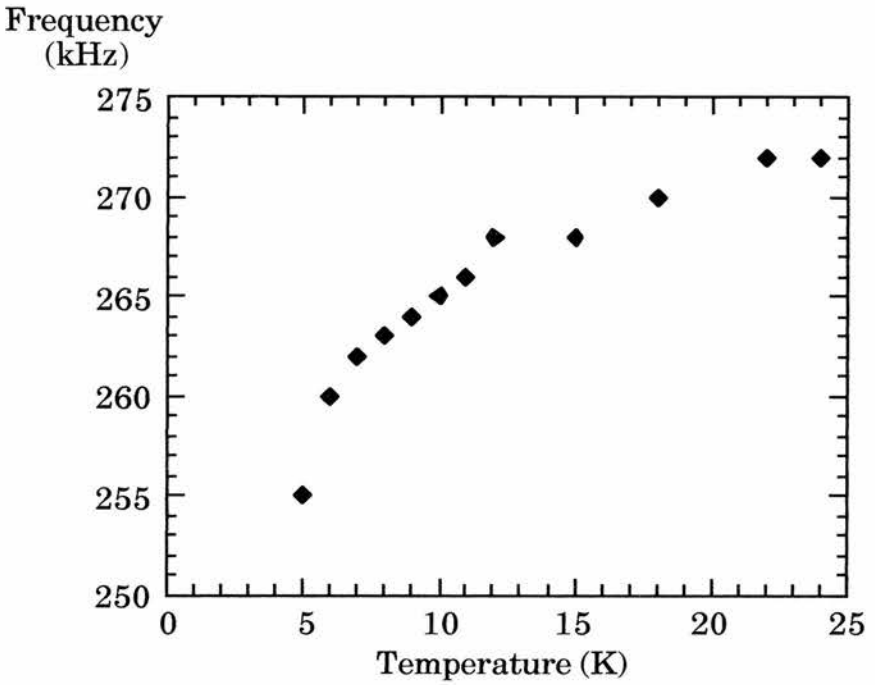

Figure 4.21. *Shift of the central peak in the low temperature proton NMR, measured relative to the excitation frequency*

Measurements of T_1 were taken using a saturating comb pulse sequence *(see Section 4.2.7)*. These are plotted on an exponential scale, as this should facilitate identification of multiple relaxations *(see Figure 4.22 (a to f)*. However, due to the large errors involved, it is impossible to see if there are one or two parts to the relaxation.

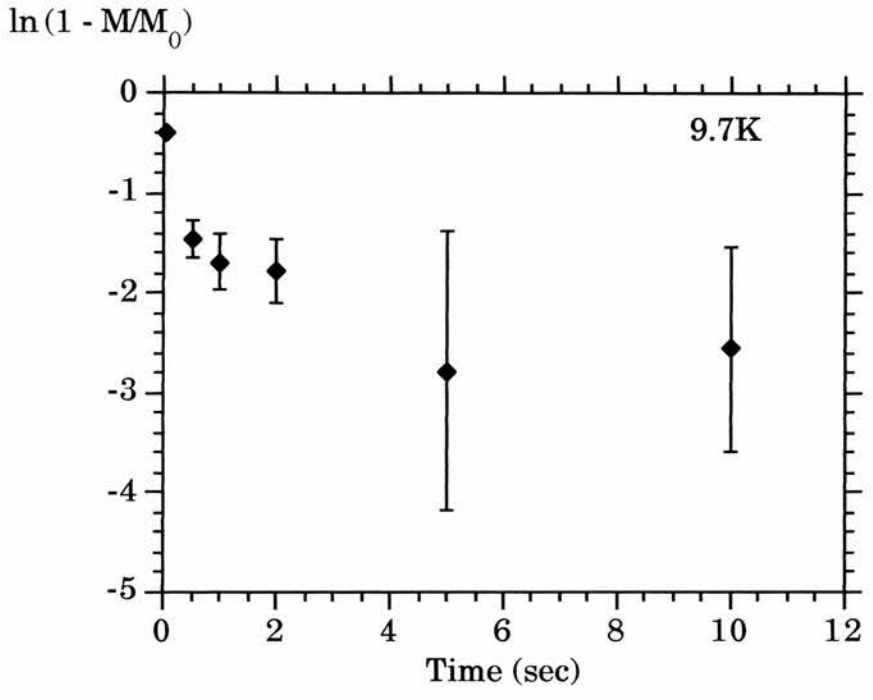

(a)

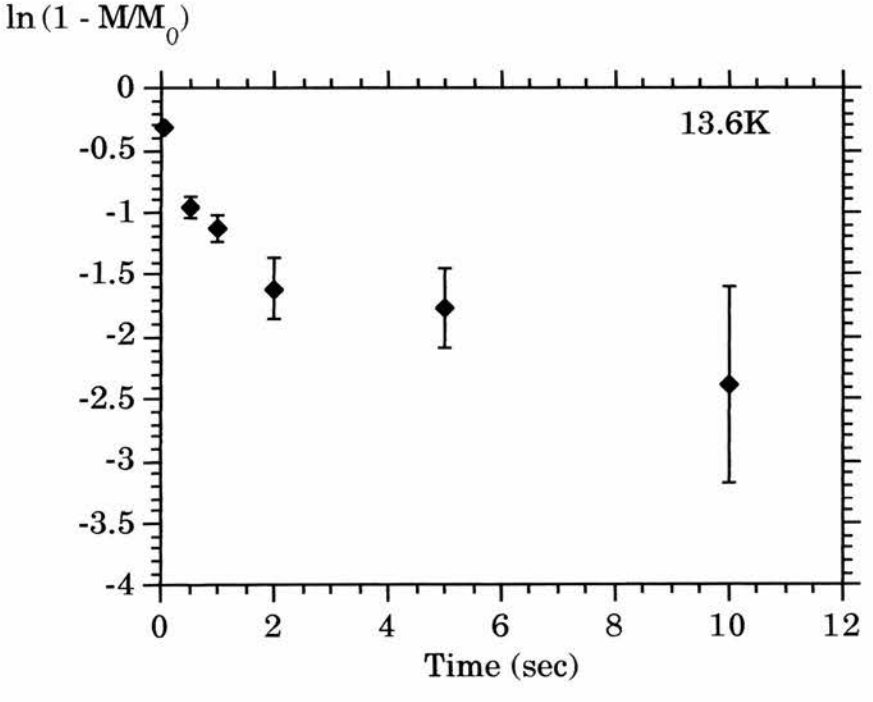

(b)

Figure 4.22. *Proton NMR T_1 measurements.*

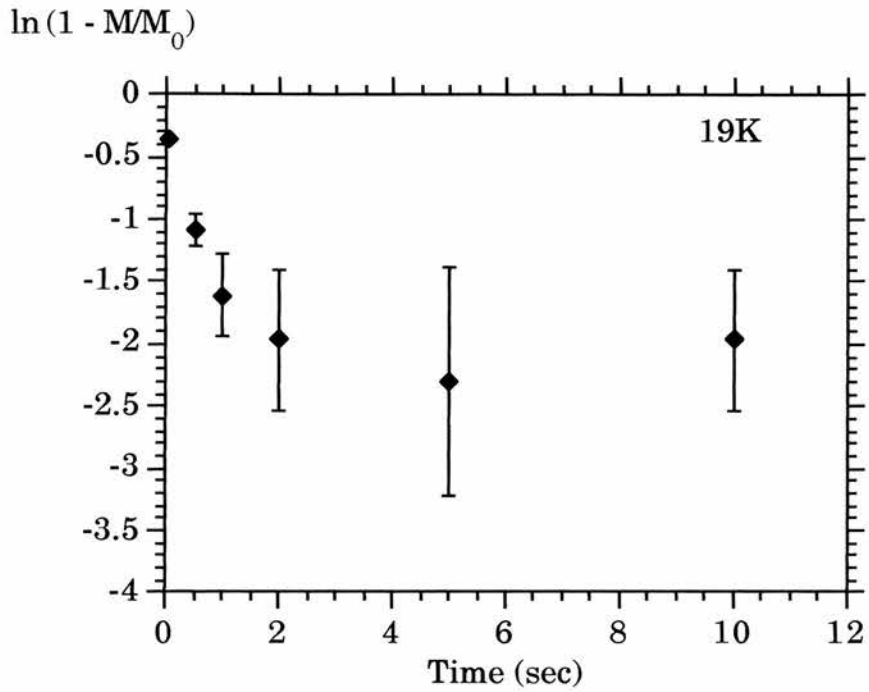

(c)

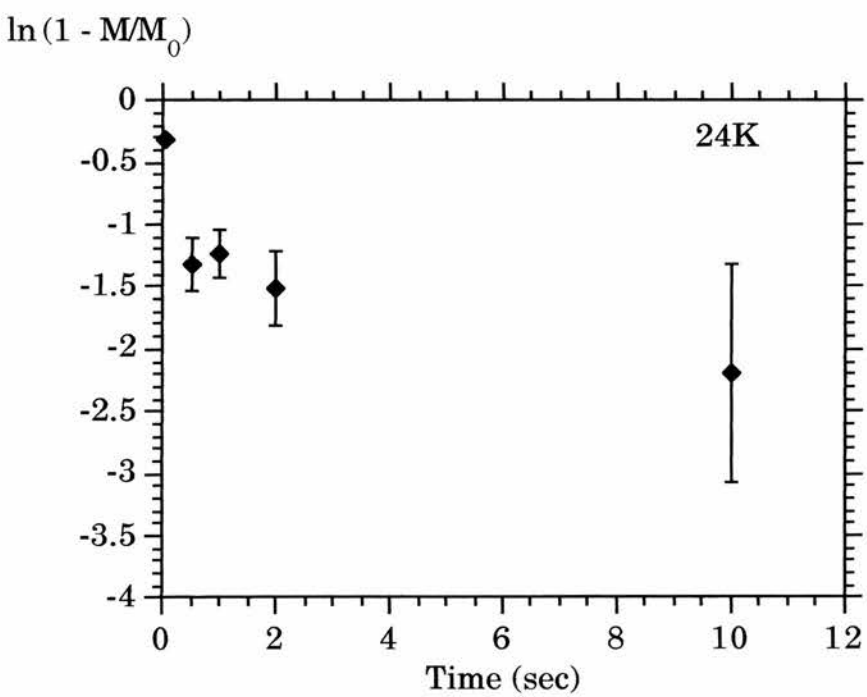

(d)

Figure 4.22. (cont.) *Proton NMR T_1 measurements.*

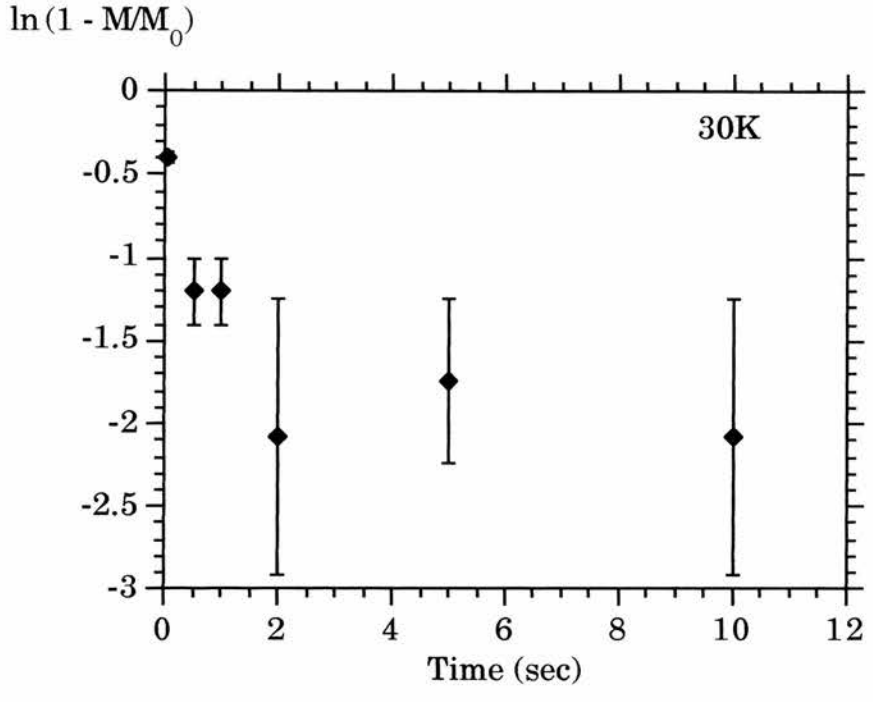

(e)

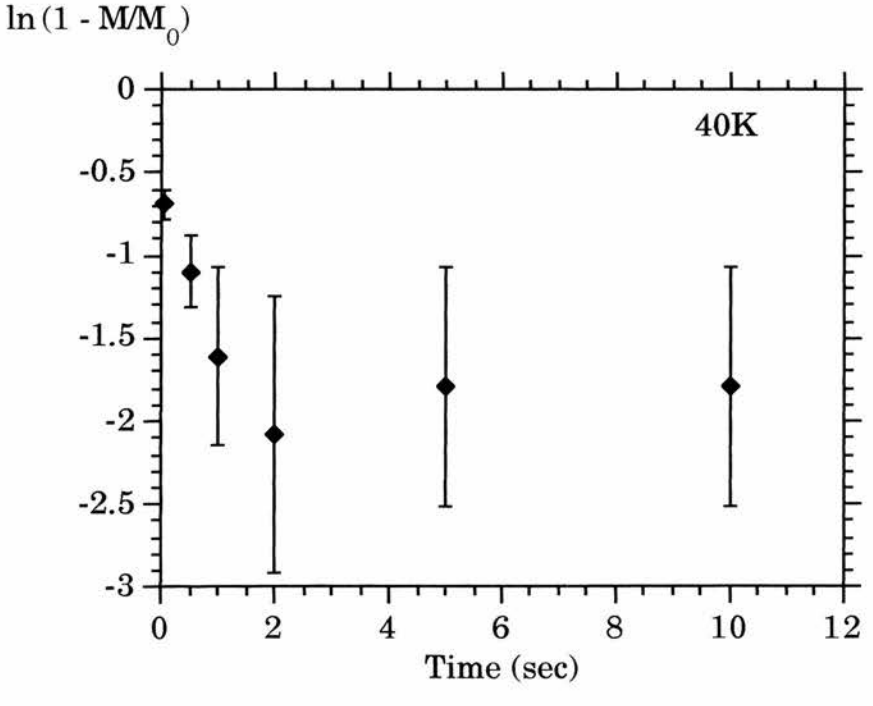

(f)

Figure 4.22. (cont.) *Proton NMR T_1 measurements.*

4.3.2. 13-C NMR.

All ^{13}C NMR was performed using a Bruker MSL500 spectrometer as described in section 4.2.8. All measurements are relative to TMS (tetramethylsilane), using a reference sample of adamantane which displays two strong peaks at 38.56 and 29.51 ppm.

Simple high-power decoupling experiments on the first sample show a number of lines at 299, 257, 177, 130, and 63ppm. Another sharp line at 193ppm was observed with HPDEC.PC, but could not be seen with CPCYCL.PC. This effect could not be investigated further, as the sample was destroyed when the rotor broke, and the 193ppm line did not appear in any spectra with the second sample. In the second sample another group of peaks centred around 30ppm appear, but these were considered to be due to impurities, as they did not appear in the first sample. Otherwise, both samples produced identical spectra. Some representative spectra are shown in Figure 4.23.

To ensure consistency between experiments on different days, the power settings on the MSL were kept constant. By sweeping through the length of the 90° pulse, the optimum pulse width could be found, and this would then remain constant. This is shown in Figure 4.24.

A baseline distortion can be seen at around 125ppm. A stack-plot *(see Figure 4.24.)* of this series of spectra taken with increasing pulse width shows that this does not cycle as the real peaks, and it is probably an artefact of the coil ringing down after a pulse has been applied. All HPDEC.PC sequences produced a "spike" at the start of acquisition (which was not related to the dead-time of the receiver) which could be artificially removed from the FID to be transformed by 'left-shifting". This reduced the size of the baseline "hump" considerably. All spectra were left-shifted an equal amount to allow comparisons between them.

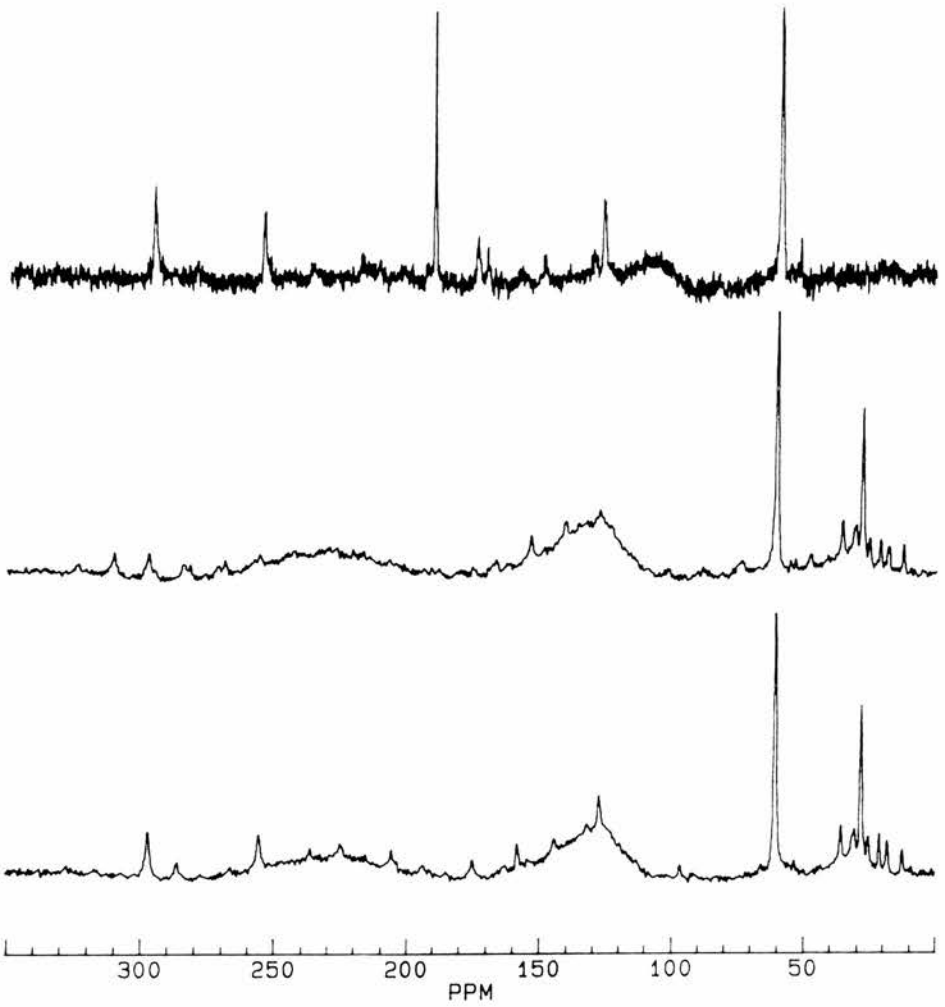

Figure 4.23. *^{13}C spectra at room temperature. The group of peaks at ~30ppm do not appear on the first sample (a), although a peak appears at 193ppm The second sample is shown at two different spinning speeds (b and c) so that real peaks can be identified.*

Cross-polarisation is a good technique for assignment of the peaks *(see Section 4.2.4.)*. By using a variable contact pulse time, those sites which are nearer protons will appear first. This is shown in figure 4.26. for the first sample (in which the 30ppm lines are not present). It can be seen that the 63 ppm line appears first, followed by the 299 and 257 ppm lines, and finally the 130 and 177 ppm lines. Assignment of these peaks will be discussed further in Chapter 7.

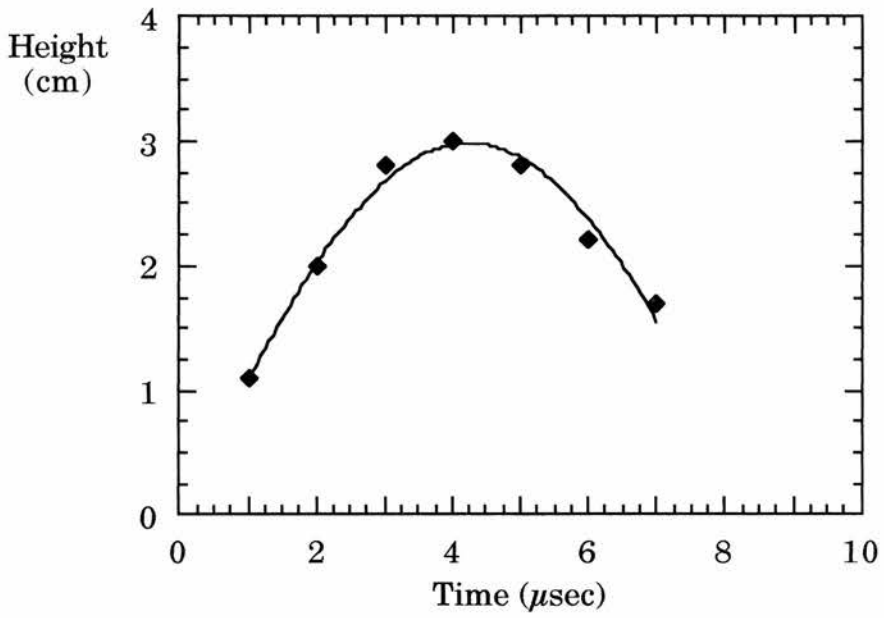

Figure 4.24. *Plot of peak height against pulse width. The optimum value for a 90° pulse is 4.25μs.*

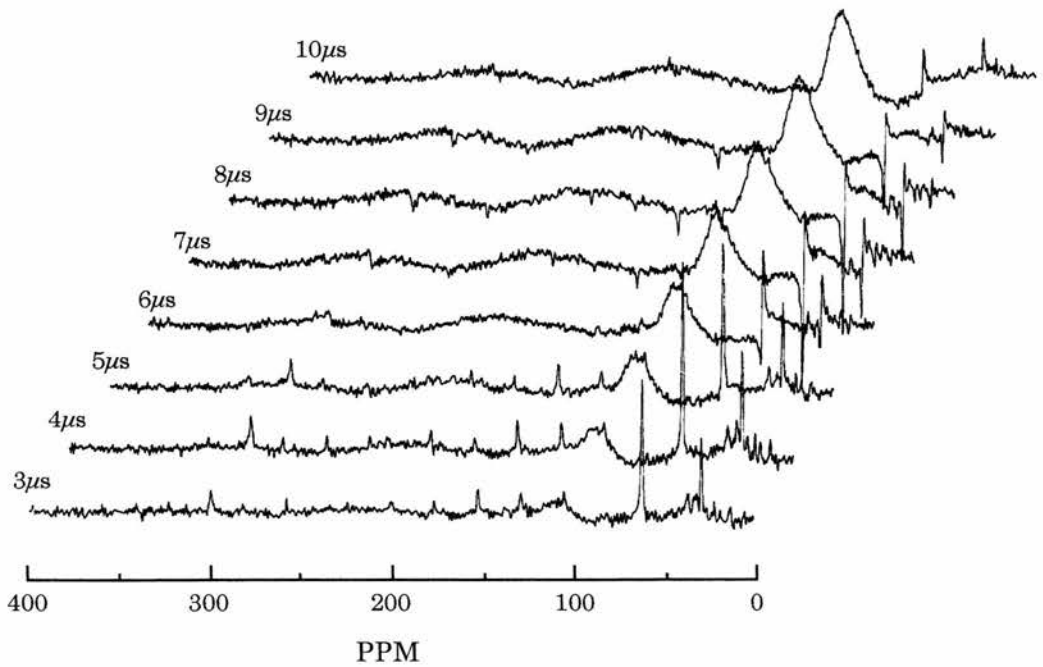

Figure 4.25. *Variation of 90° pulse width. It can be seen that the maximum signal appears at around 4.25μs. The large baseline distortion does not cycle with pulse width and is due to mechanical ring-down after the pulse.*

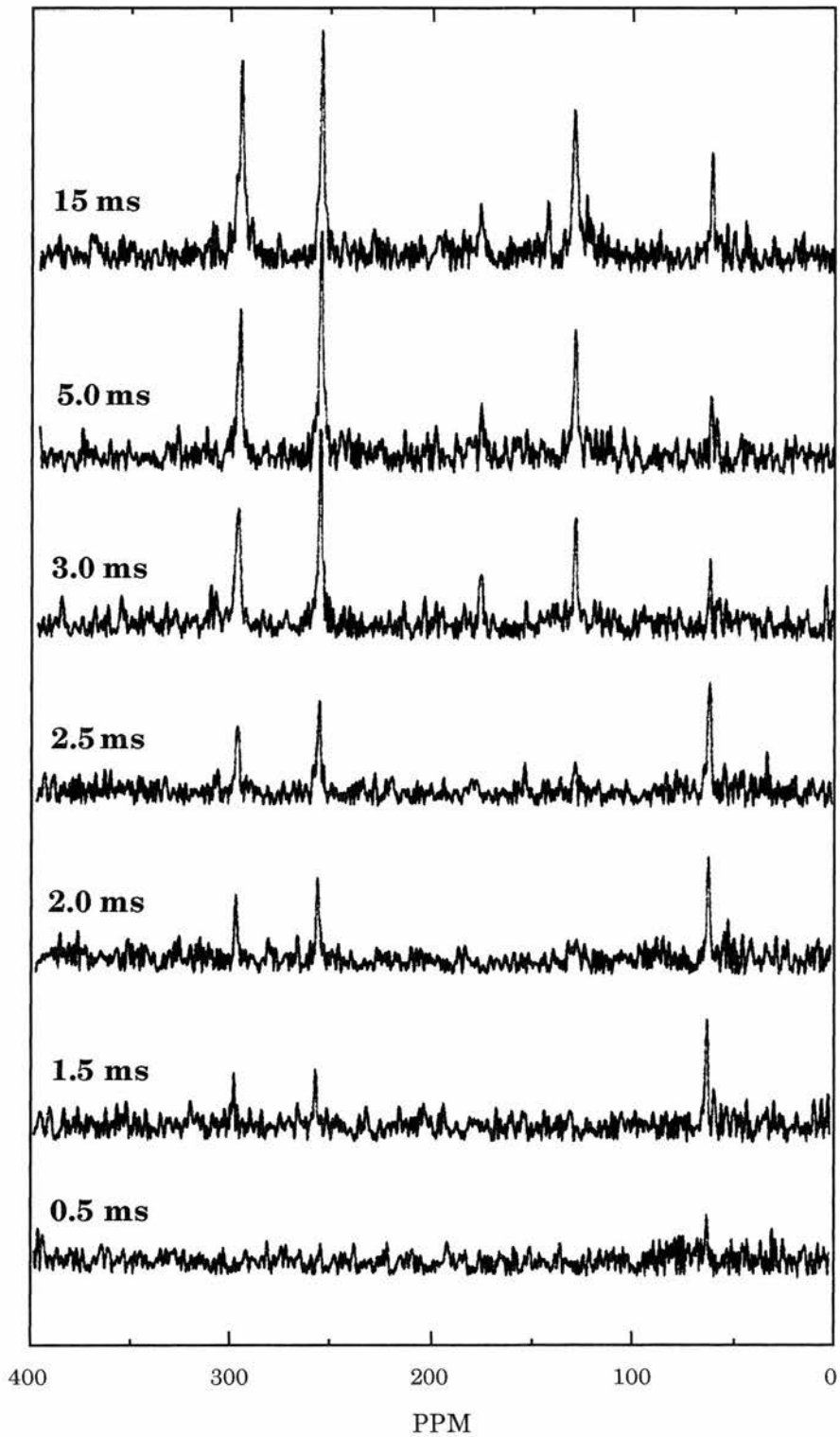

Figure 4.26. *Cross-polarisation spectra with variable contact pulse time. Those carbon sites nearest protons will appear first.*

The Non-Quaternary Suppression pulse sequence can also be used for assigning peaks. A spectrum is shown in Figure 4.27. in which it can be seen that only the 299ppm and 63ppm lines remain.

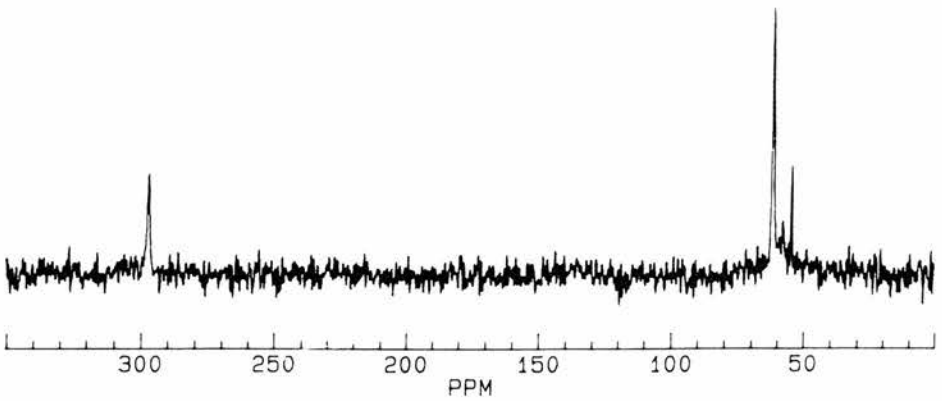

Figure 4.27. *NQS spectrum of the first sample.*

Using the Bruker MAS probe it is possible to lower the temperature to around 200K by using nitrogen as the spinning gas. Plots of peak position against temperature can be seen in Figure 4.28. *(a to c)* These show that all the peaks remain stationary, with the exception of the 177ppm peak, which shifts to 175 ppm by 235K, and the 130ppm peak which shifts to 125ppm by 235K.

Measurements of T_1 show more significant temperature dependence. Values for T_1 were calculated by fitting the equation for inversion-recovery using the "curve-fit" function of KaleidaGraph for the Apple Macintosh. Because the baseline was not completely level, an extra offset parameter was introduced to improve the fits. A sample fit is shown in Figure 4.29.

Plots of the variation of T_1 for each line (including the 30 ppm line) are shown in Figure 4.30. *(a to f).* In some cases there was insufficient data to perform a satisfactory curve fit (mainly for the weaker 177 and

257 ppm lines), so there are points missing at certain temperatures for some lines.

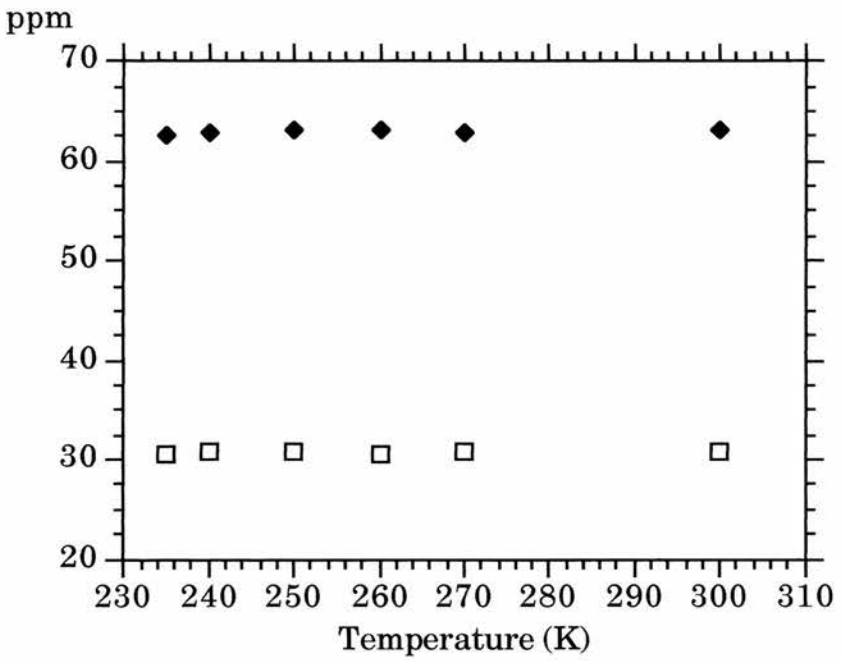

(a)

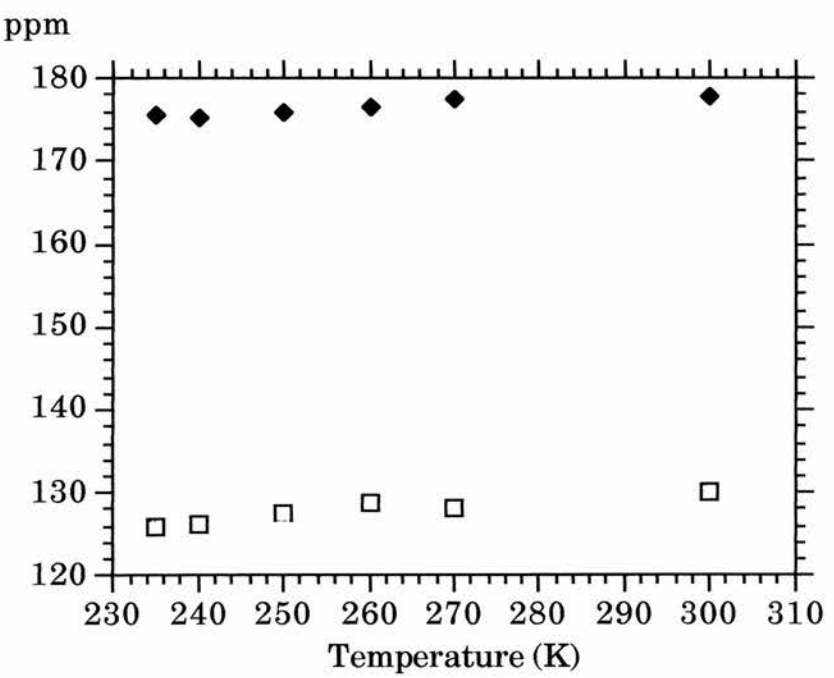

(b)

Figure 4.28. *Plots of peak position against temperature.*

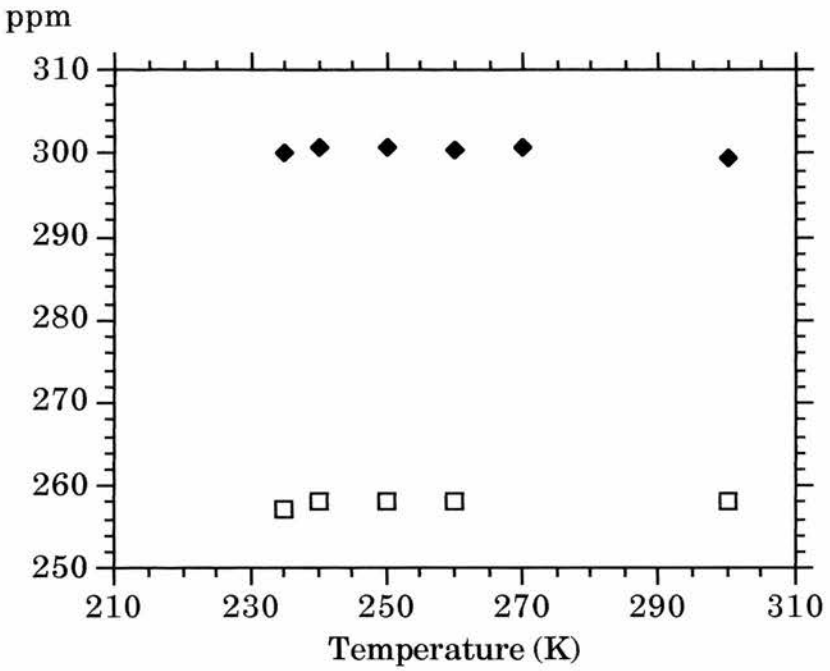

(c)

Figure 4.28. (cont.) *Plots of peak position against temperature.*

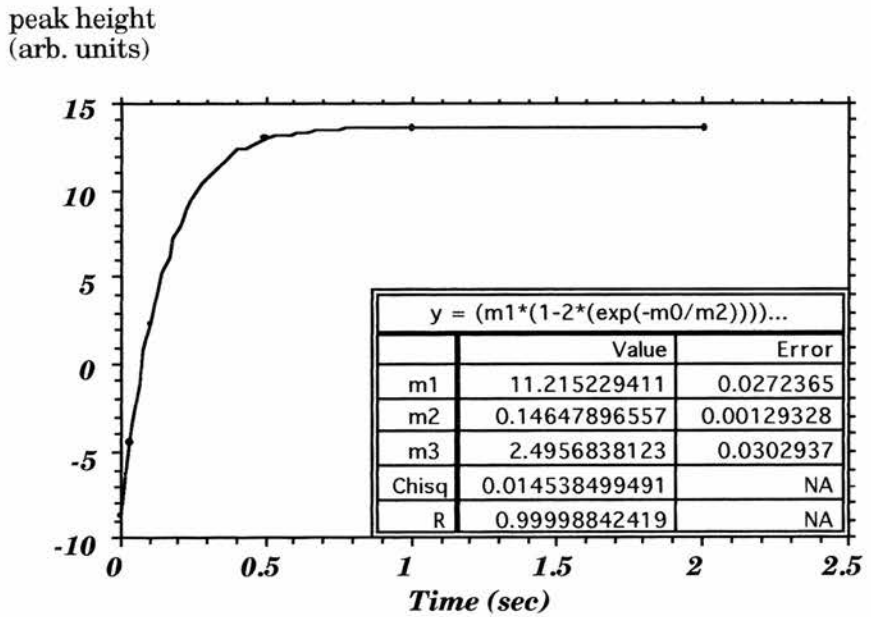

Figure 4.29. *Sample plot for calculating T1 for the 63 ppm line. The parameters are :* ***m1*** *(maximum magnetisation),* ***m2*** *(T1 in seconds) and* ***m3*** *(baseline offset).*

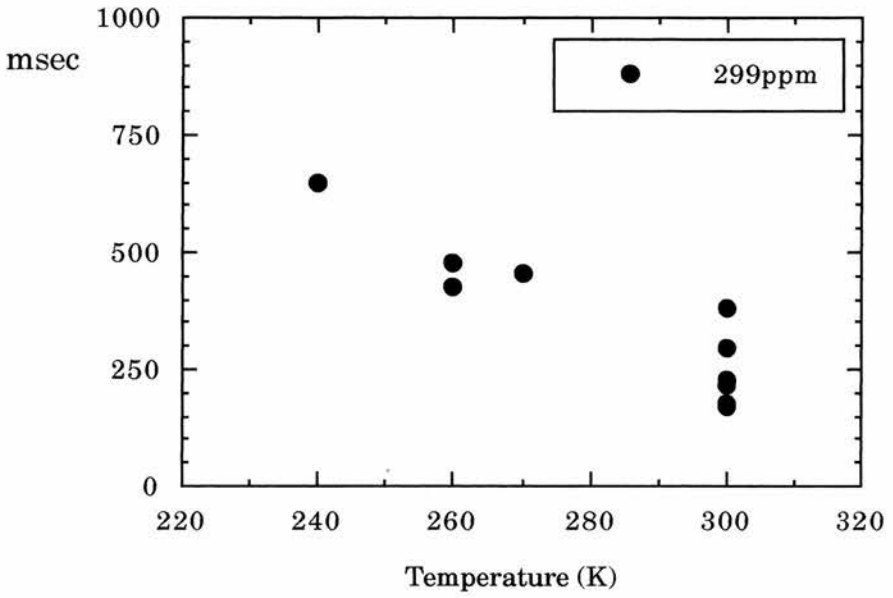

(a)

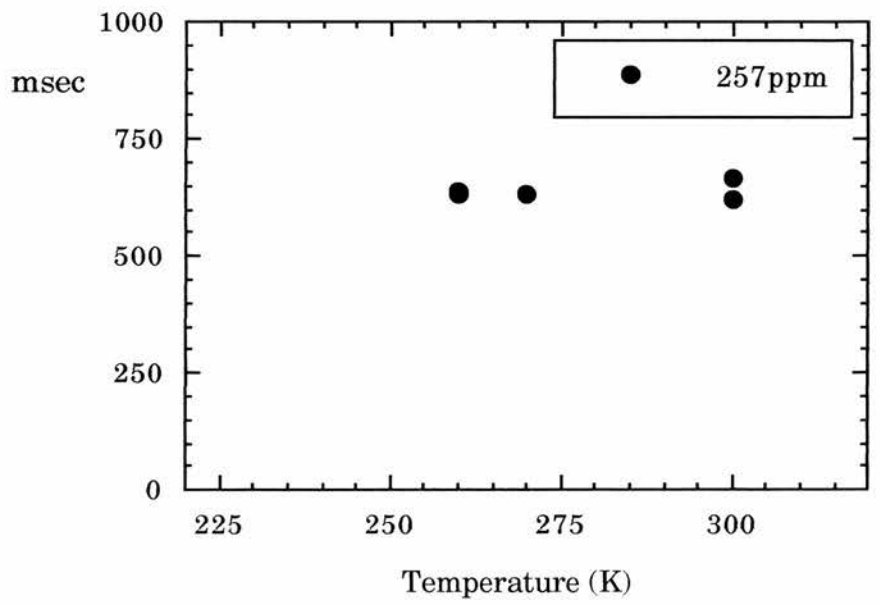

(b)

Figure 4.30. *Variation of T_1 with temperature.*

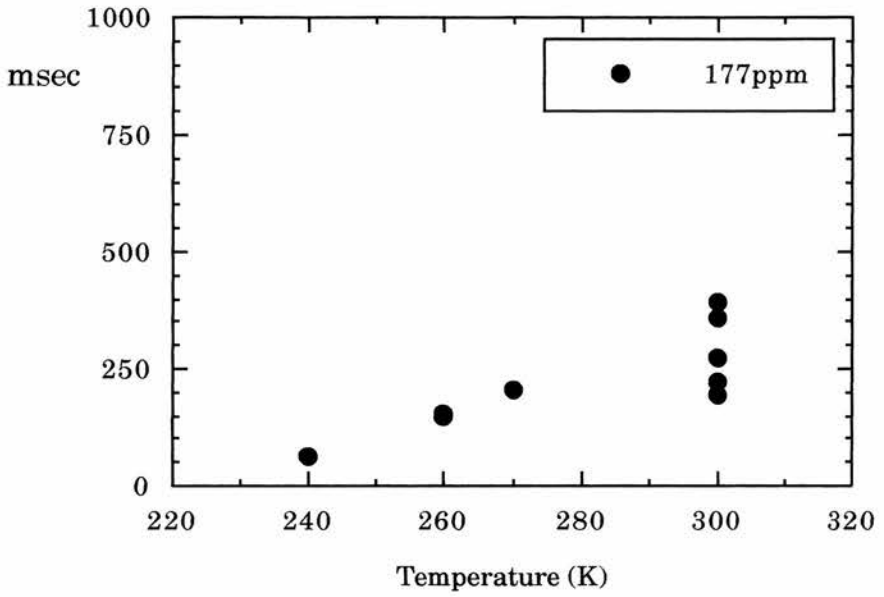

(c)

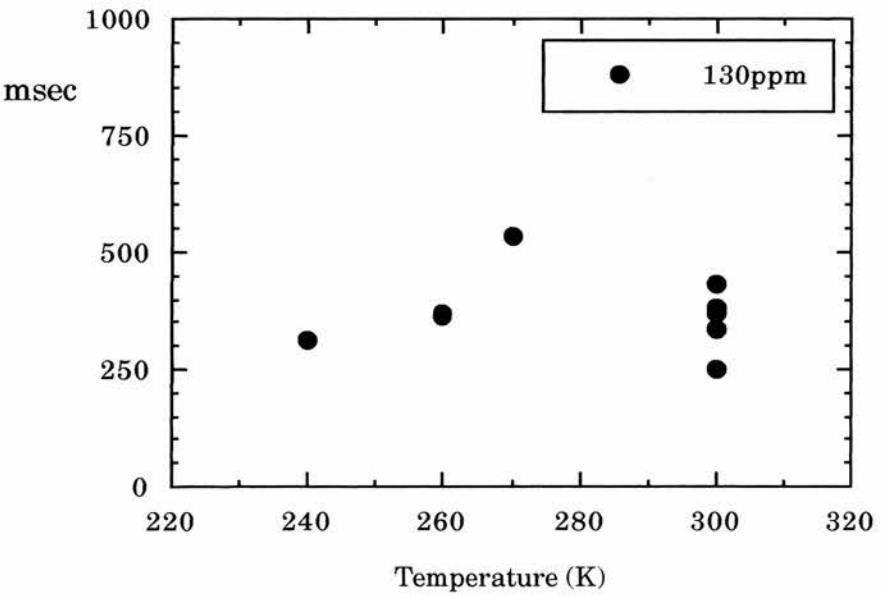

(d)

Figure 4.30. (cont.) *Variation of T_1 with temperature.*

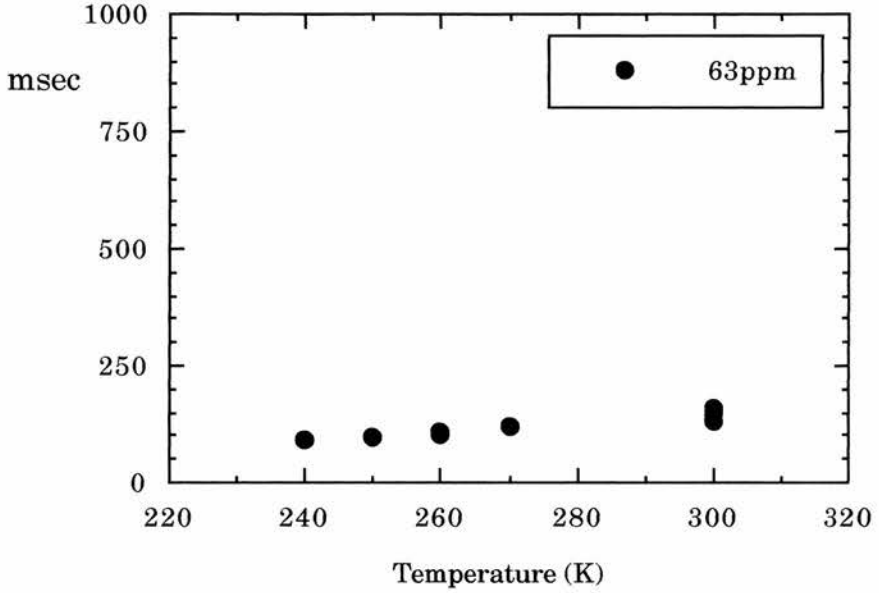

(e)

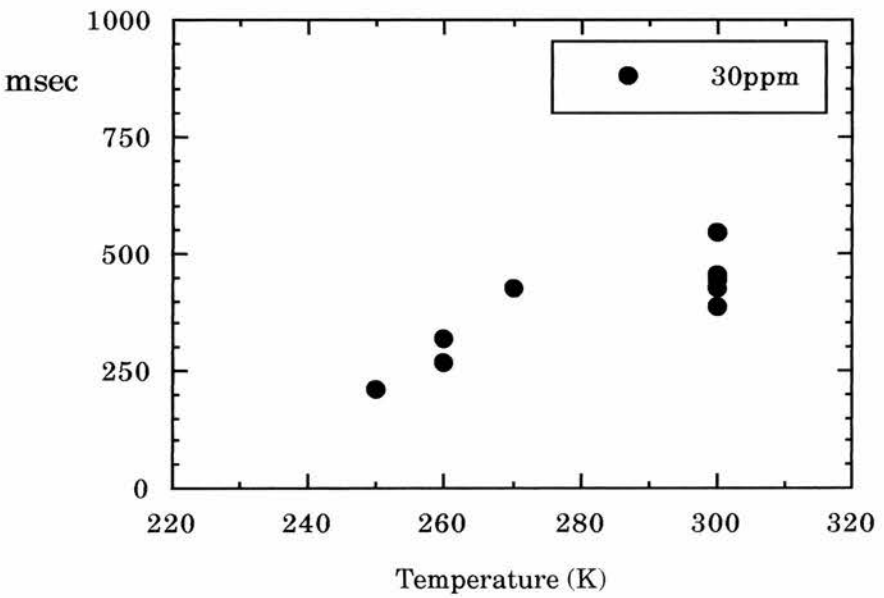

(f)

Figure 4.30. (cont.) *Variation of T_1 with temperature.*

5. Electron Spin Resonance.

5.1. Background Theory.

ESR[1] is very similar to NMR, being based on transitions between energy levels of the electron, rather than the nucleus. The theory behind these transitions is almost identical to that for NMR, with the main differences being in nomenclature. Only the major differences will be highlighted here; more comprehensive treatments are available[2,3,4].

5.1.1. Comparison with NMR.

The electron, like the nucleus, possesses spin **S**, and a magnetic moment

$$\boldsymbol{\mu}_e = -g\beta\hbar\mathbf{S}.$$

The gyromagnetic ratio here is $(g\beta)$ where β is the Bohr magneton, and g is simply called the g-value[5].

For the electron **S** = 1/2, so m_s can only take the values ±1/2. As before, in a magnetic field $\mathbf{B}_0$, the Hamiltonian is given by

---

1 ESR is sometimes referred to as Electron Paramagnetic Resonance (EPR).

2 N. M. Atherton: *Principles of Electron Spin Resonance*, Ellis Horwood (1993).

3 C. P. Slichter: *Principles of Magnetic Resonance - 3rd Edition*, Springer-Verlag (1989);

4 J. A. Weil, J. R. Bolton and J. E. Wertz: *Electron Paramagnetic Resonance*, Wiley (1994).

5 Classical models of the electron as a spinning charged sphere predicted a magnetic moment too small by a factor of two. The g-value for a free electron is 2.0023, and can be though of as a 'correction factor' for the classical approach.

$$\mathcal{H} = g\beta S_z B_0 ,$$

and the energy levels of the system are given by

$$E(m_s) = g\beta B_0 m_s ,$$

to give two levels. A transition occurs when $\hbar\omega_0 = g\beta B_0$.

5.1.2. The g-Factor.

For single crystals, the g-value depends on the orientation with respect to the magnetic field, and can therefore be described by a tensor (called the g-tensor, **g**). The Hamiltonian looks like

$$\mathcal{H} = \hbar\beta \mathbf{B} \cdot \mathbf{g} \cdot \mathbf{S} .$$

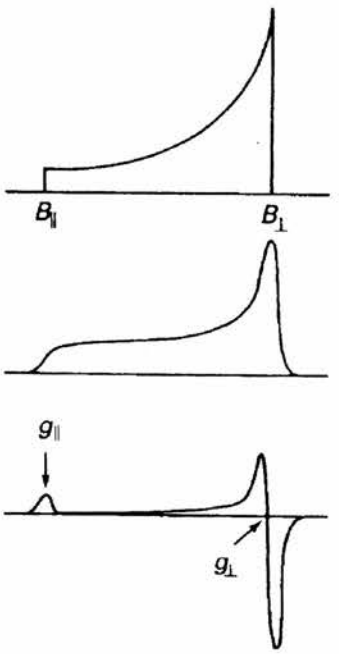

Figure 5.1. *Powder spectra for axially symmetric g-tensors. ESR spectrometers usually view the 1st derivative of the absorption lineshape. From Atherton*[2].

The g-tensor can be described in terms of its principal values, g_{xx}, g_{yy} and g_{zz}, with the value in a liquid being averaged out as $g = \frac{1}{3}\left(g_{xx} + g_{yy} + g_{zz}\right)$.

Powder spectra are similar to those for NMR, although an ESR spectrometer usually produces the derivative of the absorption lineshape, so the spectra will look like Figure 5.1.

5.1.3. Hyperfine Interactions.

As with NMR, there is interaction between the electron and nucleus in terms of the hyperfine interaction. For ESR, it is the electron levels which are affected by the presence of nearby nuclei. The (2I+1) nuclear spin states each give rise to a local field for the resonance condition, so the line is split into (2I+1) lines of equal intensity. In the first approximation, these lines will be equally spaced, although some second-order effects can produce unequal splittings.

5.1.4. The Bloch Equations.

In section 4.1.4. we introduced the Bloch equations for the classical description of NMR. These can also be applied to ESR, and solved for low $\mathbf{B_1}$.

In the rotating frame the motion of the magnetisation for an electron is given by

$$\frac{d\mathbf{M}'}{dt} = \gamma\left(\mathbf{M}'\times\left(\mathbf{B}'_0 + \frac{\omega_1}{\gamma}\right)\right) + \gamma\left(\mathbf{M}'\times\mathbf{B}'_1\right) - \frac{\left(\mathbf{i}'M_{x'} + \mathbf{j}'M_{y'}\right)}{T_2} - \frac{\mathbf{k}'\left(M_z - M_0\right)}{T_1}$$

This can be split into its component parts to give

$$\frac{dM_{x'}}{dt} = M_{y'}\left(B_0 + \frac{\omega}{\gamma}\right) - \frac{M_{x'}}{T_2}$$

$$\frac{dM_{y'}}{dt} = -M_{x'}\left(B_0 + \frac{\omega}{\gamma}\right) - M_z\omega_1 - \frac{M_{y'}}{T_2}$$

$$\frac{dM_z}{dt} = M_{y'}\omega_1 - \frac{(M_0 - M_z)}{T_1} .$$

For a steady state ($t>>T_1, T_2$) these equations all tend to zero. Therefore, with some manipulation

$$M_{x'} = \frac{-(\omega_0 - \omega)\gamma B_1}{(\omega_0 - \omega)^2 - \frac{1}{T_2^2}} M_0 \qquad M_{y'} = \frac{\gamma^2 B_1^2}{(\omega_0 - \omega)^2 - \frac{1}{T_2^2}} M_0$$

These equations correspond to the signal along the x' and y' directions. It can be seen that these equations correspond to the magnetic susceptibility equations with **M** related to **B**. The absorptive and dispersive components are shown in Figure 5.2.

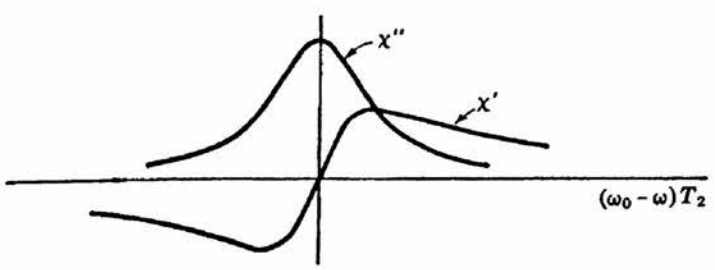

Figure 5.2. *Real and imaginary parts of the susceptibility as given by the Bloch equations. From Slichter*[3].

5.2. Experimental Techniques.

Although the theories behind the techniques of NMR and ESR are very similar the experimental techniques used are very different,

mainly because ESR uses microwaves to provide the incident energy to cause transitions between levels. Also, ESR is usually a continuous wave (c.w.) technique, although pulsed spectrometers do exist.

In this study, the two ESR spectrometers used were Bruker designed, and were very similar. Therefore, they will be described together after a section on basic spectrometer design.

The ESR experiments were performed in the Department of Chemistry, University of Birmingham with the assistance of Terry Green and P. P. Edwards, and in the Department of Biochemistry, University of St. Andrews with the assistance of Dominic Hunter and J. Ingledew.

5.2.1. Basic ESR Spectrometer.

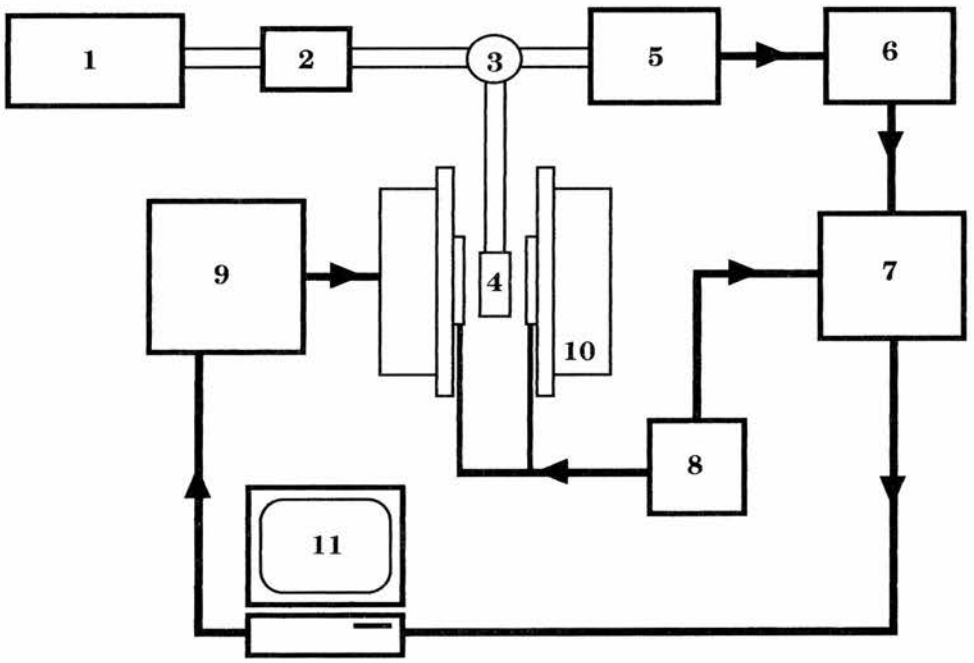

Figure 5.3. *Schematic representation of a c.w. ESR spectrometer. Adapted from Atherton*[2].

The most common type of ESR spectrometer in use today runs at a frequency of about 9.5 GHz, and is known as an X-band spectrometer. This frequency corresponds to a wavelength of about 30 mm, and a g-

value of 2 occurs at about 3300 Gauss. The principal components are shown in Figure 5.3. and are as follows:

1. ***Microwave Source.*** This is usually a Klystron, which is a vacuum tube characterised by its low-noise output.
2. ***Attenuator.*** The microwaves are passed along a waveguide through an attenuator to control the power to the cavity. The waveguides are usually rectangular brass pipes.
3. ***Circulator.*** This passes the microwaves to the sample cavity, and directs the output to the receiver side of the equipment. It acts like the T-piece in the NMR spectrometer.
4. ***Sample Cavity.*** The dimensions of the cavity match the wavelength of the microwaves so that a standing wave is set up. A small iris is located at the entrance to the cavity so that it can be tuned to match any particular sample. Then, all the power is stored in the cavity and dissipated as heat. On resonance, some power is absorbed, which changes the matching condition, and power is reflected back to the circulator. This is the received ESR signal.
5. ***Microwave Detector.*** This converts the reflected microwave signal into a d.c. signal. Because most detectors are non-linear at low levels, then usually some cavity mismatch is introduced, so the detector actually picks up differences in reflected radiation. As a d.c. signal is not readily processed, a modulated signal is introduced through modulation coils, which will be described below.
6. ***Amplifier.*** This simply amplifies the signal to be readily processed.
7. ***Phase-Sensitive Detector.*** The phase of the signal at the PSD is compared to the phase of the modulation fed to the modulation coils. This shows if the absorption has a positive or negative slope, so the first derivative of the signal can be found.

8. ***Modulation Power.*** A small oscillating component is added to the applied magnetic field through modulation coils. Usually this is at around 100 kHz. The signal at the detector will then be proportional to the slope of the absorption line.
9. ***Magnetic Field Power Supply.*** The magnetic field must be swept through the range at which the signal occurs. Normally this is an electro-magnet, as fields rarely need to be higher than 1 Tesla.
10. ***Magnet.*** Ideally this should be stable to within ±1 μT at the sample to be able to resolve complex narrow signals. A Hall probe is usually monitored to read accurately the field at the sample.
11. ***Computer.*** Most spectrometers today have some degree of computer control. In most cases it is used to control data storage and manipulation, and more recent spectrometers can automate processes such as tuning the iris.

An ESR spectrometer usually records the first derivative of the absorption signal. This can often be described by a Lorentzian or a Gaussian lineshape, which are shown in Figure 5.4. with its first and second derivatives.

The lineshape can be distorted by wrong settings of the modulation amplitude or modulation frequency. The part of the absorption line scanned during a half-cycle of the field modulation must be approximately linear for the slope of the line (or the first derivative) to be output. It follows then that the modulation amplitude should be much less than the peak to peak amplitude of the field, and that the modulation frequency must be high enough for the slope to remain linear during a half-cycle.

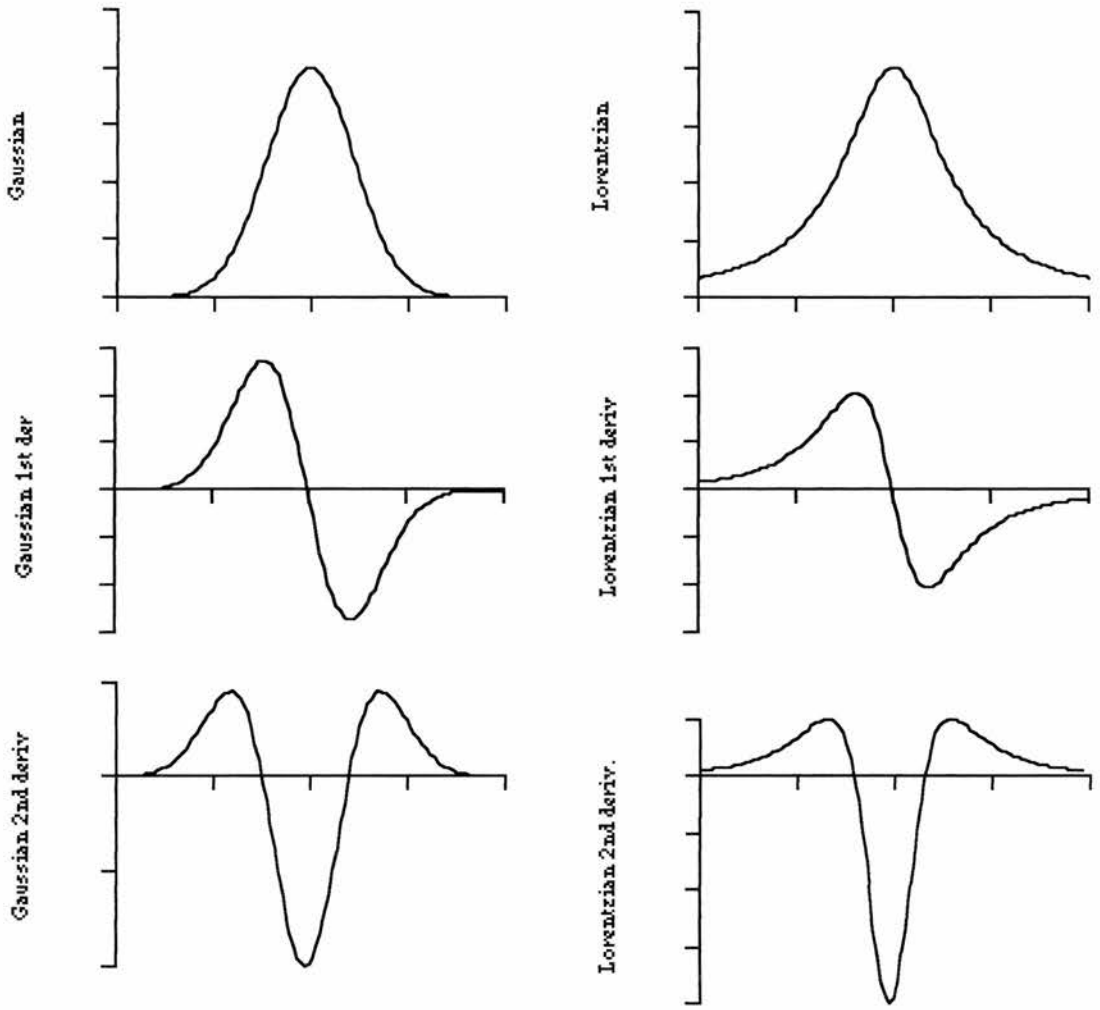

Figure 5.4. *Lorentzian and Gaussian lineshapes, with their first and second derivatives.*

5.2.2. Experimental Details.

Preliminary experiments were carried out on a Bruker ER200D spectrometer with an ESP3220 data system. A continuous flow cryostat (Oxford Instruments) cavity arrangement allowed operation at low temperatures, although in this system temperature stability and accuracy were unreliable. A single crystal sample of approximate dimensions 1mm x 0.5mm x 0.1mm was attached to a strip of overhead transparency sheet and attached with adhesive tape in a similar arrangement to the magnetic susceptibility experiments described in Chapter 6. The long axis was placed so that rotation of the crystal would

place this axis either parallel or perpendicular to the applied field. This is shown more clearly in figure 5.5.

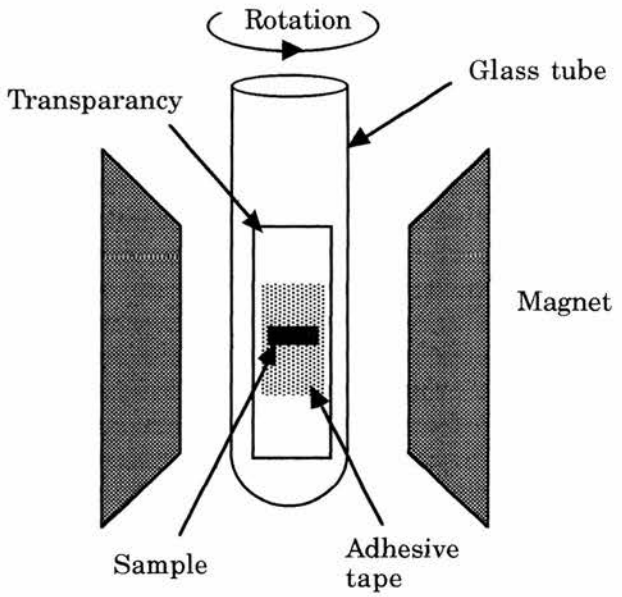

Figure 5.5. *Sample arrangements for the Bruker ESR spectrometers.*

Measurements at the lowest attainable temperature (8K) were taken for parallel and perpendicular arrangements, and also at 16K, 30K, and 50K although these temperatures may not have been accurate. An orientation study in 15° steps was also performed at 8K. After the first low-temperature experiments it was noticed that the sample had begun to fragment, although the presence of the adhesive tape may have kept many of the pieces of crystal aligned to form a pseudo-single crystal. Subsequent spectra showed slightly more structure. Attempts were made to use a liquid nitrogen-based temperature system but signals were drowned out by a large background signal from the cavity thought to be due to impurities within the cavity itself. When subtracted from the total signal, no lines could be seen, but the resultants were very noisy so further attempts were abandoned.

A more detailed study was carried out on a Bruker ESP300 spectrometer. This had a much more reliable temperature system

(Oxford Instruments), and a frequency meter (Hewlett Packard 5350B Microwave Frequency Counter) which allowed accurate calculation of g-values for each spectrum. The main operation was similar to the previous system, but with the addition of computer-controlled tuning.

A number of samples were used for the study and these are summarised in Table 5.1.

Sample	Description
x1	Single crystal approx 1.5 x 0.5 x 0.1 mm.
powd	Powder. About 100 small crystallites randomly arranged at the bottom of sample tube.
x3	Thick single crystal approx 1 x 0.5 x 0.5 mm.
x4	Thick single crystal approx 1 x 0.5 x 0.5 mm.
x5	5 x thin single crystals aligned by eye.
powd(KCl)	Powder (0.123g) mixed with KCl (0.1983g).

Table 5.1. *Summary of samples used for ESR study.*

A background signal was run with an empty cavity which produced a signal. This could be subtracted from the total signal within the computer software and produced a good resultant signal from the samples. Single crystal samples were mounted as before, using strips of overhead transparancy and adhesive tape (Sellotape Xpure). A blank sample was run to ensure that this technique produced no additional background signal. All samples were tested up to about 60K at various

temperatures. Crystal x3 was found to have shattered after the first temperature run in a similar fashion to the first sample tested, with subsequent runs showing more structure and a greatly reduced signal. Crystal x4 gave a very good single line so a detailed temperature study was carried out. Integration of the spectra to produce the area under the absorption curve was either performed with the Bruker ESP300 or the data was transferred to an Apple Macintosh.

For a more quantitative spin measurement a double-cavity measurement was performed. The sample cavity should be full, but with a full holder of $NMe_4[Ni(dmit)_2]_2$ the spectrometer would not tune. The sample was then diluted in powder with KCl which was tested separately to ensure that it contributed nothing to the signal. A reference sample from a range of $CuS0_4 \bullet 5H_2O$ samples was placed in the second cavity. This was chosen so that the signal height was closest to the $NMe_4[Ni(dmit)_2]_2$ signal. The $CuS0_4 \bullet 5H_2O$ reference spin count was 2.90×10^{19} spins/cm^3. The cavity was 2.5cm high, and the sample filled a tube of inner diameter 2.90mm to a height of 2.6cm.

5.3. Results.

5.3.1. Preliminary Results.

Preliminary ESR measurements on a single crystal of $NMe_4[Ni(dmit)_2]_2$ were performed on a Bruker ER200D spectrometer as described in section 5.2.2. Spectra taken at 8K can be seen in Figure 5.6. and 5.7. These show the two different orientations of the crystal with the long-axis parallel and perpendicular to the applied field.

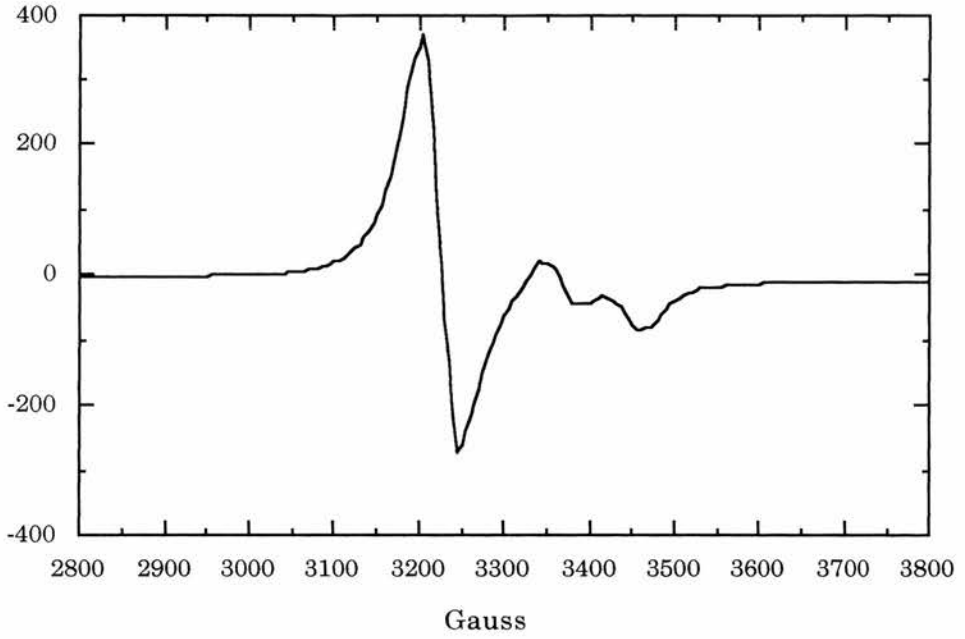

Figure 5.6. *ESR spectra at 0° orientation at 8K.*

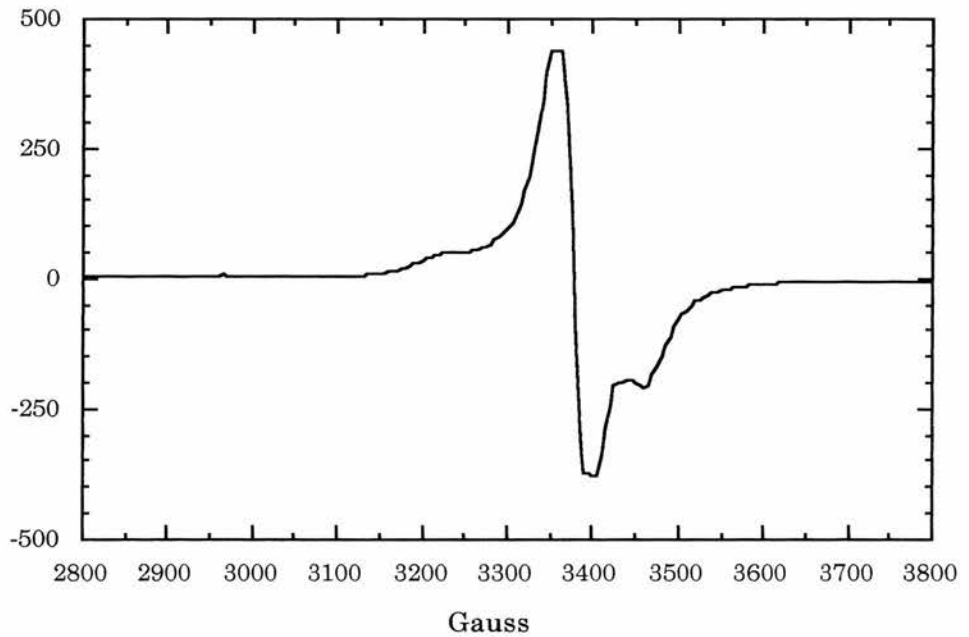

Figure 5.7. *ESR spectra at 90° orientation at 8K.*

It can be seen that the two orientations are quite different. The 90° spectrum is much larger (and was clipped in this run) and there seems to be more structure.

At 50K, "spikes" appear in the spectra *(see Figures 5.8. and 5.9.)*. These appear at the same position for both orientations, and are very narrow. The spacing is irregular, with spikes appearing at g = 1.86, 1.93, 2.06, 2.26, 2.67 and 2.83.

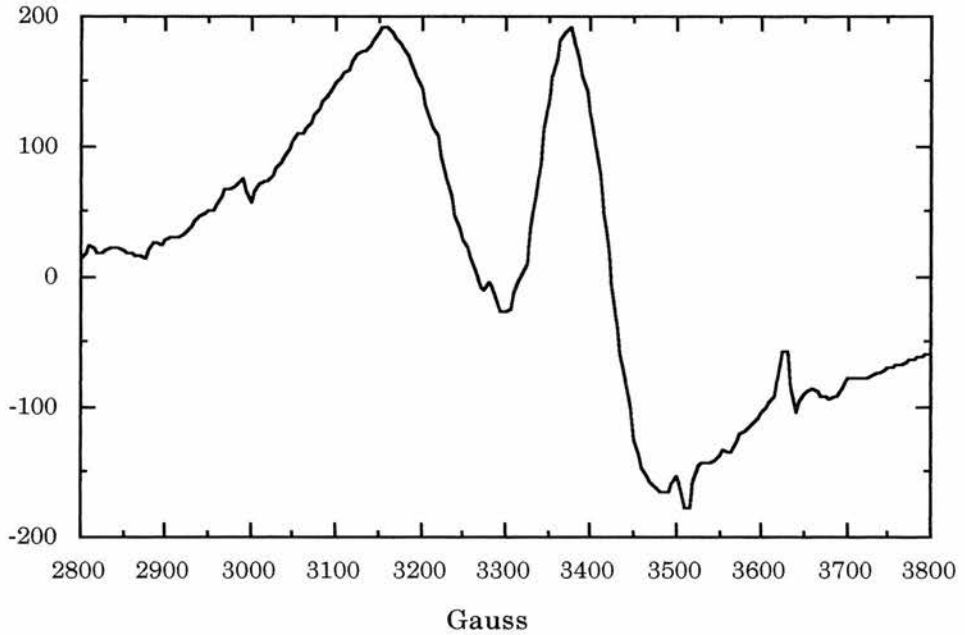

Figure 5.8. *ESR spectra at 0° orientation at 50K.*

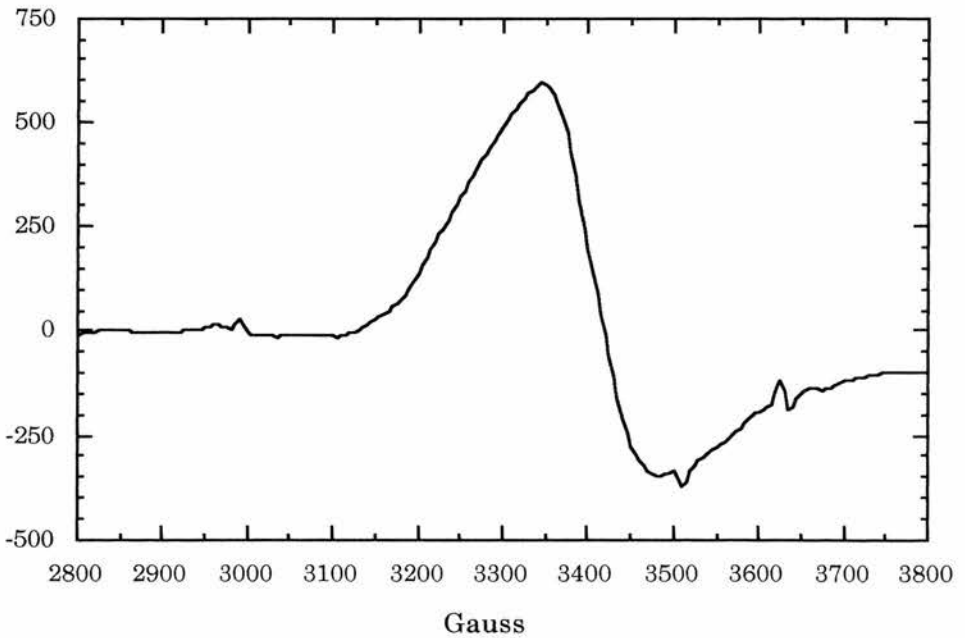

Figure 5.9. *ESR spectra at 90° orientation at 50K.*

An orientation study of this sample was performed at 8K to determine the movement of the lines as the crystal was moved from 0° to 90°. This shows the line splitting up considerably before converging again.

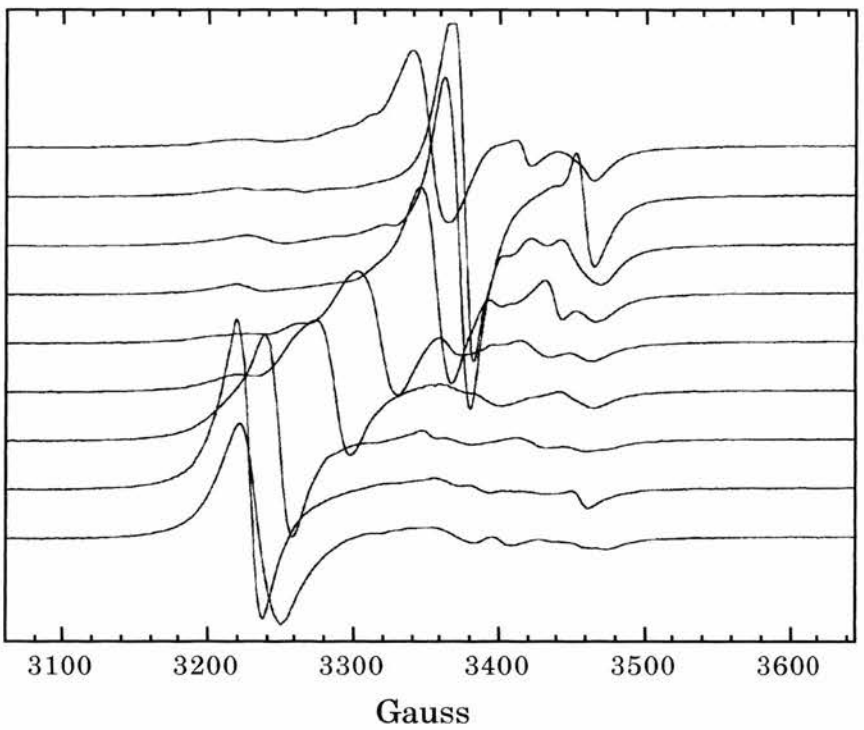

Figure 5.10. *Orientation study at 8K.*

5.3.2. Temperature Studies.

A more detailed study was carried out on the Bruker ESP300 spectrometer. The background cavity signals at 4K and 50K are shown in Figure 5.11. These could be subtracted using the spectrometer software to give the real signal. The small peak at ~3400 Gauss corresponds to g = 2 and is probably due to trace amounts of DPPH in the cavity. This did not subtract completely from the signal because the background was smoothed before subtraction to eliminate noise. This was not a problem as it could easily be identified and eliminated.

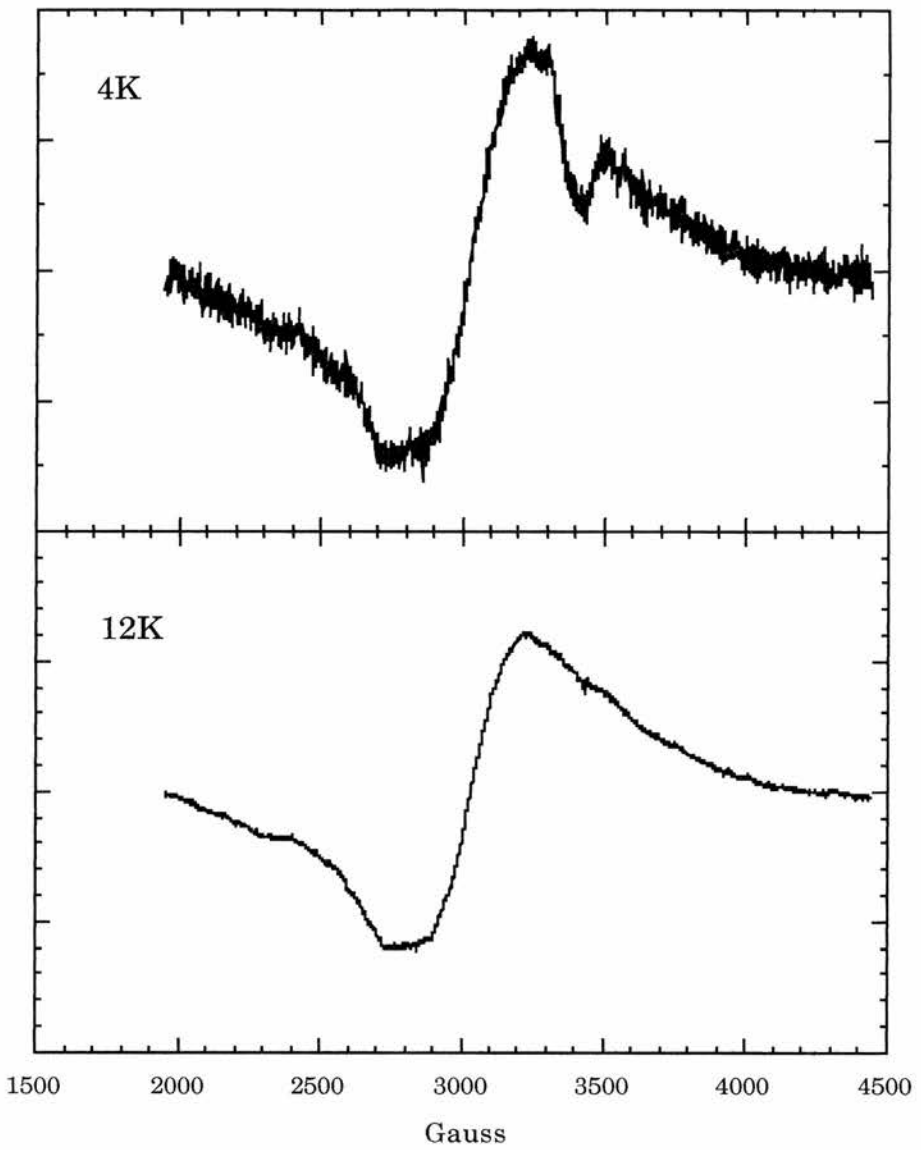

Figure 5.11. *Background ESR signals at 4K and 50K. These could be subtracted from the acquired spectra to give the true signals.*

Sample 'x1' was observed at 50K and the spectrum is shown in Figure 5.12. The "spikes" are clearly visible, but are not as well defined as in the preliminary experiments. Attempts were made to sharpen them by adjusting the modulation frequency, but without success. The magnetic field sweep was increased to 4500 Gauss, and two additional peaks can be seen above 4000 Gauss. The values of the g-factor for these lines are slightly different to the preliminary measurements, at g = 1.62,

1.67, 1.92, 1.97, 2.31, 2.73 and 2.85, and a comparison between them will be shown in the next section.

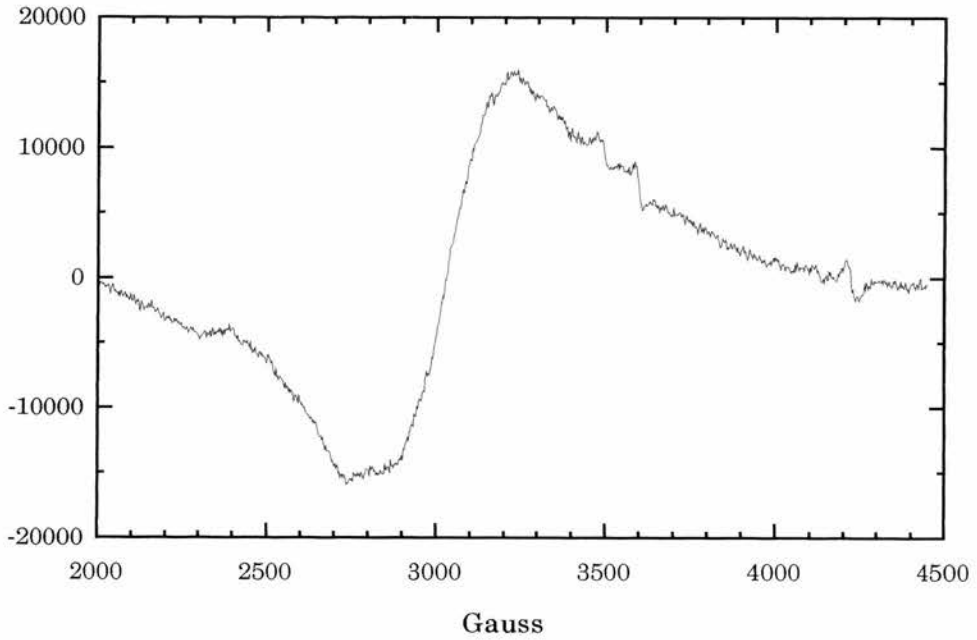

Figure 5.12. *Sample x1 spectrum at 50K*

The second sample, 'powd', was studied at 4K and 50K. Three different spectra at 4K can be seen in Figure 5.13. In each case the sample was removed, warmed to room temperature, then re-inserted into the cavity at a different orientation. It can be seen that there is a lot of structure in the main lines which is different in each run. Note that the background has not been subtracted from these spectra, as the original signals were quite noisy. When subtracting the background, the noise of the background signal was effectively doubled, making the resultant spectrum unacceptably noisy.

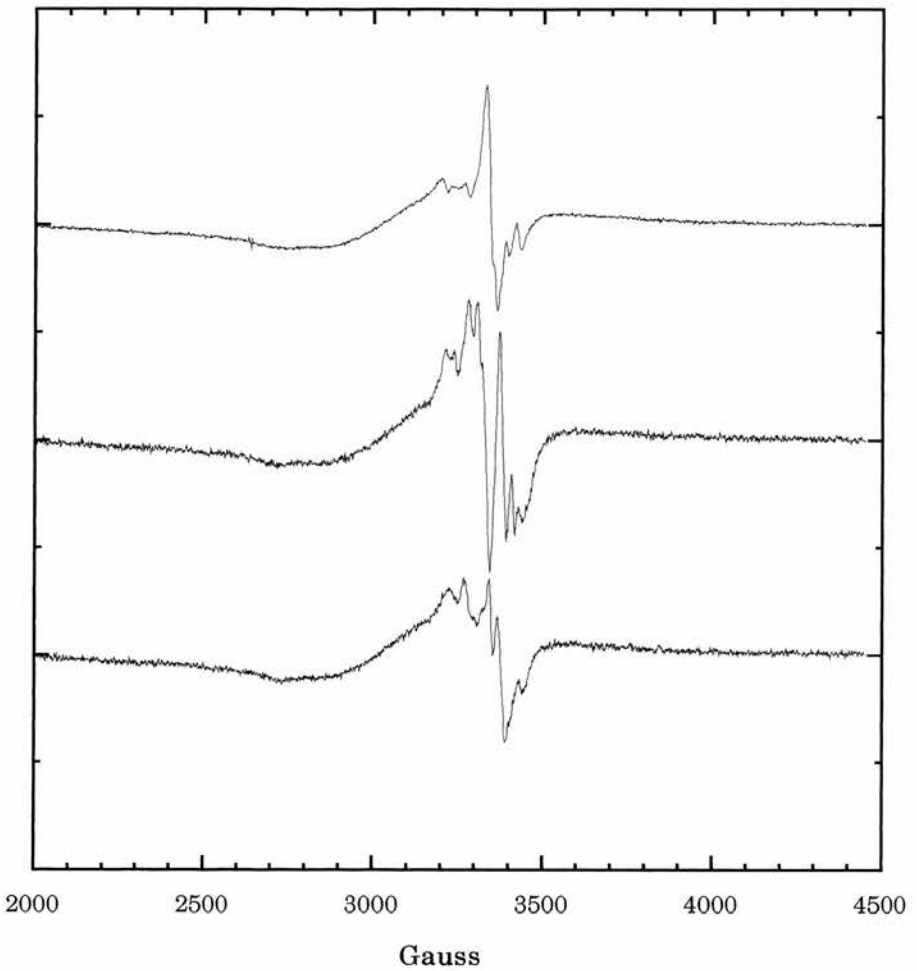

Figure 5.13. *Three different runs of sample 'powd' spectra at 4K. (Note that the background signal has not been subtracted.)*

Figure 5.14. shows two different runs of the same 'powd' sample at 50K. The spikes are once again clearly visible, and are all in the same positions as previous samples.

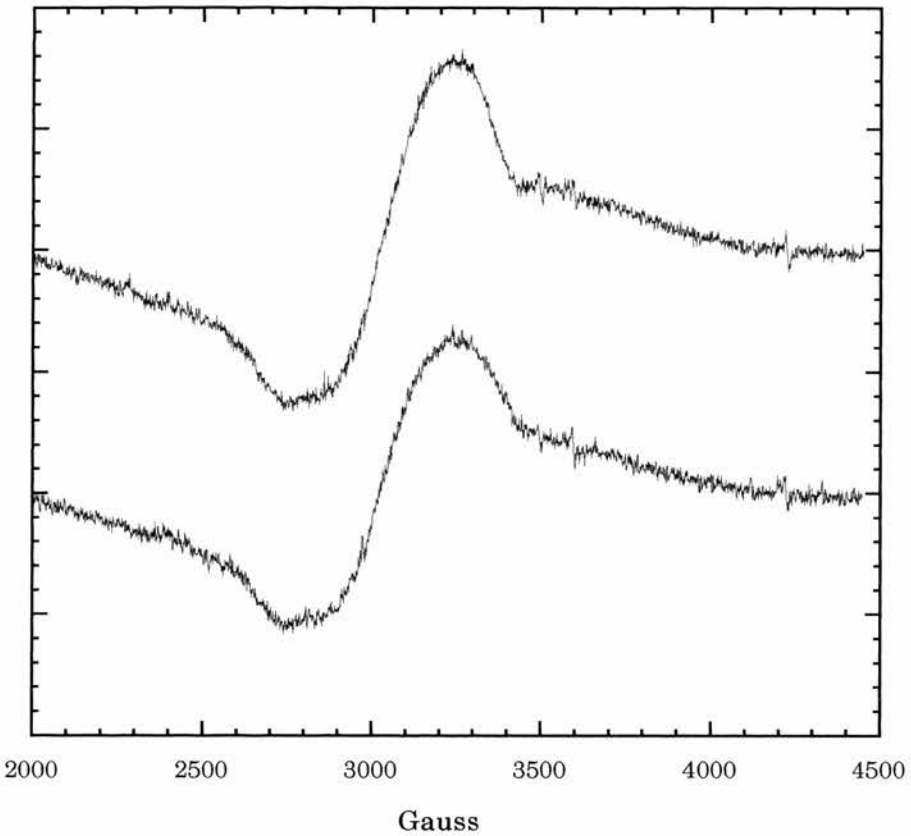

Figure 5.14. *Two different runs of sample 'powd' at 50K.*

Sample 'x3' was the large single crystal which shattered after the first low-temperature run. Figure 5.15. shows this sample on the first 4K run, and on a second run after the sample has been warmed to room temperature. The signal can be seen to have more structure, and is considerably weaker, with the main central line having disappeared. Both runs are at the same orientation.

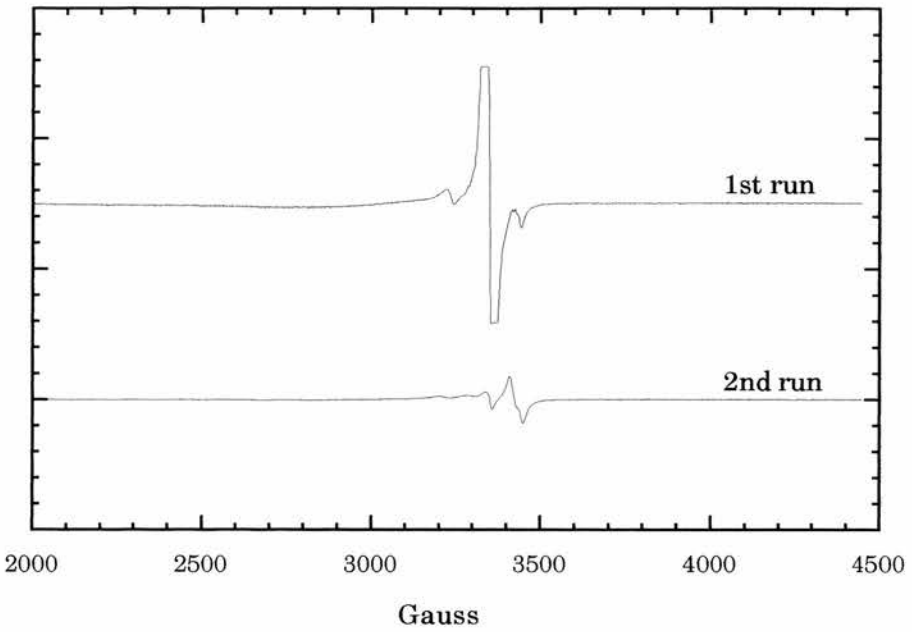

Figure 5.15. *Sample x3 spectra at 4K. The second run is after the sample had been warmed to room temperature, then cooled again.*

Sample 'x4' showed a single line at 4K so a temperature study of the area of the absorption spectrum was undertaken. The spectra at various temperatures can be seen in Figure 5.16. A graph of the area of the absorption spectrum can be seen in Figure 5.17.

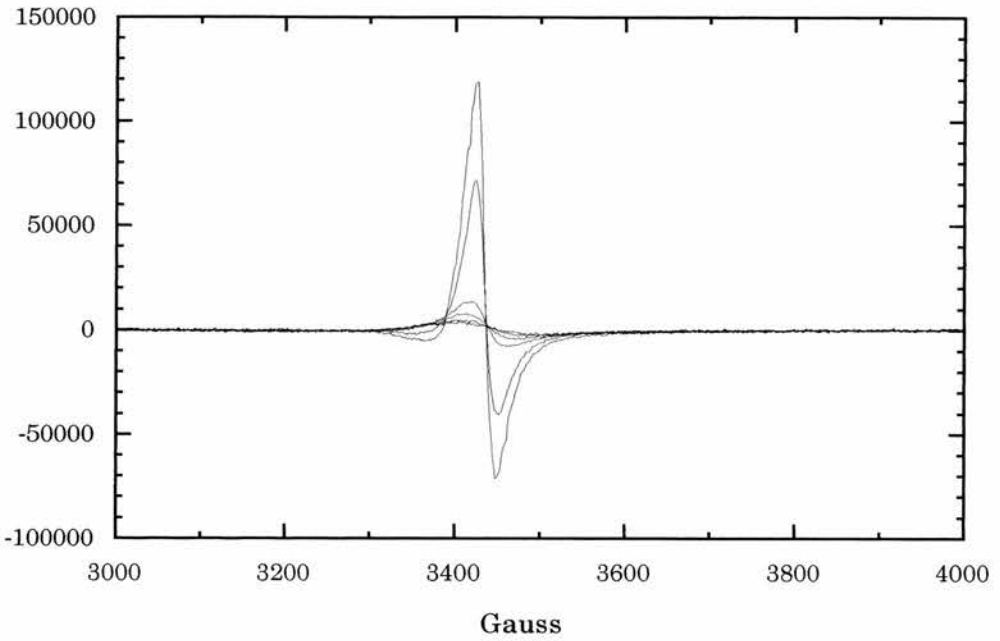

Figure 5.16. *Sample 'x4' at 4K, 7K, 10K, 15K, 20K, 25K and 30K (in order of decreasing size of peak height).*

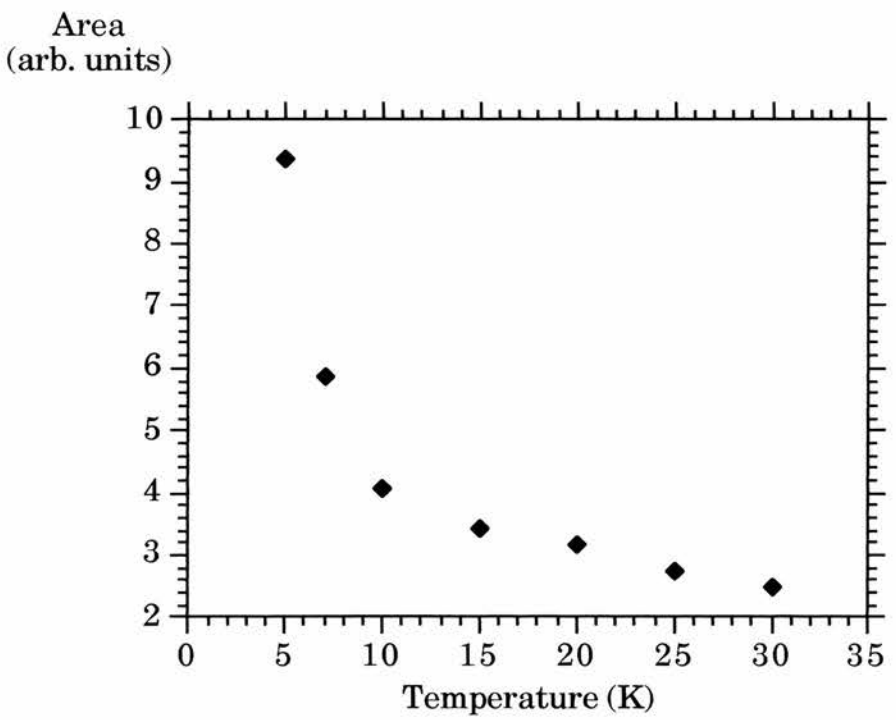

Figure 5.17. *Plot of area of absorption curve against temperature for sample 'x4'.*

Sample 'x5' showed the 50K spikes very clearly, so a temperature study of these was undertaken. The spectra can be seen in Figure 5.18. It can be seen that the spikes are not visible at 40K, and appear quite sharp at 45K before broadening out and disappearing by 60K.

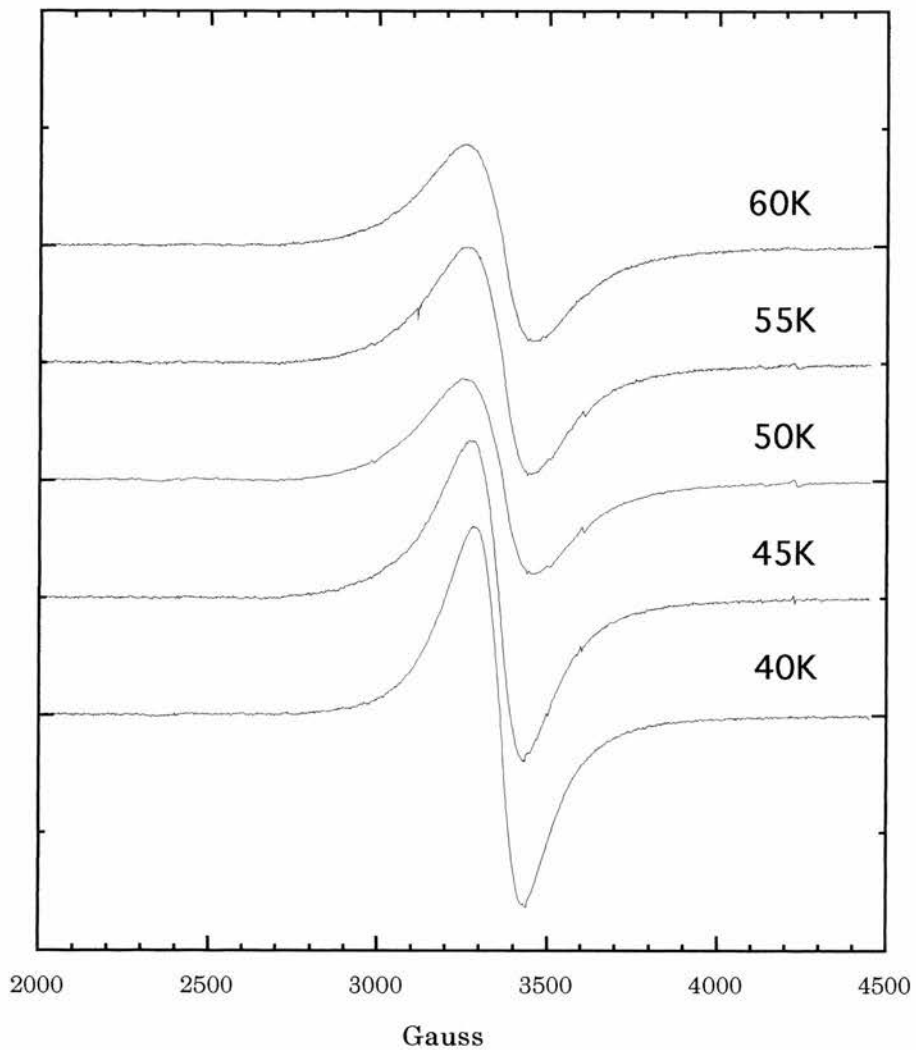

Figure 5.18. *Sample 'x5' at various temperatures showing the appearance of the 'spikes'.*

5.3.3. Comparison of ESR Results.

As a comparison, the spectra taken at 50K in St. Andrews and Birmingham are shown in Figure 5.19. plotted against the g-value. There is a slight mismatch in peak positions, but this is probably due to the frequency being more accurately known for the Birmingham experiments. Also, the field could be swept to a higher value, and two additional peaks were found. The line at g = 2.06 in the St. Andrews measurements could not be found unambiguously in the Birmingham spectra.

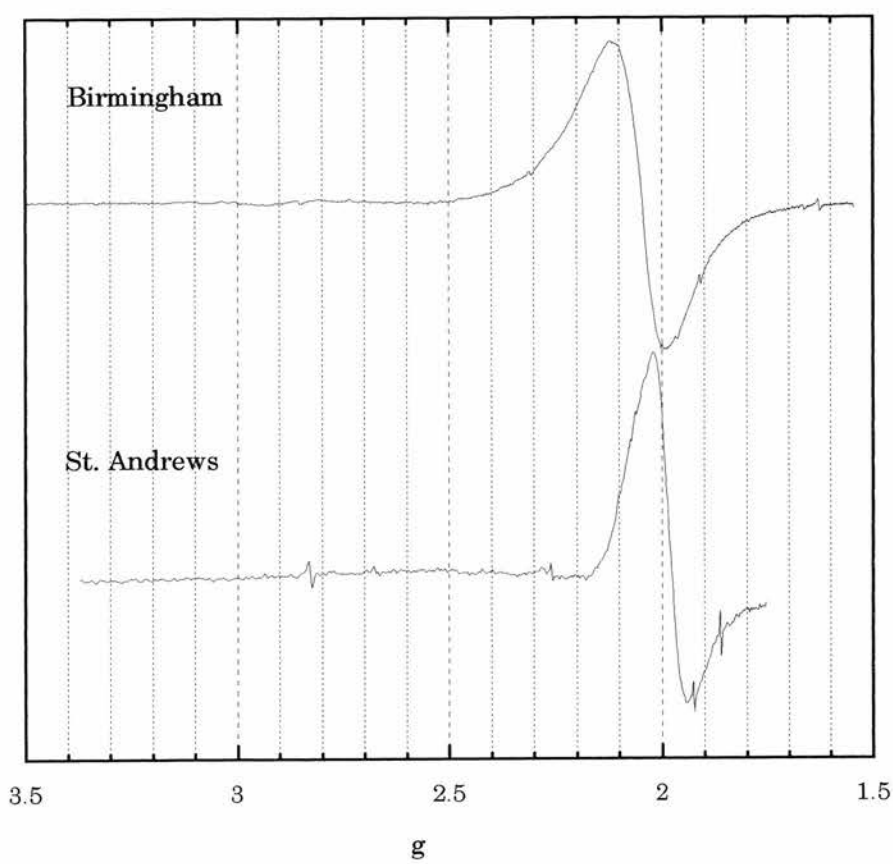

Figure 5.19. *Comparison of Birmingham and St. Andrews spectra at 50K.*

5.3.4. Double-Cavity Measurements.

Measurements using the double cavity of the Bruker ESP300 were taken with a reference sample of $CuS0_4 \bullet 5H_2O$ with 2.90 x 10^{19} spins/cm^3. The areas of the absorption curves are shown in Table 5.2.

Temperature	CuS area	powd(KCl) area
4K	291.4	376.5
10K	195.2	252.9
16K	205.5	229.6
27K	194.6	266.8

Table 5.2. *Areas under the absorption curves (in arbitrary units) for the CuS reference and the sample 'powd(KCl)'.*

6. Magnetic Susceptibility.

6.1. Background Theory.

6.1.1. Diamagnetic Contribution.

A diamagnetic material placed in a magnetic field **H**, will attain an internal magnetisation **M** opposing the applied field. The strength of this internal magnetisation is proportional to the applied field, such that

$$\mathbf{M} = \chi_{dia}\mathbf{H},$$

where χ_{dia} is the diamagnetic magnetic susceptibility[1].

Because the induced field opposes the applied field, it follows that the diamagnetic susceptibility is negative. The opposing field comes from the orbiting electrons, and is usually very weak. It is possible to calculate this from the theory of current loop, but in practice, a series of values have been produced, *Pascal's constants*[2], which are easily referred to.

6.1.2. Paramagnetic Contribution.

The magnetic susceptibility of a paramagnetic material follows the well known Curie Law,

$$\chi_c = \frac{M}{H} = \frac{\mu_0 M}{B} = \frac{C}{T}$$

---

1 Note that χ is sometimes quoted in cgs units. To convert, $\chi_{SI} = 4\pi\chi_{cgs}$.

2 See *Prog. in Inorg. Chem.*, **29**, 203 (1982).

where

$$C = \frac{\mu_0 \mu^2 N}{3k}.$$

Here, N is the number of spins, and C is known as the Curie constant.

6.1.3. Conduction Electrons.

The calculation for paramagnetic susceptibility considers all the spins to be in definite positions within the crystal. For conduction electrons this cannot apply as they are free to move, and are indistinguishable. Because the Pauli principle restricts the states they can occupy, the alignment of spins is hindered, and the susceptibility is lower than for normal paramagnetic materials. There is an excess of moments of one spin *(see Figure 6.1.)* which gives a magnetisation of

$$M = \beta^2 g(E_F) B,$$

where here $g(E_F)$ is the density of states at the Fermi surface, which can be written as $3N/2E_F$.

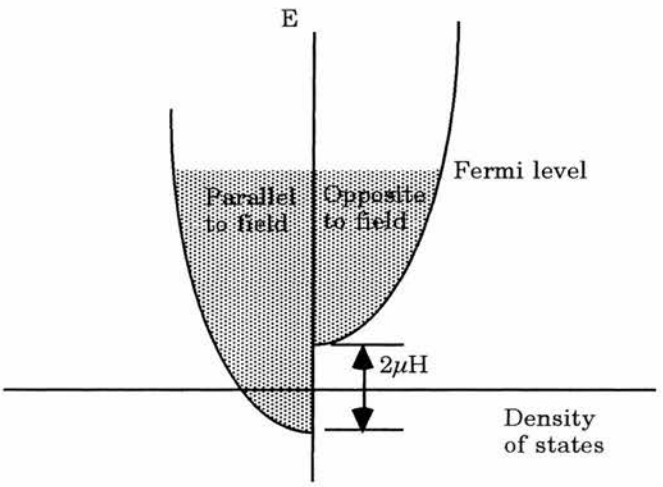

Figure 6.1. *The density of states of a metal in a magnetic field. The Pauli principle means that the susceptibility is lower.*

The susceptibility M/H is then given by

$$\chi_P = \frac{3N\mu_0\beta^2}{2E_F}.$$

This is known as the *Pauli spin susceptibility.* It can be seen that it is independent of temperature.

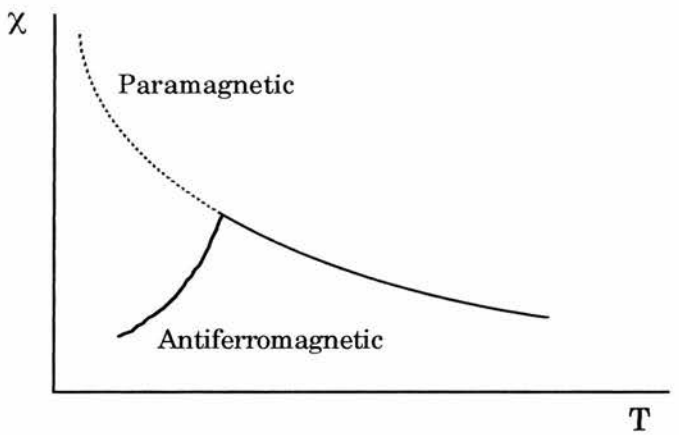

Figure 6.2. *Temperature dependent part of the susceptibility. The antiferromagnetic part follows the paramagnetic Curie law until the Neél temperature, when it starts decreasing.*

6.1.4. Antiferromagnetic Contribution.

An antiferromagnetic material has a very low susceptibility at low temperatures, because the arrangement of alternating spins is very stable. As the temperature rises, the dipole-dipole interactions are weakened, and the susceptibility rises, until at the Neél temperature,T_N, the spins are free. Above T_N the material is paramagnetic, and follows the Curie law. This behaviour, shown in Figure 6.2. is shown by a modified Curie law

$$\chi_{af} = \frac{C}{(T+\theta)}.$$

6.2. Experimental Techniques.

There are a number of techniques for measuring the spin susceptibility of a system, such as the Faraday balance, Electron Spin Resonance[3], and SQUID[4] Magnetometers. In this study the last two techniques were used, but only the SQUID Magnetometer experiments will be described in this section. The ESR experiments were part of a larger study and were explained in Chapter 5.

The SQUID measurements were carried out at the Department of Chemistry, University of Edinburgh, with the assistance of Gavin Whittaker and Andrew Harrison.

6.2.1. SQUID Magnetometer.

The system used was a Quantum Design MPMS SQUID magnetometer. This is a commercial system which is computer controlled, and capable of operation from 1.7K to 300K.

The magnetometer consists of two flux loops wound with opposite polarity *(see Figure 6.3.)* to negate the effects of external magnetic fields[5]. The sample is then inserted in a glass tube attached to the end of a probe which is lowered into the arrangement so that measurements can be made. Single crystals can be attached to plastic straws with adhesive tape instead of using the glass tube to allow alignment to the external field. A superconducting magnet can sweep the external field, but for this study it was left constant at 1000Gauss.

---

3 See Chapter 5 for general ESR references.

4 SQUID : **S***uperconducting* **QU***antum* **I***nterference* **D***evice.*

5 C. M. Pegrum: *Lecture Notes*, IRC in Superconductivity (Cambridge) Winterschool (1993).

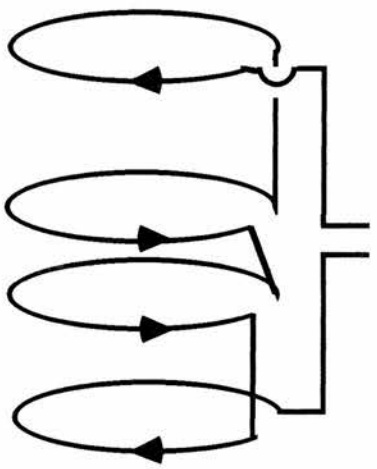

Figure 6.3. *Direction of SQUID windings to negate external magnetic fields.*

6.2.2. Experimental Details.

Two sets of samples were used in this study. The first was a pseudo-single crystal consisting of a number of single crystals of varying dimensions. These were aligned by eye and attached to a plastic straw with adhesive tape so that the crystals had the long axis perpendicular to the applied field[6]. This is shown diagramatically in Figure 6.4. A small strip of the adhesive tape was removed on either side of the sample to remove any contaminants in dust attached to the edges. This made accurate determination of the sample mass impossible, but it was estimated that the total sample mass was 1.9mg. The second sample was 42.4mg of small crystals. These were randomly arranged as a loose powder in a glass tube.

---

6 L. Brossard, E. Canadell, L. Valade, P. Cassoux: *Phys. Rev. B*, **47**, 1647 (1993).

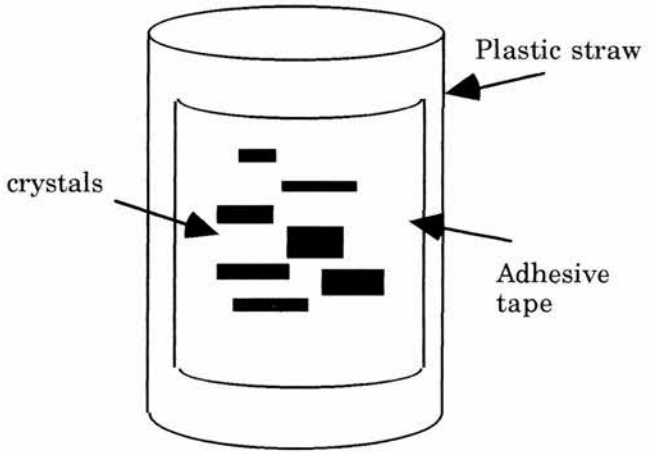

Figure 6.4. *Arrangement of crystals on a plastic straw. The crystals were aligned by eye and then attached with adhesive tape.*

Because of the unusual resistance characteristics of the $NMe_4[Ni(dmit)_2]_2$ system the magnetic susceptibility measurements were taken for both cooling and warming cycles. As the system is not as stable when cooling, care had to be taken to ensure the temperature was correct at each setting. This was done by leaving the temperature to equilibrate for a few minutes between each reading.

To convert the raw data from the SQUID into $emu.mol^{-1}$, the following relationship is used:

$$\chi_{mol} = \frac{M_{measured}}{H(gauss)} \times \frac{Mol.Wt}{Mass} .$$

Note that for all the experiments, H was kept constant at 1000 Gauss, and the molecular weight of $NMe_4[Ni(dmit)_2]_2$ is 965g.

6.3. Results.

The raw data for the first sample can be seen in Figure 6.4. There is a slight hysteresis effect that can be seen above ~50K, and a sharper increase at lower temperatures.

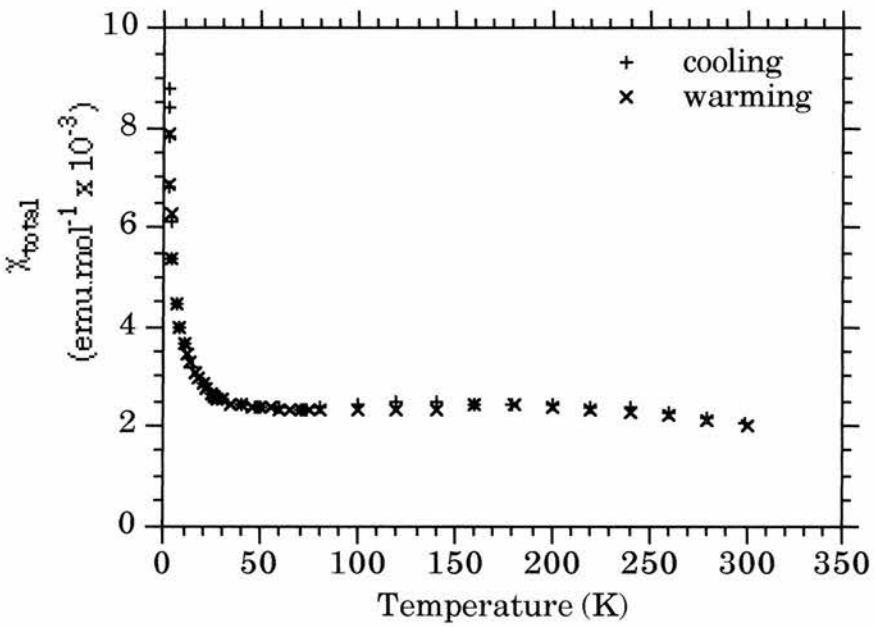

Figure 6.4. *Raw data for the pseudo-single crystal sample.*

The raw data for the powder sample can be seen in Figures 6.5. and 6.6. Two separate runs are shown, with broadly the same features, but slightly different values at higher temperatures. Both runs were only carried out at lower temperatures, and data was collected only while warming.

Analysis of this data in terms of paramagnetic impurities will be presented in the next chapter.

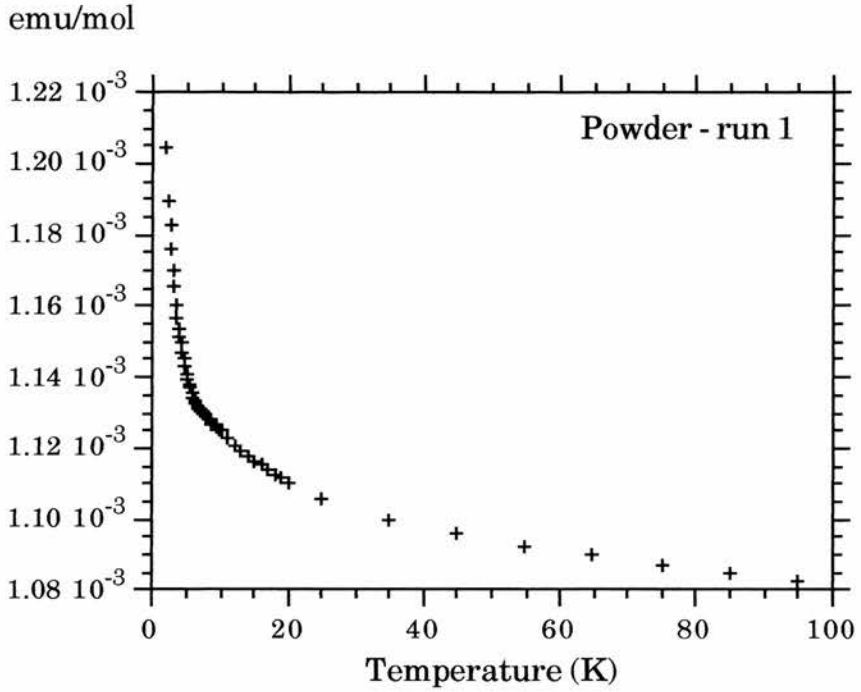

Figure 6.5. *Raw data for the powder sample - 1st run.*

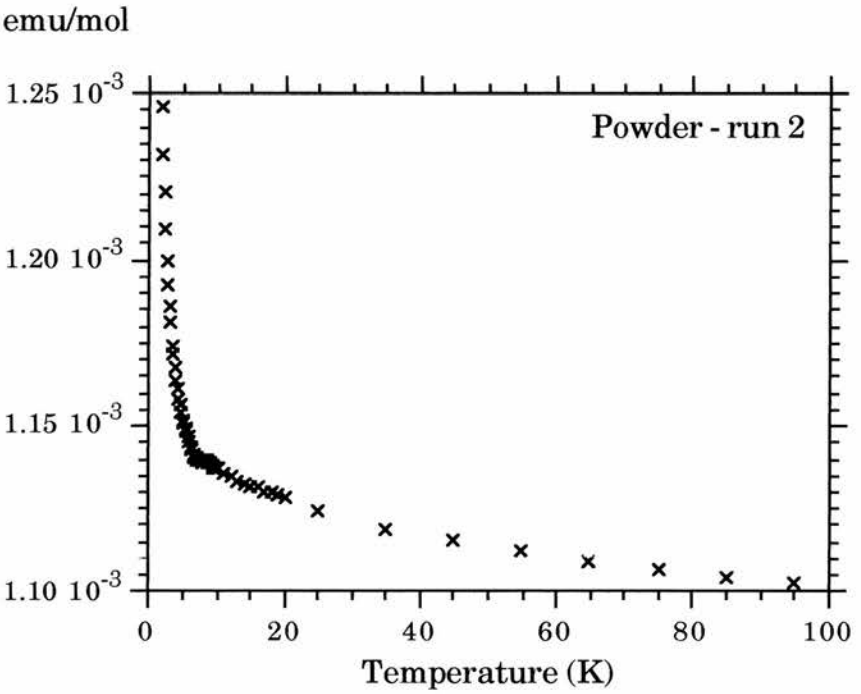

Figure 6.6. *Raw data for the powder sample - 2nd run.*

7. Discussion.

7.1. Sample Quality.

Elemental analysis for the ratio [Ni(dmit)$_2$] : x [NMe$_4$] should give x = 0.5 for NMe$_4$[Ni(dmit)$_2$]$_2$. The results in Chapter 3 give x = 0.64 ± 0.03. This excess of NMe$_4^+$ cations may be the source of the extra lines in the NMR spectra, as these correspond to the positions expected for methyl groups *(see Section 7.4)*.

Estimates of the number of paramagnetic impurities can also be found by magnetic susceptibility measurements, although this is not always representative of the actual number of impurities *(see next section)*.

7.2. Resistivity and Magnetic Susceptibility.

The electrical resistivity results *(Figure 7.1)* do not show any trace of superconductivity, as only ambient pressure results are available, but the characteristic curve does resemble the published data of Kajita *et al.*[1]. In this paper the first resistance jump at ~100K is thought to be due to the freezing of the rotational motion of the methyl groups in the NMe$_4^+$ cations as these occur at around the same temperature, although no mechanism for this is postulated. The 20K transition is thought to be due to localisation by the random potential of the frozen NMe$_4^+$ groups.

---

1 K. Kajita, Y. Nishio, S. Moriyama, R. Kato, H. Kobayashi, W, Sasaki, A Kobayashi, H. Kim, Y. Sasaki: *Sol. State Comm.*, **65**, 361 (1988).

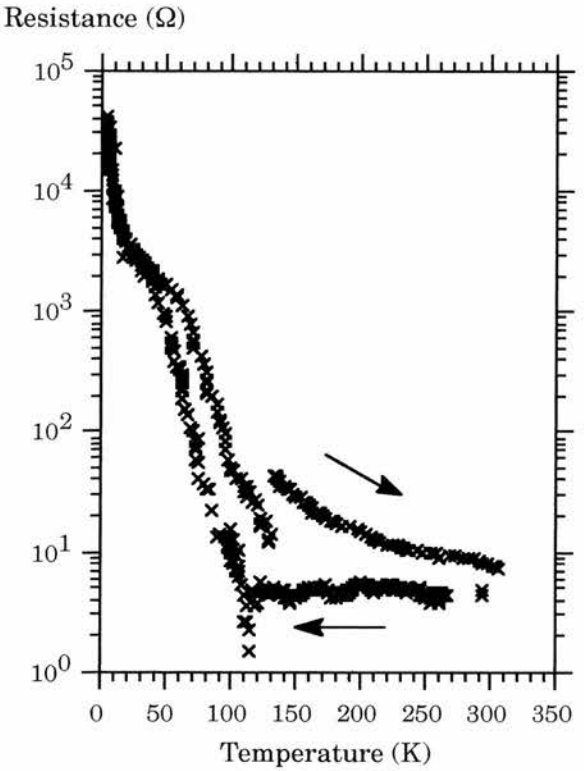

Figure 7.1. *Resistance of $NMe_4[Ni(dmit)_2]_2$ at ambient pressure. The "jump" in the warming cycle is due to the crystal cracking.*

The magnetic susceptibility curves contain components from paramagnetic impurities which must be subtracted from the raw data to give a true representation of the susceptibility. At low temperatures, the susceptibility can be thought of as being dominated by the Curie term (C/T), i.e..

$$\chi_{measured} = \chi_{sample} + \frac{C}{T}$$

$$\chi_{measured} T = \chi_{sample} T + C$$

so that a plot of χT *vs.* T will give C as the intercept. This is shown in Figure 7.2. for the crystal sample. It can be seen that there are very few points at a low enough temperature, so the straight-line fit quickly

becomes invalid. The values of C/T can then be subtracted from the raw data to give Figure 7.3.

It can be seen that there is a transition at about 20K which corresponds to the transition in the resistivity. Below this the susceptibility increases, with a turnaround at about 4K. This is reminiscent of antiferromagnetic behaviour *(see section 6.1.4)* with a Neél temperature, T_N, of 4K. A plot of emu^{-1} *vs.* T in the region 4K to 25K gives a good fit for antiferromagnetic behaviour. The gradient gives 1/C (C = 0.11) and the intercept gives θ/C (θ = 74K). The ratio θ / T_N is therefore 18.5, which is higher than would normally be expected[2].

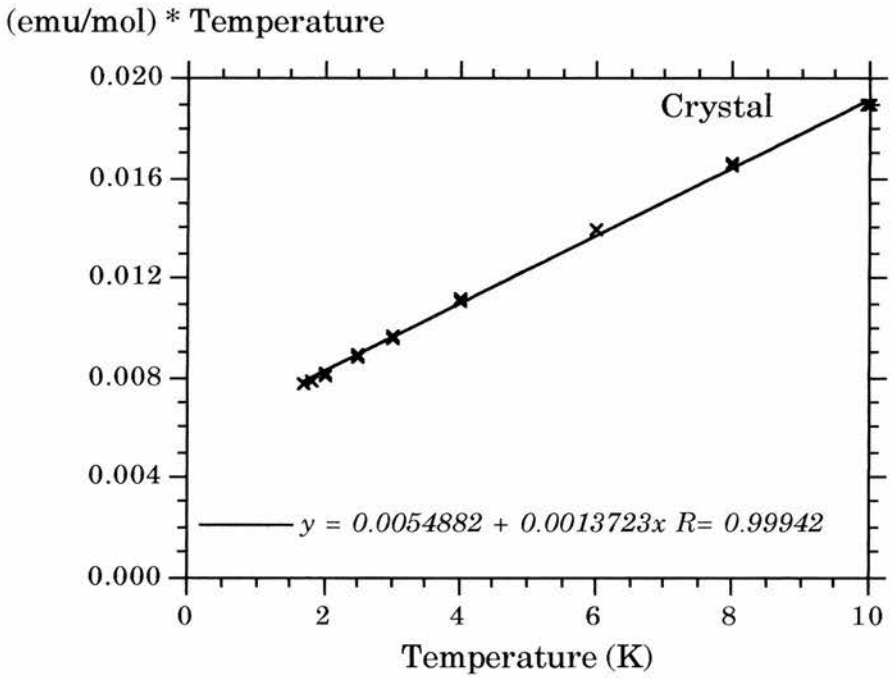

Figure 7.2. *Plot of χT vs T to give the Curie constant for the crystal data.*

2 See for example: C. Kittel, *Introduction to Solid State Physics,* Wiley.

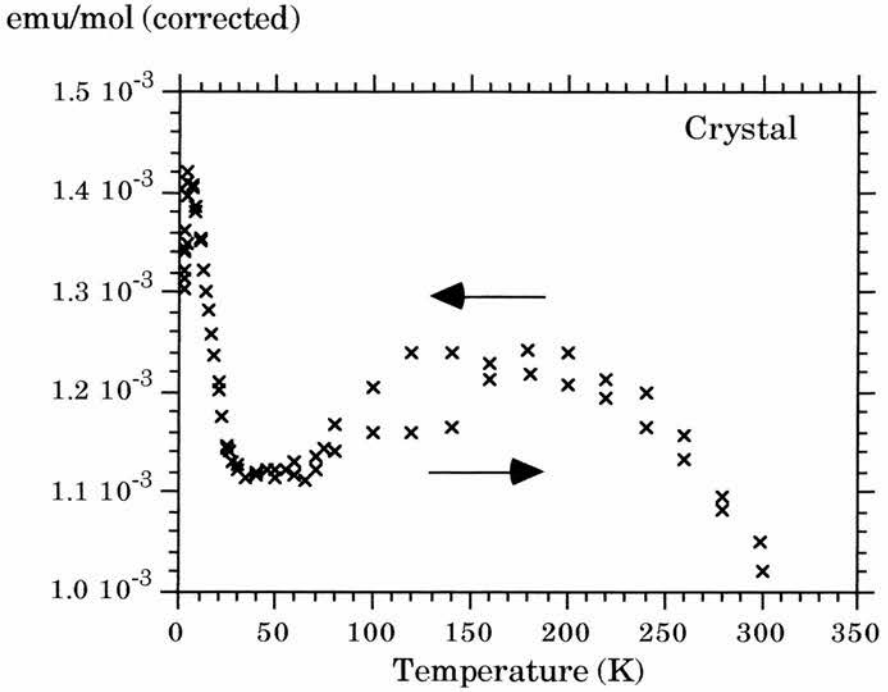

Figure 7.3. *Corrected data with C/T term subtracted for the crystal sample.*

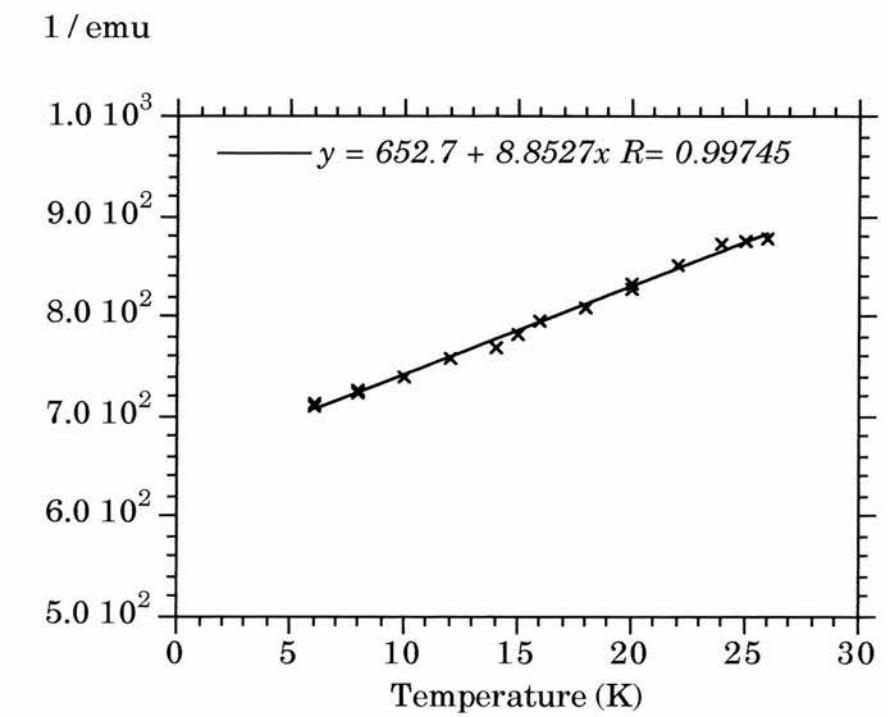

Figure 7.4. *Plot of $1/\chi$ vs T to show antiferromagnetic behaviour in the region 5 to 25K.*

A similar approach can be used for the powder sample. The Curie fits are shown in Figures 7.5 and 7.6, and the resultant susceptibilities shown in Figure 7.7, along with the powder data. Pascal's constants give an estimate of the diamagnetic contribution to the susceptibility *(see Chapter 6)* and are calculated to give χ_{dia} = -4.55 x 10-4 emu/mol for $NMe_4[Ni(dmit)_2]_2$. This has been subtracted from the total susceptibility to give the spin susceptibility.

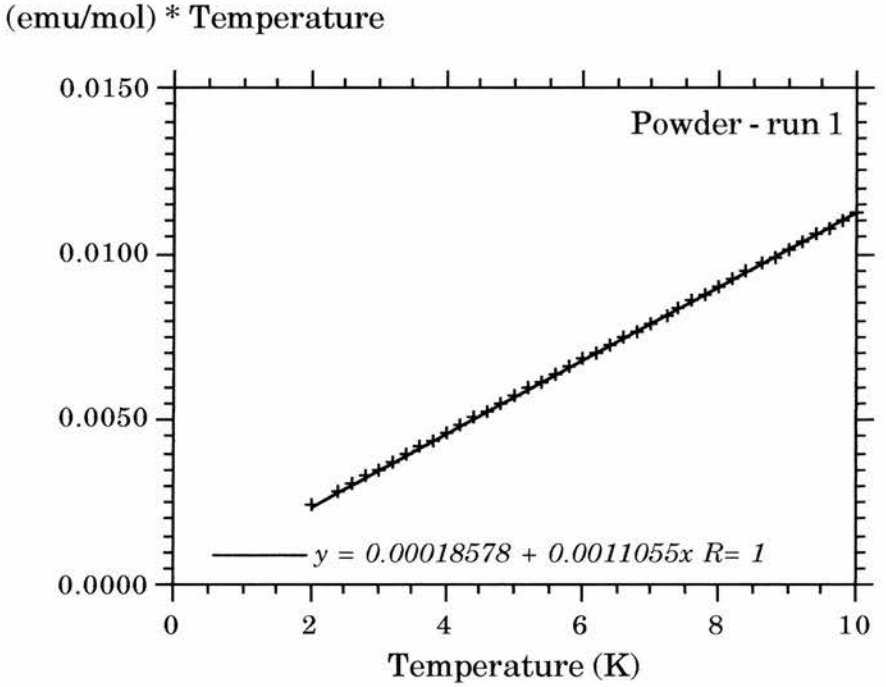

Figure 7.5. *Curie fit for the first powder run.*

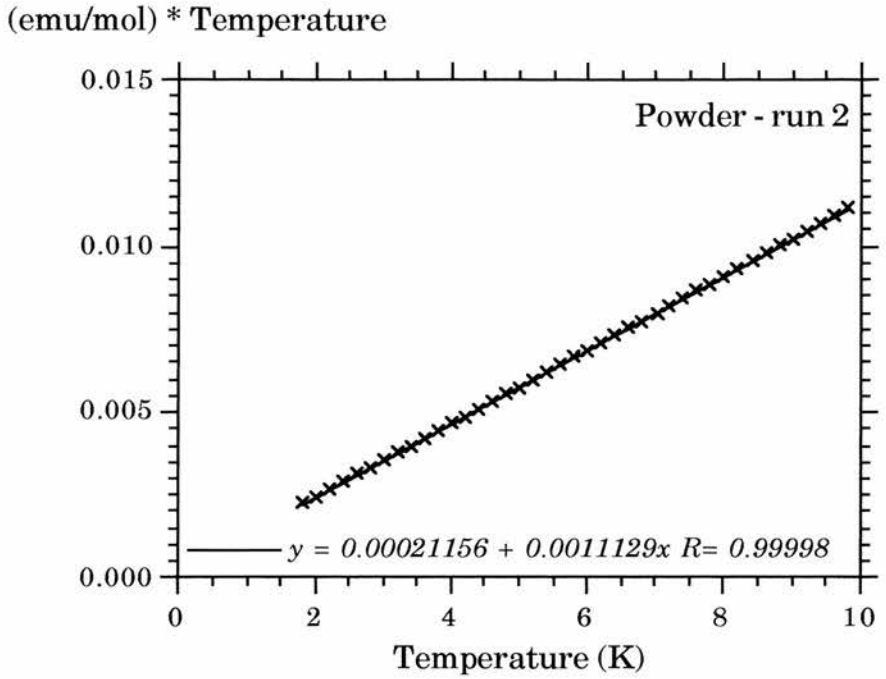

Figure 7.6. *Curie fit for the second powder run.*

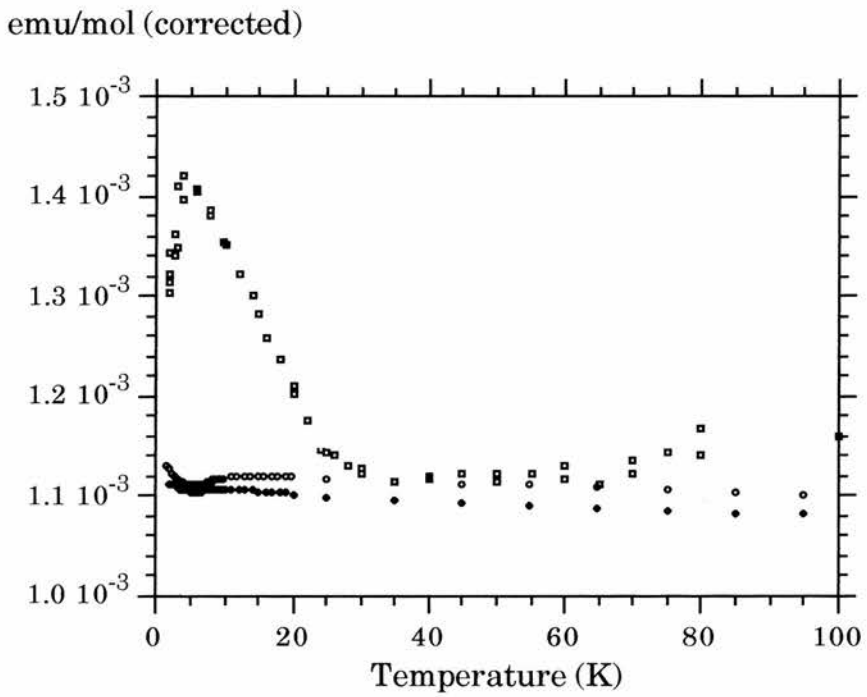

Figure 7.7. *Combined susceptibility graphs for the crystal and powder runs.*

The susceptibilities from the samples match closely throughout the temperature-independent region, but deviate significantly below ~25K. It is possible that the powder causes the antiferromagnetic behaviour to be masked, as this is a well-known phenomenon in High-Tc superconductors[3]. Small amounts of impurities (~1%) can destroy the antiferromagnetism in La_2CuO_4. The single crystal sample came from an earlier batch of samples; the powder batch would be more likely to contain impurities.

Between 20K and 90K the susceptibility becomes temperature independent, which is expected from metallic behaviour. However, as the temperature increases there is a hysteresis effect observed between the cooling and warming curves. This may be related to the hysteresis observed in the resistivity measurements as the splitting occurs at a similar temperature. The jump in the resistivity has been proposed as being due to the freezing of the rotational motion of the methyl groups[4]. A possible mechanism for these effects at 100K involves a co-operative rotational motion of the methyl groups. If, when synthesised, the rotation of these are independent of one another then on freezing they will align randomly. This would give a random potential along the $Ni(dmit)_2$ stacks which would inhibit the conductivity. As the system is warmed, groups may start rotating again, interacting with near-neighbours to produce a common rotation. When frozen again, these would have the same orientation, and provide less of a resistance to the current flow. As this process is repeated, more methyl groups will move together, and, when frozen in alignment, these will keep reducing the

---

3 See for example H. Alloul: *Magnetic Properties of the Cuprates*, in High Temperature Superconductors *(ed. D. P. Tunstall and W. Barford)*, Adam Hilger (1991).

4 H. Kim, A. Kobayashi, Y. Sasaki, R. Kato, H. Kobayashi: *Chem. Lett.*, **1987,** 1799 (1987).

resistance. On warming, if the frozen state persists until a slightly higher temperature, the warming resistivity will be slightly higher at any given temperature than the cooling resistivity. In this scenario, each successive cooling curve will have a jump at the same temperature, when the methyl groups freeze, but this will be reduced in size for each successive cycle.

The Curie constant, C, can be used to estimate the number of paramagnetic impurities using the formula

$$C = \frac{Ng^2\mu_B^2 J(J+1)}{3k},$$

which, for g = 2, μ_B = 9.27 x 10^{-21} erg/gauss, and k = 1.381 x 10^{-16} erg/K gives

$$N = 6.0199 \times 10^{23} C \qquad \text{(spin-1 e.g. } Ni^{2+}\text{)}$$

$$N = 1.6053 \times 10^{24} C \qquad \text{(spin-1/2)}$$

For the crystal sample (C = 0.005 cgs K/mol) this corresponds to 1.3% impurities per formula unit for spin-1/2, or 0.5% for spin-1. For the powder samples (C = 0.0002 cgs K/mol) this corresponds to 0.05% for spin-1/2, or 0.02% for spin-1.

Often in organic materials, the concentration of Curie spins does not directly correspond to the number of impurities[5]. Because the slightest disorder in low-dimensional systems can lead to localisation of states, the signal can arise from strains and defects in the molecular lattice. This may be the reasoning behind the apparent correlation

---

5 J. C. Scott: *Highly Conducting Quasi-One-Dimensional Organic Crystals*, Semiconductors and Semimetals (ed. E. Conwell), **27**, 385 (1988).

between those samples in which there was a large low temperature ESR signal and those that were destroyed by thermal cycling. It is possible that these samples had a large number of stresses that destroyed the crystals during thermal cycling.

7.3. Electron Spin Resonance.

7.3.1. Low Temperature Results.

The large peaks in the low temperature ESR spectra can be attributed to paramagnetic impurities, as with the magnetic susceptibility results. This is likely, as all samples show different low-temperature spectra, so the impurities must be very sample-dependant A plot of the area under the absorption spectra for sample x4 shows a Curie-like dependence.

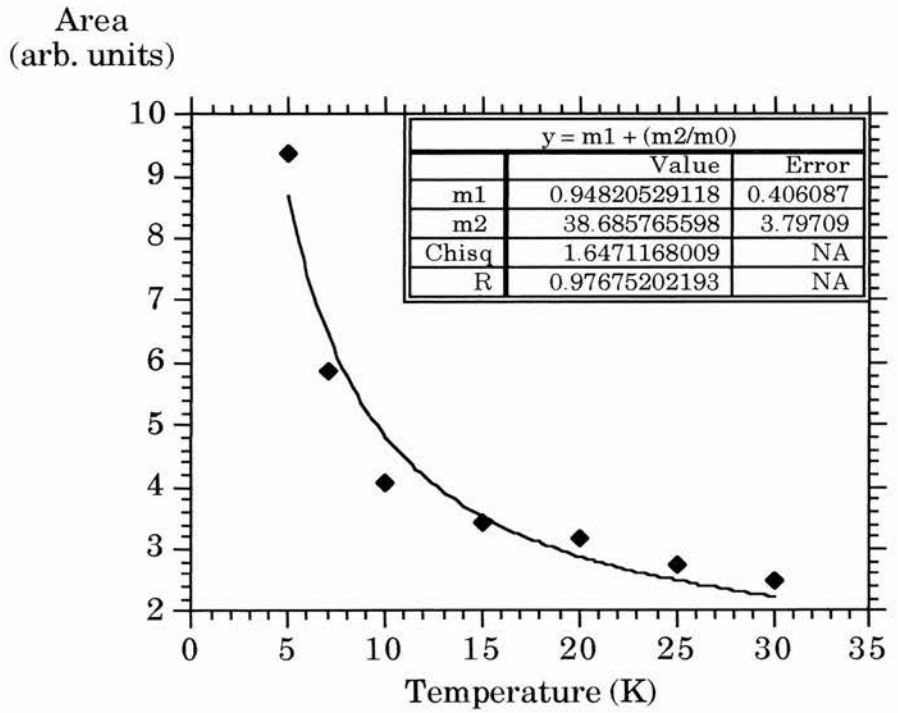

Figure 7.8. *Curie-like dependence of ESR low-temperature spectra.*

Often, the single cavity measurements will not give a true representation of the temperature dependence, as many factors can change between spectra, therefore a comparison with a standard reference in a dual cavity is better. The dual-cavity measurements give some indication of the spin concentration contributing to the signal. Because the $CuSO_4 \bullet 5H_2O$ reference should follow a 1/T dependence, then this can be translated to give the real sample areas. This is shown in Table 7.1.

Temperature	Actual $CuSO_4 \bullet 5H2O$ Area	Calculated $CuSO_4 \bullet 5H2O$ Area	Actual $NMe_4[Ni(dmit)_2]_2$ Area	Calculated $NMe_4[Ni(dmit)_2]_2$ Area
4K	291.4	291.4	376.5	376.5
10K	195.2	116.6	252.9	151.1
16K	205.5	72.8	229.6	81.4
27K	194.6	43.17	266.8	59.2

Table 7.1. *Corrected Areas for the dual-cavity measurements.*

If this data is fitted to a Curie-like dependence then a good fit is obtained (see Figure 7.9.).

To calculate the susceptibility, the formula

$$\chi = \frac{C}{T} = \frac{Ng^2\mu_B^2 J(J+1)}{3kT}$$

is used. For $CuSO_4 \bullet 5H_2O$, N = 2.9 x 10^{19} cm^{-1} which gives

$$\chi = \frac{1.80 \times 10^{-5}}{T} emu / cm^3 .$$

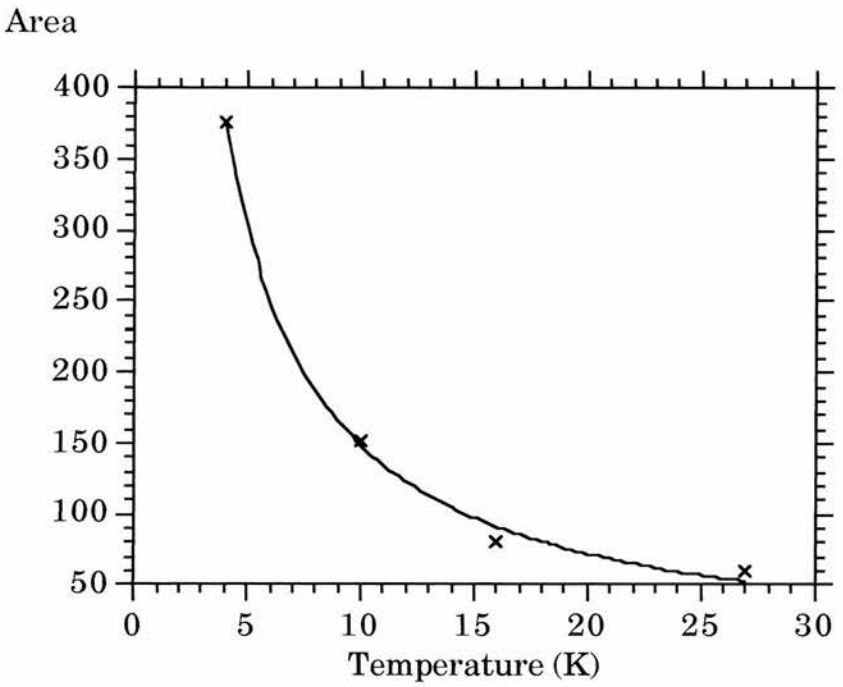

Figure 7.9. *Curie-like dependence of dual-cavity data.*

The average of the ratios between the sample and reference areas is 1.27, which means the sample susceptibility is

$$\chi = \frac{2.31 \times 10^{-5}}{T} emu / cm^3.$$

For $NMe_4[Ni(dmit)_2]_2$, ρ = 2 g/cm^3 [6] and the formula weight = 965 g/mol which gives

$$\chi = \frac{1.114 \times 10^{-2}}{T} emu / mol.$$

---

6 See for example: B. Pomaréde, B. Garreau, I. Malfant, L. Valade, P. Cassoux, J-P. Legros, A. Audouard, L. Brossard, J.-P. Ulmet, M.-L. Doublet and E. Canadell: *Inorg. Chem.*, **1994**, 3401 (1994).

At 4K, χ = 2.78 x 10^{-3} emu/mol. This is a factor of 2 greater than that measured by the SQUID magnetometer.

7.3.2. Anomalous "Spikes"

The origin of the "spikes" are more difficult to explain. The fact that they appear identical in all samples, even when the low-temperature data is very different implies that they are definitely from the $NMe_4[Ni(dmit)_2]_2$ and not impurities.

As ESR lines are often Lorentzian *(see Chapter 5)* then a fit to a derivative of a Lorentzian line can be performed. This is given by[7]

$$Y' = -Y_{\max}\frac{2\Gamma^2(x-x_r)}{\left[\Gamma^2+(x-x_r)^2\right]^2},$$

and the absorption signal is given by

$$Y = Y_{\max}\frac{\Gamma^2}{\left[\Gamma^2+(x-x_r)^2\right]}.$$

This can then be integrated to give the area under the curve. For the spectra obtained, the high-field peak at ~4250 Gauss is the largest, and therefore the best with which to attempt a fit. The 40K and 60K spikes were too small to be fitted; the others are shown in Figures 7.10 (a to c). The results are shown in Table 7.2.

---

7 J. A. Weil, J. R. Bolton, J. E. Wertz: *Electron Paramagnetic Resonance,* Wiley (1994).

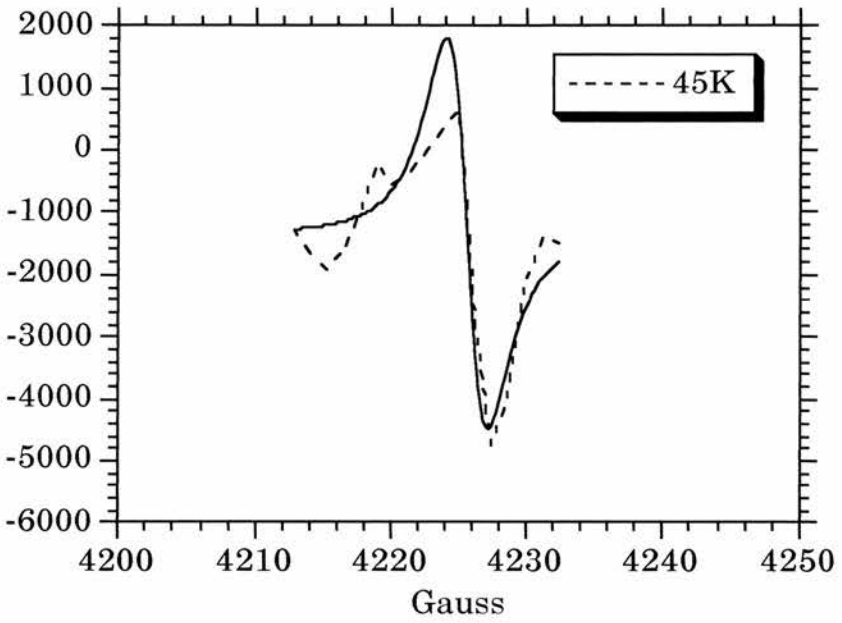

(a)

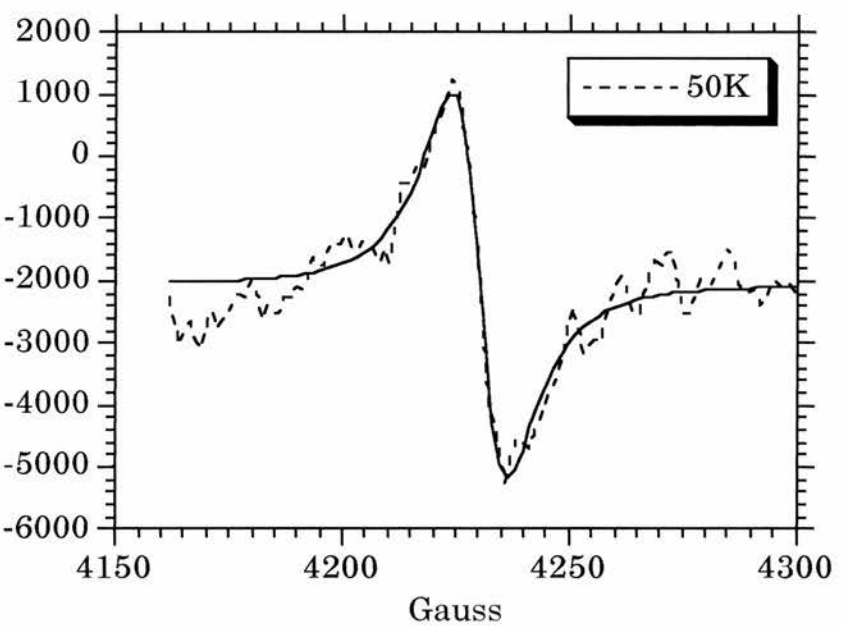

(b)

Figure 7.10. *Lorentzian line fits to the 4230 Gauss spike.*

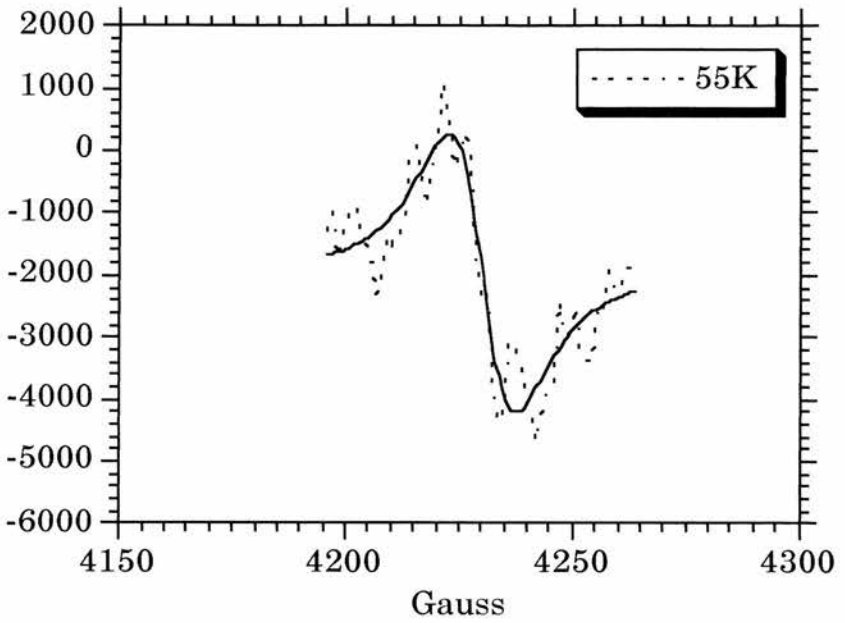

(c)

Figure 7.10. (cont.) *Lorentzian line fits to the 4230 Gauss spike.*

Temp.	Offset	Y_{max}	Γ	x_r	Area
45K	-1344	12768	2.63	4225	104726
50K	-2061	51715	10.83	4230	1710717
55K	-1963	44294	12.84	4230	1727989

Table 7.2. *Results of Lorentzian line fits for the 4230 Gauss spike.*

It can be seen that the area is small for the first line is small, but the other two are approximately the same. As the area is a measurement of the susceptibility, a temperature-independent region would imply metallic, or Pauli-spin susceptibility. Unfortunately, the lines broaden

before any other areas can be calculated. Also, as the lines are not calibrated, susceptibility measurements cannot be relied upon.

The peak positions do not change with orientation, which is an indication of metallic behaviour and this is consistent with the temperatures at which they appear. It is unusual to see a feature over such a small range of temperature although the disappearance at about 60K is probably due to the relaxation time increasing so as to broaden the line. The appearance of the spikes at 45K is unusual, as they are extremely narrow. This may be some form of phase transition, although no other evidence of transitions exists at this temperature

With organic conductors, it is often possible to see ESR signals up to room temperature, as the one-dimensionality inhibits the broadening mechanisms normally present[8]. In this study, no signal was seen at room temperature which implies some two-dimensional character exists (as is seen in resistivity measurements). As the temperature increases, it is possible that there is more interaction between adjacent stacks, leading to the two-dimensional nature which broadens the spikes.

There are at least 7 spikes observed in the spectra, with another one seen in the St. Andrews results, but not conclusively seen in the Birmingham results. There is no obvious relationship between the positions, although the three pairs of spikes all have separations of about 120 Gauss. In the $Ni(dmit)_2$ molecules there are six carbon atoms whose π-orbitals create the molecular orbitals.

It is possible to envisage a system of "filaments" being created along which the current can flow when the system becomes metallic. As the temperature increases, these smear into a two-dimensional system. This is shown diagramatically in Figure 7.11. In $NMe_4[Ni(dmit)_2]_2$ there

---

8 J. C. Scott: *Highly Conducting Quasi-One-Dimensional Organic Crystals*, Semiconductors and Semimetals (ed. E. Conwell), **27**, 385 (1988).

are two directions of stacks, which may lead to the doubling of the ESR lines. This model does not explain the other lines that appear. These are not spaced as the other pairs, and may be due to some other artefact, such as conduction through the central nickel atoms.

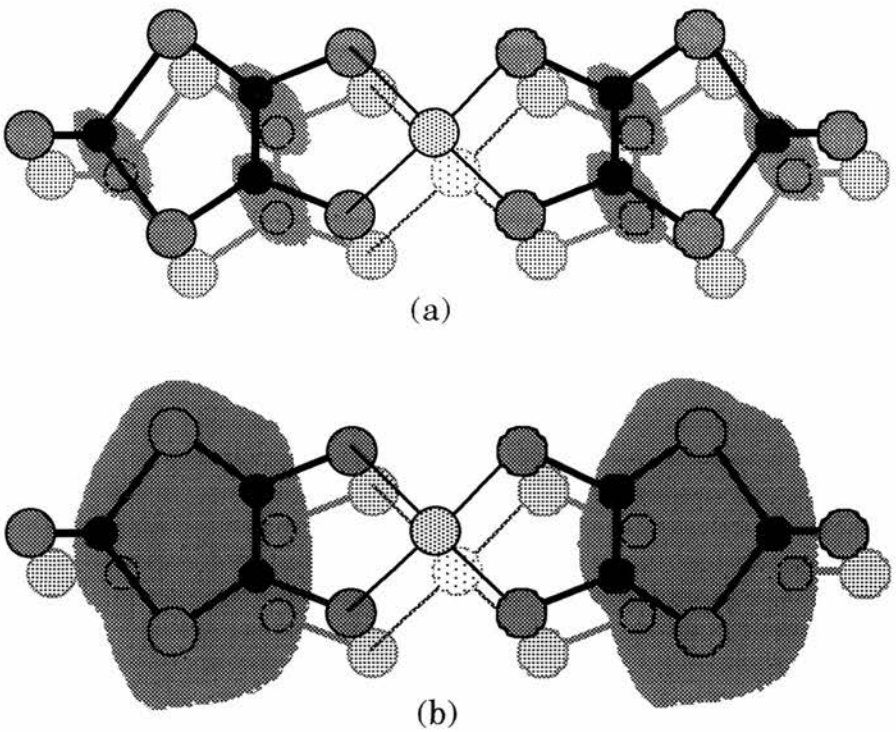

Figure 7.11. *Possible arrangement of conducting "filaments". (a) shows low-temperature conducting filaments along overlapping carbon atoms, with (b) showing higher temperatures where the filaments have more two-dimensional character.*

However, normally in organic conductors the lines appear close to g = 2 [9]. One mechanism for lines at different values is in a SDW. If the field exceeds a critical value (~0.4T for the Bechgaard salts) then the ESR line splits into at least two resonances. It is unlikely that these spikes are due to a SDW though, as these are normally associated with a low temperature insulating phase, and this system is metallic at the temperatures at which the spikes appear.

---

9 J. C. Scott: *Highly Conducting Quasi-One-Dimensional Organic Crystals*, Semiconductors and Semimetals (ed. E. Conwell), **27**, 385 (1988).

7.4. Nuclear Magnetic Resonance.

7.4.1. ^{1}H N.M.R.

Proton NMR measurements at room temperature show two peaks of almost equal intensity. This is not expected from the $NMe_4[Ni(dmit)_2]_2$ system, as all hydrogen sites should be equal, as they are rotating, which should average any splitting. The second peak may be due to methyl impurities, as the position of the line falls within the range (1.5 to 2.0 ppm)[10] at which these should appear. The second line falls within the range given for methyl groups attached to nitrogen (2.2 to 3.5 ppm). This would also correspond to the extra lines seen in the ^{13}C NMR spectra which fall in the range for methyl groups (*see next section*).

The low temperature spectra are consistent with the triplet seen for frozen methyl groups[11], with the lines being broad enough to mask the double-peak structure seen at room temperature.

If there was an antiferromagnetic transition taking place the lines would be expected to broaden out and disappear below the transition temperature, as in $NMe_4[Pd(dmit)_2]_2$ at 12K[12]. Instead, the peaks can be seen to decrease in intensity as the temperature increases, which is the Curie-like behaviour expected of a paramagnetic material. In $NMe_4[Pd(dmit)_2]_2$ a double exponential relaxation is also seen below 20K. A similar relaxation may be present in $NMe_4[Ni(dmit)_2]_2$, but the data was not sufficient to be analysed.

There is also a shift in the central peak position as the temperature decreases. This is due to the dipolar interaction of the spins

---

10 Bruker Almanac.

11 R. E. Richards, J. A. Smith: *Trans. Faraday. Soc.*, **47**, 1261 (1951).

12 K. Seya, Y. Kobayashi, T. Nakamura, T. Takahashi, Y. Osako, H. Kobayashi, R. Kato, A. Kobayashi, H. Iguchi: *Synth. Metals,* **70**, 1043 (1995)

on the Ni atoms at the NMe_4^+ cation sites. Geometrically, the arrangement of the sites is shown in Figure 7.12.

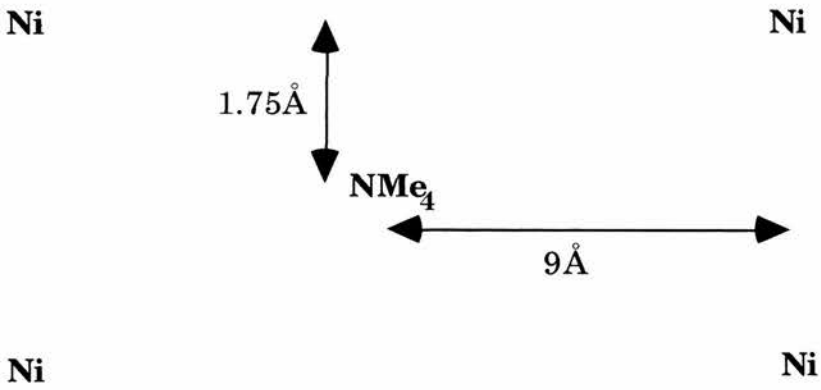

Figure 7.12. *Geometrical arrangement of Ni sites around the NMe_4^+ cation.*

The magnetic moment produced by the Ni atoms is given by the Brillouin function[13]

$$M = Ng\mu_B JB_J(y),$$

where

$$B_J(y) = \left\{\left(\frac{2J+1}{2J}\right)\coth\left[\frac{2J+1}{2J}y\right] - \left(\frac{1}{2J}\right)\coth\left[\frac{y}{2J}\right]\right\}$$

and

$$y = \frac{g\mu_B JB}{kT}.$$

---

13 J. S. Blakemore: *Solid State Physics (Second Edition)*, Cambridge (1985).

The dipolar field associated with this is given by

$$B_d = \frac{\mu_0 \mu_B}{4\pi r^3}\left(3\cos^2\theta - 1\right).$$

The field produced at the NMe_4^+ cations is shown in Figure 7.13. This model assumes half a spin per $Ni(dmit)_2$ molecule, according to the molecular formula, and it can be seen that there is a close correlation. It therefore appears that the shift is due to the dipolar interaction with the nearest-neighbour nickel sites, and the next-nearest need not be taken into account.

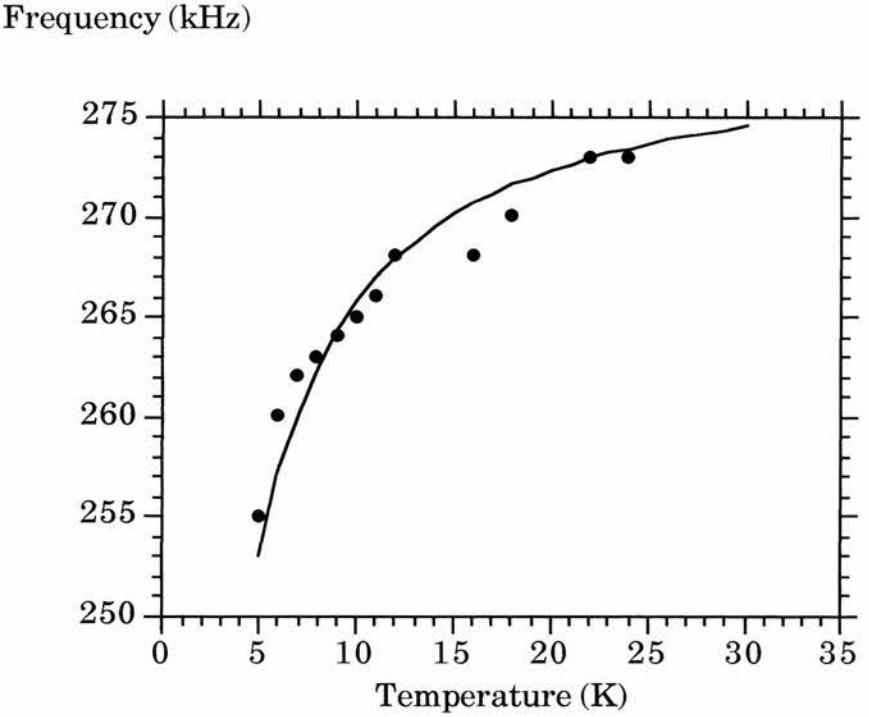

Figure 7.13. *Peak position of low-temperature ^1H peak. The solid curve is the predicted shift using a nearest neighbour dipolar interaction.*

This model assumes that there will be an alignment of the molecules in the magnetic field, as normally the orientation of the axis to the field will be random. If the long axis of the crystals align

perpendicular to the field then this will leave the unit cell in the correct alignment for the above calculation.

7.4.2. ^{13}C N.M.R.

The assignment of peaks is reasonably clear from the cross-polarisation spectra. The 299 and 257 ppm peaks are from the end carbon sites, with the 177 and 130 ppm lines from the central carbon sites. The 63 ppm line is from the methyl carbon. The lines at 30ppm are from impurities as they only appear in the second sample. The positions correspond to those for methyl groups, as does the proton NMR *(see last section)*. The NQS spectrum shows only the 299ppm and 63ppm lines. Normally the methyl lines should be suppressed, but often the rapid rotation overcomes this. The other lines would not be expected to be suppressed, but often are in these systems[14]. Lines are suppressed when strong coupling, usually from protons, causes the decay during a decoupling window in the pulse sequence.

In a normal non-conducting dmit system, lines usually appear at ~135 ppm (often a doublet) and at ~205 ppm[15]. This means that the lines seen in $NMe_4[Ni(dmit)_2]_2$ are shifted by the amounts shown in Table 7.3.

Atoms	Position (ppm)	Shift (ppm)
C = S	299	94
C = S	257	52
C = C	177	22
C = C	130	-5

Table 7.3. *Knight shifts of ^{13}C NMR lines from expected positions.*

14 G. J. Stockham and D. P. Tunstall: Unpublished results on $Sn(dmit)_2$ systems.

15 G. J. Stockham: Unpublished results on $Sn(dmit)_2$ systems.

According to the Korringa relation, the shifts should follow

$$K^2 T_1 T = \frac{\hbar}{4\pi k}\left(\frac{g\mu_B}{\hbar\gamma_N}\right)^2$$

which for $\gamma_N = 6.72828 \times 10^7\ T^{-1}s^{-1}$ gives $K^2T_1T = 4.1534 \times 10^{-6}$ Ks. For the 299 ppm line, this corresponds to a T_1 of ~1.5 seconds at 300K, instead of the measured value of 250ms. It is also clear that the Korringa relationship does not hold, as for the lines in which there is no shift in position, then T_1 should be inversely proportional to T. The Korringa relationship assumes that the electronic states are of purely *s*-character. It is possible to imagine a system in which the positive shift of the *s*-states in counteracted by a negative shift from the *p*-character of the carbon atomic orbitals which make up the molecular orbitals of the $Ni(dmit)_2$ blocks, as these play a significant role in the formation of the conduction bands.

Then, the system would be described by the equations:

$$K = K_s + K_p$$

$$\frac{1}{T_1} = \frac{1}{T_{1_s}} + \frac{1}{T_{1_p}}$$

$$K_s^{\,2} T_{1_s} T = \frac{\hbar}{4\pi k}\left(\frac{g\mu_B}{\hbar\gamma_N}\right)^2 \quad \text{and} \quad K_p^{\,2} T_{1_p} T = \frac{\hbar}{4\pi k}\left(\frac{g\mu_B}{\hbar\gamma_N}\right)^2 .$$

Using these formulae, only particular combinations of the four variables fit with the observed data. These are shown in Tables 7.4 to 7.7.

T	K	$1/T_1$	K_s	K_p	T_{1s}	T_{1p}
300	94	3.33	190	-96	0.4	1.66
260	94	2.10	168	-74	0.56	2.90
240	94	1.54	152	-58	0.74	5.13

Table 7.4. *Shift and relaxation data for 299ppm line.*

T	K	$1/T_1$	K_s	K_p	T_{1s}	T_{1p}
300	52	1.43	122	-70	0.92	2.81
270	52	1.43	128	-76	0.93	2.64
260	52	1.43	130	-78	0.94	2.61

Table 7.5. *Shift and relaxation data for 257ppm line.*

T	K	$1/T_1$	K_s	K_p	T_{1s}	T_{1p}
300	22	2.86	174	-122	0.52	1.06
270	21	4.40	194	-173	0.40	0.51
260	20	5.70	224	-204	0.31	0.38

Table 7.6. *Shift and relaxation data for 177ppm line.*

T	K	$1/T_1$	K_s	K_p	T_{1s}	T_{1p}
300	-5	2.85	138	-143	0.72	0.67
260	-8	2.50	138	-146	0.83	0.75
240	-10	3.08	158	-168	0.69	0.61

Table 7.7. *Shift and relaxation data for 130ppm line.*

In most organic conductors, the shifts decrease as the temperature is lowered, but here, the shifts increase for three of the lines. The Knight shift is proportional to the spin susceptibility *(see Section 4.1.6)*. Over this small temperature range, the susceptibility is rising as the temperature is lowered, so this phenomenon is not surprising.

8. Conclusions and Further Work.

8.1. Conclusions.

- The samples studied have a number of impurities, seen as extra lines in ^{1}H and ^{13}C NMR experiments, and from the elemental analysis. The ^{13}C NMR lines were not seen in the first batch of samples, and can be assumed not to be from the $Ni(dmit)_2$ molecules.
- The large number of sample-dependent impurities seen in low-temperature ESR measurements are probably from stresses within the crystal, as those with the largest number of impurities were destroyed by thermal cycling. These have a Curie-like temperature dependence, and estimates range from 0.05% to 1.3% for spin 1/2, or 0.02 to 0.5% for spin-1 impurites.
- The ground state of the system appears to be antiferromagnetic in origin from magnetic susceptibility measurements, as the susceptibility curves show a characteristic peak at about 4K. Results from ^{1}H NMR can not confirm this as the lines would be expected to broaden below this temperature, and this is not seen approaching 4K.
- The magnetic susceptibility curves show a transition at 20K which corresponds to the resistivity transition at this temperature. There is also a hysteresis effect observed in both resistivity and magnetic susveptibility curves, and a possible mechanism for this has been postulated, in which there is a co-operative rotation of the methyl groups with each thermal cycle.

- A number of unusual "spikes" appear in the ESR spectra between 40K and 60K. They are isotropic, and very narrow at 40K, and broaden out at 60K. It is difficult to estimate the susceptibilities by integrating the absorption spectra as the lines are so small. A possible explanation for this phenomenon is that conduction takes place along one-dimensional filaments which "smear" out at higher temperatures, but this would only account for 6 lines, whereas 7, or possibly 8 can be seen in the spectra.
- The spikes appear at g-values far from g=2, and there is no signal at room temperature, which is unusual for organic conductors.
- The proton NMR spectra are typical of frozen methyl groups, with a shift described by a simple dipolar interaction of spins on the Ni sites. This would imply that the paramagnetic terms in the magnetic susceptibility are due to these spins, and not impurities. However, the ESR lines at low temperature are sample dependent, which implies impurities.
- The ^{13}C NMR spectra show 4 peaks due to the $Ni(dmit)_2$ molecules at 299, 257, 177, and 130ppm, and one from the NMe_4 molecules at 63ppm. The Ni(dmit) lines are assigned to the C=S site (299 and 257ppm) and the C=C sites (177 and 130ppm).
- The ^{13}C NMR Knight shifts do not follow the simplest Korringa relationship, but instead appear to be determined by contributions from both *s*- and *p*-character orbitals.

8.2. Further Work.

- If larger crystals could be grown, a confirmation of superconductivity at higher pressures could be obtained.

- One of the most interesting phenomena are the spikes in the ESR spectra. A more detailed study of the these would be necessary.

- Low-temperature ^{13}C NMR measurements. The Bruker MSL is limited in its temperature range. A DOTY MAS probe was purchased which should have been capable of temperatures close to 10K, but this failed to function properly, after much testing. A replacement probe has recently been delivered which should work to 30K. Of particular interest is the region around 50K where the spikes appear in the ESR spectra.

Appendices.

A. Computer Programs.

A1. High-Pressure Resistance Experiment.

```
REM                    *** Hipress ***
REM    A program to control High-Pressure Resistance Expt.
REM    Written by GJS 19/08/94
REM    Adapted from 'LIAVDP' and 'SOLAR2' by PJM

REM    $INCLUDE: 'C:\LW\INCLUDE\LWSYSTEM.INC'
REM    $INCLUDE: 'C:\LW\INCLUDE\GPIB.INC'
REM    $INCLUDE: 'C:\LW\INCLUDE\GRAPHICS.INC'

DECLARE SUB LIA.START()
DECLARE SUB LIA.reset()
DECLARE SUB Lia.check.report(vr#,dev1#,dev2#,res#)
DECLARE SUB Set.Gain(sens%)
DECLARE SUB Set.OscV(sens%)
DECLARE SUB Start.trace()
DECLARE SUB Trace.average(itrace%,avg#,dev#,sens%)
DECLARE SUB LIA.WRITE (a$)
DECLARE SUB LIA.READ(a$,v#)
DECLARE FUNCTION pjmstr$(xx#,nsig%)
DECLARE SUB itc4.readtemp(sensor%,tmp#,done%)

DIM SHARED t#, tempcryo#,vsens#(30),lia%,offset#,expf%,temperature#,pressure#
DIM SHARED LiaValData%,LiaNameF$,LiaVs#
DIM SHARED report3$,LiaVy#,LiaVSy#
DIM SHARED  vv AS STRING *100
DIM SHARED sens1%,sens2%,oscv#


sens1%=26 : sens2%=26


REM ========================= MAIN PROGRAM ==================================

CALL ResetDevs
CALL solartron.init.v(addr%, ran%)
CALL Lia.Start
nextmeasurement: i%=0
WHILE i% <= 15
       ink$=LCASE$(INKEY$)
        IF ink$ = "s" THEN END
        SLEEP 1 : i%=i%+1
WEND
CALL solartron.measure(addr%, ran%, ssflag%, res$, sread#)
resistance# = (sread# / 0.01)
CALL itc4.readtemp(1,tempcryo#,check%)
CALL itc4.readtemp(2,t#,check%)
highp# = 2.0
lowp# = -2.0
pressure# = 0.0
CALL res.calc(RatP0#, t#)
resratio# = resistance# / RatP0#
nexttime:
       IF INKEY$ = "s" THEN END
       IF t# > 77 THEN
            ratio# = 0.9994 + (0.3518 * pressure#) + (0.05837 * pressure#^2)
```

```
        ELSE
              ratio# = 0.9967 + (0.3719 * pressure#) + (0.05974 * pressure#^2)
        ENDIF
       IF ABS(ratio# - resratio#) < 0.00000000001 THEN
             GOTO contin
        ENDIF
       IF ratio# > resratio# THEN
             highp# = pressure#
        ELSE
             lowp# = pressure#
        ENDIF
       pressure# = (lowp# + highp#) / 2
GOTO nexttime
contin:

CALL LIA.reset
PRINT report3$
GO TO nextmeasurement
END


REM=============================================================================

SUB LIA.START

vsens#(0)=2e-9 : vsens#(1)=5e-9 : vsens#(2)=1e-8
i%=3
WHILE i% <= 26
      vsens#(i%)=vsens#(i%-3)*10.0 : i%=i%+1
WEND
LiaNameF$="gjs"+MID$(DATE$,4,2)+LEFT$(DATE$,2)+".dat"
t1$="                RESISTOR              STANDARD"
t2$="  time      Voltage     %dev      Voltage      %dev     Resistance     Temp
Press"
t3$="                                                 Ohms        K           GPa"
PRINT t1$ : PRINT t2$ : PRINT t3$

LIA% = OpenDev%("", "lia")
IF lia% <= 0 THEN PRINT "Unable to open device for LIA " : END
IF ilpad%(lia%, 8) < 0 THEN PRINT "Unable to find address of LIA" : END
IF iltmo%(lia%, 11) < 0 THEN PRINT "Unable to set timeout for LIA" : END
CALL LIA.WRITE("OUTX1")                              'Directs output to GPIB
CALL LIA.WRITE("SMOD0")                          'Selects single screen display
CALL LIA.WRITE("OEXP1,0,1")     'Removes offset and expansion from X values
offset#=0.0 : expf%=1
CALL LIA.WRITE("TRCD1,1,0,0,1")          'Trace 1 set to store values of X
CALL LIA.WRITE("TRCD2,2,0,0,1")          'Trace 2 set to store values of Y
CALL LIA.WRITE("SRAT8")                      '16 values stored per second
CALL LIA.WRITE("SLEN100")                     'length of scan 100 seconds
CALL LIA.WRITE("SEND0")                                    'Single shot

   CALL LIA.WRITE("IGND1")                        'Grounds input shielding
   CALL LIA.WRITE("FREQ27")                     'Sets frequency to 27.5 Hz
   CALL LIA.WRITE("ISRC1")                       'Selects A-B configuration
  CALL LIA.WRITE("SYNC1")   'Switches ON synchronous filtering below 200 Hz
   CALL LIA.WRITE("OFLT8")                      'Sets time constant to 100ms
   CALL LIA.WRITE("AUXV1,0")          'Sets relay to connect LIA to sample
   CALL LIA.WRITE("SLVL1")  : SLEEP 1          'Sets amplitude of SINE OUT

   CALL SET.GAIN(sens1%)       'Sets appropiate LIA sensitivity for sample
   CALL LIA.READ("OUTP?1",vx#)                       'Reads the value of X
   oscv#=10e-6/vx#
  'Adjusts oscillator voltage so that voltage across sample = 10 microvolts
   CALL Set.OscV(sens1%)                    'AND readjusts LIA sensitivity
CALL Start.Trace         'Starts recording values of voltage across sample
END SUB

REM=============================================================================

SUB LIA.reset
```

```
LiaValData%=0 : report3$="" : dev2#=0.0
CALL Trace.average(1,LiaVr#,dev1#,sens1%) 'Reads and averages recorded values
of voltage
CALL Trace.average(2,LiaVy#,devy#,sens1%) 'Reads and averages recorded values
of voltage
IF LiaValData% > -11 THEN GO TO measurestandard

PRINT "LIA OFF SCALE attempting to reset"
sens1%=26
CALL SET.GAIN(sens1%)           'Sets appropiate LIA sensitivity for sample
CALL Start.Trace          'Starts recording values of voltage across sample
SLEEP 10
CALL Trace.average(1,LiaVr#,dev1#,sens1%) 'Reads and averages recorded values
of voltage

measurestandard:
IF sens2% > sens1% THEN a$="SENS"+STR$(sens2%): CALL LIA.WRITE(a$)
CALL LIA.WRITE("AUXV1,5") : SLEEP 1    'Sets relay to connect LIA to standard
CALL SET.GAIN(sens2%)          'Sets appropiate LIA sensitivity for standard
CALL Start.Trace:SLEEP 10 'Starts recording values of voltage across standard
CALL Trace.average(1,LiaVs#,dev2#,sens2%) 'Reads and averages recorded values
of voltage
CALL Trace.average(2,LiaVSy#,dev2y#,sens2%) 'Reads and averages recorded values
of voltage
res#=LiaVr#*1.0e03/LiaVs#
CALL LIA.check.report(LiaVr#,dev1#,dev2#,res#)

CALL LIA.WRITE("AUXV1,0") :            'Sets relay to connect LIA to sample
   'Adjusts oscillator voltage so that voltage across sample = 10 microvolts
CALL Set.OscV(sens1%)                          'AND readjusts LIA sensitivity
CALL Start.Trace          'Starts recording values of voltage across sample
END SUB

REM=============================================================================

SUB LIA.check.report(vr#,dev1#,dev2#,res#)
meas$="A"

CALL setdisplaymode(0)                    'Returns monitor to printing mode
xtime$=LEFT$(TIME$,2)+","+MID$(TIME$,4,2) : PRINT xtime$;
pdev1#=dev1#*100.0/vr#
pdev2#=dev2#*100.0/LiaVs#
PRINT USING "#######.###";vr#*1e6;
PRINT USING "###.####";pdev1#;
PRINT USING "#######.###";LiaVs#*1e6;
PRINT USING "###.####";pdev2#;
PRINT USING "#######.###";res#;
PRINT USING "#######.#";t#;
PRINT USING "#######.####";pressure#
PRINT "     ";       : PRINT USING "#######.###";LiaVy#*1e6;
PRINT "       "; : PRINT USING "#######.###";LiaVsy#*1e6;
PRINT "                    "; : PRINT USING "#####.#";tempcryo#
OPEN LiaNameF$ FOR APPEND AS #1
PRINT #1, xtime$;
P  R  I  N  T                        #  1  ,                        U  S  I  N  G
"#######.###";vr#*1e6;pdev1#;LiaVs#*1e6;pdev2#;res#;t#;pressure#
PRINT #1, "     ";       : PRINT #1, USING "#######.###";LiaVy#*1e6;
PRINT #1, "       ";     : PRINT #1, USING "#######.###";LiaVsy#*1e6
CLOSE #1

vmeas#=10e-6
oscv#=oscv#*vmeas#/vr#
END SUB

REM=============================================================================

SUB Set.Gain(sens%)
lastsens%=0
setsensitivity:
IF sens% <  7 THEN sens%=7
IF sens% > 26 THEN sens%=26
```

```
IF sens%=lastsens% THEN EXIT SUB ELSE lastsens%=sens%
a$="SENS"+STR$(sens%) : CALL LIA.WRITE(a$) : SLEEP 1    'Sets LIA sensitivity
CALL LIA.READ("OUTP?3",vr#)        'Reads the value of R (voltage amplitude)
IF vr# > 0.8 THEN
       CALL LIA.WRITE("SLVL0.05") :
       PRINT "Unacceptable voltage detected" : END
END IF
ratio# =vr#/vsens#(sens%)
ratio1#=vr#/vsens#(sens%-1)
IF ratio# <= .80 AND ratio1# > .80 THEN EXIT SUB
IF ratio# < .0080 THEN sens%=sens%-6 : GO TO setsensitivity
IF ratio# > .80   THEN sens%=sens%+3 : GO TO setsensitivity
WHILE vr# < vsens#(sens%)*0.80
       sens%=sens%-1
WEND
sens%=sens%+1
GO TO setsensitivity
END SUB

REM=============================================================================

SUB Set.OscV(sens%)
IF oscv# < .05 THEN oscv#=.05#
IF oscv# > 5.0 THEN oscv#=5.0#
oscv#=CINT(oscv#*500)/500
a$="SLVL"+pjmSTR$(oscv#,4) : CALL LIA.WRITE(a$)     'Sets amplitude of SINE OUT

CALL LIA.READ("SLVL?",oscv#)                'Reads amplitude of SINE OUT
CALL Set.Gain(sens%)                              'Adjusts LIA sensitivity
END SUB

REM=============================================================================

SUB Start.trace
CALL LIA.WRITE("REST")                        'Erases contents of data buffer
CALL LIA.WRITE("STRT")                                          'Starts scan
END SUB

REM=============================================================================

SUB Trace.average(itrace%,avg#,dev#,sens%)
DIM iarray%(200)
avg#=0.0 : dev#=0.0
CALL LIA.WRITE("PAUS")                                          'Stops scan
CALL LIA.READ("SPTS?1",nv#)           'Reads no of points stored in trace 1
npts%=CINT(nv#)-1
IF itrace%=2 AND npts% > 99 THEN npts%=99
IF npts% < 10 THEN PRINT "Insufficient points in trace " : END

j%=0 : sum#=0.0 : nsum%=0  : sum2#=0.0 : lastsum#=0.0 : lastno%=0
WHILE j% <= npts%
       k%=npts%-j%+1
       IF k% > 100 THEN k%=100
     a$="TRCL?"+STR$(itrace%)+","+STR$(j%)+","+STR$(k%) : CALL LIA.write(a$)
      ii%=ilrdi%(lia%,iarray%(),400)
       i%=0 : blocksum#=0.0
       WHILE i% <= k%-1
             x#=iarray%(2*i%)*2#^(iarray%(2*i%+1)-124)
              sum#=sum#+x#
              sum2#=sum2#+x#*x#
              nsum%=nsum%+1
             blocksum#=blocksum#+x#
      IF npts%-nsum% < 80 THEN lastsum#=lastsum#+x# : lastno%=lastno%+1
               i%=i%+1
       WEND
      blockavg#=blocksum#/i%
      IF j%=0 THEN maxblock#=blockavg# : minblock#=blockavg#
      IF blockavg# > maxblock# THEN maxblock#=blockavg#
      IF blockavg# < minblock# THEN minblock#=blockavg#
       j%=j%+k%
WEND
```

```
IF nsum% <> npts%+1 THEN PRINT "no of points error ",j%,npts%,nsum%
IF nsum% < 10 THEN PRINT "Insufficient points in trace " : END
avg#=sum#/nsum%
dev2#=(sum2#-sum#*sum#/nsum%)/nsum%
IF dev2# > 0 THEN dev#=SQR(dev2#)
lastavg#=lastsum#/lastno%
vavg#=offset#*vsens#(sens%)/100.0+avg#
ptest#=(maxblock#-minblock#)*100.0/vavg#
IF ABS(ptest#) > 5 THEN avg#=lastavg# : report3$="Unstable reading" :
LiaValData%=-1
outv1#=ABS(maxblock#*expf%*10.0/vsens#(sens%))
outv2#=ABS(minblock#*expf%*10.0/vsens#(sens%))
outv3#=ABS( lastavg#*expf%*10.0/vsens#(sens%))
IF outv1# > 10 OR outv2# > 10 OR outv3# > 10 THEN
       report3$="LIA OFF SCALE" : LiaValData%=-10
        avg#=lastavg#
        IF outv3# > 10 THEN LiaValData%=-100
END IF
avg#=offset#*vsens#(sens%)/100.0+avg#
END SUB

REM=============================================================================

SUB LIA.WRITE (a$)
b$ = a$ + CHR$(10)
l% = LEN(b$)
IF ilwrt%(LIA%, b$, l%) <= 0 OR ibcnt% <> l% THEN
       PRINT "Unable to write to LIA   ";a$ : END
END IF
END SUB

REM=============================================================================

SUB LIA.READ(a$,v#)
vv$=""
CALL LIA.WRITE(a$)
ii%=ilrd%(LIA%,vv$,100)
v#=VAL(vv$)
END SUB

REM=============================================================================

FUNCTION pjmstr$(xx#,nsig%)
a$ = ""  : x#=xx#
IF x# < 0 THEN a$=a$+"-": x#=-x#
a$=a$+LTRIM$(RTRIM$(STR$(FIX(x#))))+"."
n% = 1
WHILE n% <= nsig%
x# = (x# - FIX(x#)) * 10
a$ = a$ + LTRIM$(RTRIM$(STR$(FIX(x#))))
n% = n% + 1
WEND
pjmstr$=a$
END FUNCTION


REM =============================================================================

SUB res.calc(RatP0#, temp#)
CALL temp.coeff(rT#, temp#)
RatT77# = 0.0937
RatP0# = RatT77# * rT#
END SUB


REM =============================================================================

SUB temp.coeff(coeff#, temp#)
r1# = 0.97689
r2# = (2.27613e-4) * temp#
r3# = (9.4825e-6) * (temp# ^ 2)
```

```
r4# = (3.85803e-8) * (temp# ^ 3)
r5# = (6.359763255e-11) * (temp# ^ 4)
r6# = (1.844378863e-14) * (temp# ^ 5)
coeff# = r1# - r2# + r3# - r4# + r5# - r6#
END SUB


REM ===========================================================================

SUB solartron.init.v(bd%,range%)
bd% = OpenDev% ("", "solartronv")
IF bd% <= 0 THEN PRINT "Unable to open device for solartron V "
IF ilpad%(bd%,12) < 0 THEN PRINT "Unable to find address of solartron V"
IF ilclr%(bd%)   <= 0 THEN PRINT "Unable to clear solartron V"
IF iltmo%(bd%,11)   < 0 THEN PRINT "Unable to set timeout for solartron V"
range%=0
a$="I4N0M0R0Y2T1D0"+CHR$(10)
IF ilwrt%(bd%,a$,15)<=0 OR ibcnt%<>15 THEN PRINT "Unable to initialise
solartron settings V"
CLS
LOCATE 15,5:PRINT "DO YOU WANT TO RESET PRESSURE GAUGE? (Y/N)"
SLEEP
inp$ = INKEY$
IF (inp$="y") OR (inp$="Y") THEN
      LOCATE 10,5:PRINT "SWITCH OFF CURRENT SUPPLY TO PRESSURE GAUGE"
       LOCATE 12,5:PRINT "   THEN PRESS ANY KEY"
        SLEEP
       a$ = "Z1"+CHR$(10)
      www% = ilwrt%(bd%,a$,3)
       SLEEP 10
      LOCATE 16,5:PRINT "NOW SWITCH ON CURRENT, THEN PRESS ANY KEY"
       SLEEP
ENDIF
CLS
END SUB

REM ===========================================================================

SUB solartron.init.i(bd%,range%)
bd% = OpenDev% ("", "solartroni")
IF bd% <= 0 THEN PRINT "Unable to open device for solartron I"
IF ilpad%(bd%,12) < 0 THEN PRINT "Unable to find address of solartron I"
IF ilclr%(bd%)   <= 0 THEN PRINT "Unable to clear solartron I"
IF iltmo%(bd%,11)   < 0 THEN PRINT "Unable to set timeout for solartron I"
range%=3
a$="I4N0M0R0Y2T1D1"+CHR$(10)
IF ilwrt%(bd%,a$,15) <= 0 OR ibcnt%<>15 THEN PRINT "Unable to initialise
solartron settings I "
END SUB

REM ===========================================================================

SUB solartron.range (bd%,range%,sflag%,sola$)
rangestart:
sflag%=0
CALL solartron.measure (bd%,range%,sflag%,sola$,reading#)
IF ABS(reading#) < 2 THEN
       IF range%=2 THEN EXIT SUB
       range%=2 : a$="R2"+CHR$(10)
ELSE
       IF range%=3 THEN EXIT SUB
       range%=3 : a$="R3"+CHR$(10)
END IF
IF   ilwrt%(bd%,a$,3)<=0   OR   ibcnt%<>3      THEN   CALL
solartron.reset(bd%,range%,sflag%,sola$)
GO TO rangestart
END SUB

REM ===========================================================================

SUB solartron.measure (bd%,range%,sflag%,sola$,reading#)
```

```
DIM a AS STRING * 17, b AS STRING * 1
t#=TIMER
a$="*************+++++**"

measurestart:
ii%=ilrd%(bd%,a$,17)
IF ASC(MID$(a$,16,1))=13 AND ASC(MID$(a$,17,1)) =  10 THEN
                          IF ASC(MID$(a$,11,1)) <> 32 THEN sflag%=sflag%+1
       reading#=VAL(LEFT$(a$,9))
        EXIT SUB
ELSE
        ich%=0
        b$="*"
        WHILE ich% <> 10
            IF TIMER-t# > 10 THEN GO TO timeisup
                ii%=ilrd%(bd%,b$,1)
                ich%=ASC(b$)
        WEND
      sflag%=sflag%+CINT((TIMER-t#)*5)
END IF
GO TO measurestart

timeisup:
CALL solartron.reset(bd%,range%,sflag%,sola$)
t#=TIMER : a$="*************+++++**"
GO TO measurestart
END SUB

REM=============================================================================

SUB solartron.reset(bd%,range%,sflag%,sola$)

CALL setdisplaymode(0)
PRINT "***********************************"
PRINT "***** Unable to read solartron ";sola$;"****"
PRINT "***********************************"
sflag%=999
idummy%=CloseDev%(bd%)
SLEEP 10
IF sola$ = "V" THEN CALL solartron.init.v(bd%,range%)
IF sola$ = "I" THEN CALL solartron.init.i(bd%,range%)
SLEEP 5
END SUB

REM=============================================================================

SUB solartron.write(bd%,range%,sflag%,sola$,solwrt$)
writeagain:
ls%=LEN(solwrt$)
IF ilwrt%(bd%,solwrt$,ls%) <= 0 OR ibcnt%<>ls% THEN
      CALL solartron.reset(bd%,range%,sflag%,sola$)
ELSE
       EXIT SUB
END IF
GO TO writeagain
END SUB
```

A2. Digital Oscilloscope Control.

```
REM   $INCLUDE: 'C:\LW\INCLUDE\LWSYSTEM.INC'
REM   $INCLUDE: 'C:\LW\INCLUDE\GPIB.INC'
REM   $INCLUDE: 'C:\LW\INCLUDE\FORMATIO.INC'
REM   $INCLUDE: 'C:\LW\INCLUDE\GRAPHICS.INC'
```

```
REM   $INCLUDE: 'C:\LW\INCLUDE\ANALYSIS.INC'
REM     $INCLUDE: 'C:\LW\INSTR\hp54501a.inc'        ' HP 54501A Digitizing
Oscilloscope

dim wave(500) as double
common shared/wave/wave () as double
OPEN "SCOPE.LOG" FOR INPUT AS #2
INPUT #2, numf%
CLOSE #2

CALL hp54501a.init(7,1,1,1,1,14)
npts%=500
memno%=1
WHILE memno%<=4
      CALL hp54501a.read.memory (memno%, wave#(), sp#, tz#, npts%)
       CALL GrfReset (4)
       CALL SetPlotMode (0)
       CALL GrfYCurv2D (wave#(), 500)

       numf%=numf%+1
      namef$="SCOPE"+RTRIM$(LTRIM$(STR$(numf%)))+".DAT"

       OPEN namef$ FOR OUTPUT AS #1
       PRINT #1, sp#,tz#,npts%
              i%=0
              WHILE i% <= npts%
                     PRINT #1, wave#(i%)
                      i%=i%+1
              WEND
       CLOSE #1
      memno%=memno%+1
WEND
OPEN "SCOPE.LOG" FOR OUTPUT AS #2
PRINT #2, numf%
CLOSE #2
END
```

A1. Proton NMR Spectum Analysis.

```
REM   $INCLUDE: 'C:\LW\INCLUDE\LWSYSTEM.INC'
REM   $INCLUDE: 'C:\LW\INCLUDE\GPIB.INC'
REM   $INCLUDE: 'C:\LW\INCLUDE\FORMATIO.INC'
REM   $INCLUDE: 'C:\LW\INCLUDE\GRAPHICS.INC'
REM   $INCLUDE: 'C:\LW\INCLUDE\ANALYSIS.INC'
REM   $INCLUDE: 'C:\LW\INCLUDE\RS232.INC'


COMMON SHARED asize%,pi2#,n%
asize% = 4096
pi2# = 1.570796327
DIM SHARED x#(1 TO 4096)
DIM SHARED time#(1 TO 2048)


FUNCTION ibitr% (j%,nu%)
       ib% = 0
       for i = 1 to nu%
              j2% = fix(j%/2)
              ib% = (ib% * 2) + (j% - (2 * j2%))
              j% = j2%
              next i
       ibitr% = ib%
```

```
END FUNCTION


SUB post (inv%)
      nn2% = fix(n%/2)
      nn4% = fix(n%/4)
      for l% = 1 to nn4%
            i% = l% + 1
            m% = nn2% - i% + 2
            ipn2% = i% + nn2%
            mpn2% = m% + nn2%
            rp# = x#(i%) + x#(m%)
            rm# = x#(i%) - x#(m%)
            ip# = x#(ipn2%) + x#(mpn2%)
            im# = x#(ipn2%) - x#(mpn2%)
            arg# = (pi2#/nn4%) * (i% - 1)
            ic# = cos(arg#)
            if inv% = 1 then
                  ic# = -ic#
            endif
            isl# = sin(arg#)
            ipcos# = ip# * ic#
            ipsin# = ip# * isl#
            rmsin# = rm# * isl#
            rmcos# = rm# * ic#
            x#(i%) = rp# + ipcos# - rmsin#
            x#(ipn2%) = im# - ipsin# -rmcos#
            x#(m%) = rp# - ipcos# +rmsin#
            x#(mpn2%) = -im# - ipsin# - rmcos#
        next l%
END SUB


SUB SHUFFLE (inv%)
      IF inv% = 0 then
            celdis% = fix(n%/2)
            celnum% = 1
            parnum% = fix(n%/4)
      elseif inv% = 1 then
            celdis% = 2
            celnum% = fix(n%/4)
            parnum% = 1
      endif

      DO UNTIL (((inv% = 0) AND (celdis% < 2)) OR ((inv% = 1) AND (celnum% =
0)))
            i% = 2
            for j = 1 to celnum%
                  for k = 1 to parnum%
                        xtemp# = x#(i%)
                        ipcml% = i% + celdis% -1
                        x#(i%) = x#(ipcml%)
                        x#(ipcml%) = xtemp#
                        i% = i% + 2
                  next k
                  i% = i% + celdis%
            next j
            if inv% = 0 then
                  celdis% = fix(celdis%/2)
                  celnum% = celnum% * 2
                  parnum% = fix(parnum%/2)
            elseif inv% = 1 then
                  celdis% = celdis% * 2
                  celnum% = fix(celnum%/2)
                  parnum% = parnum% * 2
            endif
      LOOP
END SUB

SUB fft1 (inv%)
```

```
nu% = 0
n1% = fix(n%/2)
n2% = n1%
while n1% >= 2
       nu% = nu% + 1
       n1% = fix(n1%/2)
       wend
for i% = 1 to n2%
      k% = ibitr%(i%-1,nu%) + 1
       if i% > k% then
              ipn2% = i% + n2%
              kpn2% = k% + n2%
              tr# = x#(k%)
              ti# = x#(kpn2%)
              x#(k%) = x#(i%)
             x#(kpn2%) = x#(ipn2%)
              x#(i%) = tr#
              x#(ipn2%) = ti#
       endif
next i%


i% = 1
while i% <= n2%
       k% = i% + 1
       kpn2% = k% + n2%
       ipn2% = i% + n2%
       k1# = x#(i%) + x#(k%)
       x#(k%) = x#(i%) - x#(k%)
       x#(i%) = k1#
      k1# = x#(ipn2%) + x#(kpn2%)
      x#(kpn2%) = x#(ipn2%) - x#(kpn2%)
       x#(ipn2%) = k1#
       i% = i% + 2
wend
deltay# = pi2#
celnum% = fix(n2%/4)
parnum% = 2
celdis% = 2

do until celnum% = 0
       index% = 1
       y# = 0
       for i2% = 1 to parnum%
              if y# <> 0 then
                     cosy# = cos(y#)
                     siny# = sin(y#)
                     if inv% = 1 then
                            siny# = -siny#
                      endif
              endif
       for l% = 0 to celnum% - 1
             i% = (celdis% * 2) * l% + index%
             j% = i% + celdis%
             ipn2% = i% + n2%
             jpn2% = j% + n2%
             if y# = 0 then
                    k1# = x#(i%) + x#(j%)
                   k2# = x#(ipn2%) + x#(jpn2%)
                   x#(j%) = x#(i%) - x#(j%)
                  x#(jpn2%) = x#(ipn2%) - x#(jpn2%)
              else
                    r2cosy# = x#(j%) * cosy#
                    r2siny# = x#(j%) * siny#
                    i2cosy# = x#(jpn2%) * cosy#
                    i2siny# = x#(jpn2%) * siny#
                    k1# = x#(i%) + r2cosy# + i2siny#
                    k2# = x#(ipn2%) - r2siny# + i2cosy#
                    x#(j%) = x#(i%) - r2cosy# - i2siny#
                   x#(jpn2%) = x#(ipn2%) +r2siny# - i2cosy#
              endif
```

```
                x#(i%) = k1#
                x#(ipn2%) = k2#
            next l%
            y# = y# + deltay#
            index% = index% + 1
            next i2%

          celnum% = fix(celnum%/2)
          parnum% = parnum% * 2
          celdis% = celdis% * 2
          deltay# = deltay# / 2

    LOOP
END SUB

SUB draw.ft(tit$,st%,fin%,num%)
    CALL GrfReset (12)
    CALL SetTitle (tit$)
    CALL SetAxAuto (0, 0)
    CALL SetCrvColor (12)
    CALL SetAxName (0, "")
    CALL SetAxRange (0, st%, fin%, 10)
    CALL GrfYCurv2D (x#(),num%)
END SUB

SUB draw.mag.ft(filename$)
    for h% = 1 to fix(n%/2)
        a# = x#(h%)
        b# = x#(h% + (fix(n%/2)))
        x#(h%) = SQR((a#*a#) + (b#*b#))
    next
    CALL GrfReset (12)
    CALL SetTitle (filename$ + "  : Magnitude")
    CALL SetAxName (0, "MHz")
    CALL SetAxAuto (0, 0)
    CALL SetCrvColor (13)
    CALL SetAxRange (0, 0, time#(fix(n%/2)), 10)
    CALL GrfCurv2D (time#(),x#(), fix(n%/2))
END SUB

SUB move.cursor(num%,num2%,sp#,tz#)
    CALL GrfMsg ("Move cursor with < & > keys (use SHIFT for speed), then
press SPACE", 5)
    CALL MaxMin (x#(), num2%, xmax#, xmaxin%, xmin#, xminin%)
    timestart% = 1
    resp$ = "2"
    while resp$<> " "
        resp$ = inkey$
        IF resp$ = "."  THEN timeadd% = 1
        IF resp$ = ","  THEN timeadd% = - 1
        IF resp$  = ">" THEN timeadd% = 5
        IF resp$  = "<" THEN timeadd% = - 5
        timestart%=timestart% + timeadd%
        CALL SetPlotMode (0)
        CALL SetCrvColor (15)
        CALL SetPointStyle (10)
                    CALL  GrfPoint2D  (time#(timestart%-timeadd%),
timeadd%))
        CALL SetCrvColor (0)
        CALL SetPointStyle (5)
        CALL GrfPoint2D (time#(timestart%-timeadd%), xmax#)
        CALL SetPlotMode (0)
        CALL SetCrvColor (12)
        CALL SetPointStyle (10)
        CALL GrfPoint2D (time#(timestart%), x#(timestart%))
        CALL SetCrvColor (15)
        CALL SetPointStyle (5)
        CALL GrfPoint2D (time#(timestart%), xmax#)
        timeadd% = 0
    WEND
```

```
        for k% = 0 to 2048
              x#(1+k%) = x#(timestart% + k%)
        next
        tz# = tz# + (sp# * (timestart%-1))
        for s% = 1 to num%
              time#(s%) = (((s%-1) *sp#) + tz#) * 1000000
        next s%
        CALL GrfReset (4)
       CALL SetAxName (0, "milliseconds")
        CALL SetCrvColor (9)
       CALL GrfCurv2D (time#(), x#(), num%)
       CALL GrfMsg ("Press a key to continue", 5)
       if inkey$ = "" then sleep
END SUB

check% = 1
do
CALL SetDisplayMode (0)

input "Enter Filename (RTN to exit) :";file$
if file$ = "" then end
input "How many points in transform (RTN for maximum) :";numpt%
if numpt% >= 4096 then
       numpt%=4096
elseif numpt% >= 2048 then
       numpt%=2048
elseif numpt% >= 1024 then
       numpt%=1024
elseif numpt% >= 512 then
       numpt%=512
elseif numpt% >= 256 then
       numpt%=256
else numpt% = 4096
endif
write numpt%


filename$ = file$ + ".dat"
open filename$ for input as #1
input #1, sp#, tz#, npts%
z% = 0
while z% <= npts%
       input #1, x#(z%)
        z% = z% + 1
wend
close #1
if numpt% > npts% then
       for q% = npts%+1 to numpt%
              x#(q%) = 0
        next
endif
for s% = 1 to npts%
      time#(s%) = (((s%-1) *sp#) + tz#) * 1000000
next s%
CALL GrfReset (12)
CALL SetTitle (filename$)
CALL SetAxName (0, "microseconds")
CALL SetAxAuto (0, 0)
CALL SetAxRange (0, time#(1), time#(npts%), 10)
CALL GrfCurv2D (time#(), x#(), npts%)
CALL move.cursor(npts%,numpt%,sp#,tz#)

n% = numpt%
tottime# = n% * sp# *1000
freqsp# = (1/tottime#)/1000
for g% = 1 to fix(n%/2)
      time#(g%) = (g%-1) * freqsp#
next
CALL GrfMsg ("Please wait : Shuffling...", 5)

shuffle(0)
```

```
CALL GrfMsg ("Please wait : Transforming array...", 5)
fft1(0)
CALL GrfMsg ("Please wait : Post processing...", 5)
post(0)

CALL draw.ft(" Real FT",1,fix(n%/2),fix(n%/2))
CALL draw.ft(" Imaginary FT",(fix(n%/2))+1,n%,n%)
CALL draw.mag.ft(filename$)

CALL GrfMsg ("Do you want to save to disc (Y/N)", 9)
resp$ = ""
do
resp$ = inkey$
loop until resp$ <> ""
if resp$ = "Y" or resp$ = "y" then
      msg$ = "Saving to disc as "+file$+".fft  :*"
      CALL GrfMsg (msg$, 9)
      counter# = fix (n%/2) /10
       count# = 0
      open file$+".FFT" for output as #2
      for j% = 1 to fix(n%/2)
             print #2, j%,
            print #2, using "######.####";time#(j%),
            print #2, using "######.####";x#(j%)
             count# = count# + 1
             if count# >= counter# then
                    msg$ = msg$ + "*"
                    count# = 0
                    CALL GrfMsg (msg$, 9)
              endif
       next
       close #2
endif
resp2$ = inkey$
loop until resp2$ = "N" or resp2$ ="n"
end
```

B. Bruker MSL500 Pulse Programs.

B1. HPDEC.PC

```
; INVERSE GATED HETERONUCLEAR DECOUPLING
; CW DECOUPLING DURING D7 ONLY
; SEE OPERATORS MANUAL CHAP. V. 6.

PROT F1 XT
START,              D1 [XT +X]
                    D1 [F1 @PLS1 F2 +X RGATE XT +X]
                                ; 90 DEGREE PULSE AND DECOUPLING
                    D3 [STA F2 +X RGATE]   ; DECOUPLING AND TRIGGER
                    D7 [F2 +X]             ; ACQUISITION
                    D0
                    5U ++PLS1
GOTO START

BEGIN LISTS
PLS1,               +X +X -X -X
RLS,                +X +X -X -X
END LISTS

; RECEIVER MODE : RPN
; TRIGGER MODE : NT
; DECOUPLER MODE : DO
```

B2. CPCYCL.PC

```
; CROSS POLARISATION PULSE SEQUENCE
; WITH PHASE ALTERNATION

PROT NONE

START,              D11 [XT +X]
                    D11 [F2 @PLS1 XT +X]          ;PROTON 90 DEG. +/-
                    D5 [F2 -Y F1 @PLS2 RGATE XT +X] ; CONTACT PULSE
                    D3 [F2 -Y RGATE STA]           ; DEAD TIME DELAY
                    D7 [F2 -Y]
                    D0
                    5U ++PLS1
                    5U ++PLS2
GOTO START

BEGIN LISTS
PLS1,               +X -X
PLS2,               +X +X -X -X
RLS,                +X -X -X +X
END LISTS

; RECEIVER MODE : RPN
; TRIGGER MODE : NT
; DECOUPLER MODE : DO

; NS = 8*N
```

B3. NQS.PC

```
; CROSS POLARISATION PULSE SEQUENCE WITH PHASE ALTERNATION
; INTERRUPTED DECOUPLING SUPPRESSES SIGNAL OF STRONGLY
; DIPOLAR COUPLED NUCLEI.
```

```
; SEE OPELLA S.J. & FREY D.M.H., J.A.C.S., 101, (1979), 5855

PROT NONE

START,              D11 [F2 @PLS1]              ;PROTON 90 DEG. +/-
                    D5 [F2 -Y F1 @PLS2 RGATE]   ; CONTACT PULSE
                    D3 [STA RGATE]              ; DEAD TIME DELAY
                    D7 [F2 -Y]
                    D0
GOTO START

BEGIN LISTS
PLS1,               +X -X
PLS2,               +X +X
RLS,                +X -X
END LISTS

; RECEIVER MODE : RPN
; TRIGGER MODE : NT
; DECOUPLER MODE : DO
; D3 = 30 - 100US IS USUALLY SUITABLE
; NS = 8*N
```

B4. GJSNMRT1.PC

```
; INVERSE GATED HETERONUCLEAR DECOUPLING
; CW DECOUPLING DURING D7 ONLY
; SEE OPERATORS MANUAL CHAP. V. 6.
; ADAPTED 22/5/94 BY GJS

PROT F1 XT
START,              D2 [XT +X]
                    D2 [F1 @PLS1 F2 +X RGATE XT +X]
                              ; 180 DEGREE PULSE AND DECOUPLING
                    VD                    ; VARIABLE DELAY
                    D1 [XT +X]
                    D1 [F1 @PLS1 F2 +X RGATE XT +X]
                             ; 90 DEGREE PULSE AND DECOUPLING
                    D3 [STA F2 +X RGATE]   ; DECOUPLING AND TRIGGER
                    D7 [F2 +X]             ; ACQUISITION
                    D0
                    5U ++PLS1
GOTO START

BEGIN LISTS
PLS1,               +X +X -X -X
RLS,                +X +X -X -X
END LISTS

; RECEIVER MODE : RPN
; TRIGGER MODE : NT
; DECOUPLER MODE : DO
```

B5. ONEF2.PC

```
; PROTON F2 PULSE FOR SET UP
; PUTS OUT 0 DEGREE PHASE PULSES ON F2 CHANNEL

PROT F1 F2 XT

START,              D11 [F2 +X RGATE]  ; F2 CHANNEL X PULSE
                    D3 [STA RGATE]     ; DEAD TIME DELAY AND TRIGGER
```

```
                    D0                  ; RECYCLE DELAY
GOTO START

; RECEIVER : F2
; TRIGGER MODE : NT
; DECOUPLER MODE : DO
; QPF, RPF
```

C. Publications and Presentations.

Magnetic Resonance Investigation of the Organic Superconductor $NMe_4[Ni(dmit)_2]_2$.

G. J. Stockham, D. P. Tunstall, (Dept. of Physics, University of St. Andrews)
J. T. S. Irvine, (Dept. of Chemistry, University of St. Andrews)
S.M. Doidge-Harrison, (Dept. of Chemistry, University of Aberdeen)

Poster presented at the CMMP conference, Liverpool, Dec. 1995.

Magnetic Susceptibility of the Organic Superconductor $NMe_4[Ni(dmit)_2]_2$.

G.J. Stockham, D. P. Tunstall, (Dept. of Physics, University of St. Andrews)
A. Harrison, G. Whittaker, (Dept. of Chemistry, University of Edinburgh)
S.M. Doidge-Harrison, (Dept. of Chemistry, University of Aberdeen)

Poster presented at the CMMP conference, Warwick, Dec. 1994.

A 13-C NMR Investigation of the Organic Superconductor $NMe_4[Ni(dmit)_2]_2$.

G.J. Stockham, D. P. Tunstall, (Dept. of Physics, University of St. Andrews)
S.M. Doidge-Harrison, J.T.S. Irvine, (Dept. of Chemistry, University of Aberdeen)

Poster presented at the M2S-HTSC conference, Grenoble, Jun. 1994.